Photoalignment Control of Nanodomains in Liquid Crystalline Block Copolymer Thin Films

MORIKAWA Yuichi

Graduate School of Engineering

Nagoya University

2007

Contents

Chapter 1

General Introduction

Fabrications of nanomaterials through building up atoms or molecules one by one are the final goal and the cherished desire for chemists. The nanomaterials have widely attracted increasing interest in various fields such as optical electronics, biomaterials, energy materials and materials science, etc. On the other hand, biological systems create hierarchical and distinct structures with nanoscopic and microscopic scale based on the difference of the combination of molecules and the molecular orientations. The imitation of the hierarchical structural formation carried out in biological systems should give large possibility to the development of nanomaterials having high performances.

The molecules form structures of a high order via self-assembly and self-organization, denoted as the bottom-up approach. Besides, the photoresposible molecules are controlled molecular structure and orientation states by light illumination. Therefore, it is expected that the light exposure in molecules during a bottom-up process brings about the formations of hierarchical structure having each of information relevant to molecules and nanostructures. The utilizing photoprocess may make it possible to pattern similarly as photolithography representing the top-down approach. In this motivation, the aim of this study is establishment of the novel concept neither bottom-up nor top-down for formation and alignment controls of hierarchical nanostructures. For the materials forming hierarchical structures, block copolymes are attracting increasing interest. These polymers provide microphase separated structures

with nanometer ordered periodicity, through self-assembly.[1,2] From the viewpoint of optics approach, azobenzene (Az) as a photochromic molecule will be favorably applied. Due to the angular-selected photoreaction excited by linearly polarized light (LPL) irradiation and cooperative motions most favorably in a liquid crystalline state, Az chromophores aligned in the in-plane and out-of-plane directions.[3]

This doctoral thesis describes my novel approach on the on-demand 3D alignment control and patterning of hierarchical nanostructures in Az-containing diblock copolymers. Background and aim of this thesis are described in below.

1.1 Nanostructures in block copolymers

In general, block copolymers consisting of chemically distinct polymer segments, i.e. hydrophobic and hydrophilic segments or hard and soft segments, provide microphase separated structures of sphere, cylinder and lamellar, etc., through self assembly. As shown in Figure 1-1, the AB diblock copolymers exhibit the periodic nanostructures depending on the relative volume fractions of the two blocks.[1,2] The important parameters to describe phase separation leading to the formation of nanostructures are the total degree of polymerization, the Flory-Huggins χ parameter and volume fractions of two blocks. Additionally, block copolymers have various properties resulting from the natures of blocks.

The diblock copolymers connecting a polymer possessing mesogenic groups at the side-chains and an isotropic polymer exhibit liquid crystallinity, and provide hierarchical structures consisting of microphase separated structures and liquid crystalline (LC) layer structures within the block copolymer domain. The LC mesogens prefer to orient homogeneously with respect to the interface between the two polymer

a

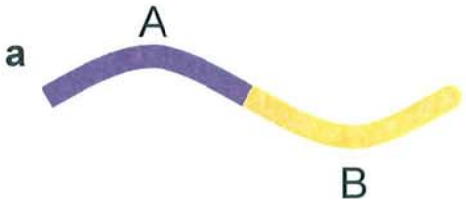

b

Nature of patterns	Spheres (SPH) (3D)	Cylinders (CYL) (2D)	Double gyroid (DG) (3D)	Double diamond (DD) (3D)	Lamellae (LAM) (1D)
Space group	$Im\bar{3}m$	p6mm	$Ia\bar{3}d$	$Pn\bar{3}m$	pm
Blue domains: A block	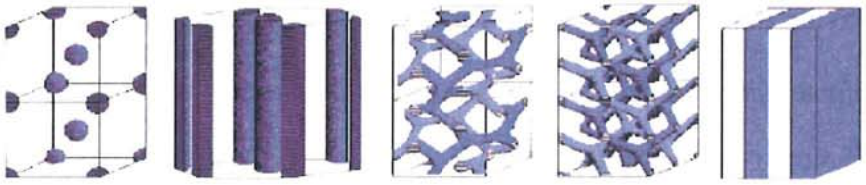				
Volume fraction of A block	0-21%	21-33%	33-37%		37-50%

Figure 1-1 (**a**) Schematic illustration of AB diblock copolymer. (**b**) Schematic phase diagram showing various microphase separated structures by AB diblock copolymer. (taken from Ref. 2)

phases, denoted as the intermaterial dividing surface (IMDS).[4,5] Ober and coworkers demonstrated that both the axes of the mesogenic groups and the lamellar interfaces orient parallel to the film surface since mesogens are anchored at the IMDS (Figure 1-2).[4] Hammond's group revealed the influence of the length of LC spacer on orientation direction within the layers.[6] Hexyl spacer systems provide the parallel arrangement of mesogens to a lamellar morphology. The longer decyl spacer systems, however, exhibit the perpendicular arrangement of mesogens to lamellae. It is assumed that these results, which have not been observed in other LC block copolymer systems, are the consequence of the decoupling of the mesogens from the polymer main chain.

1.2 Thickness dependence of nanostructures in block copolymer thin films

In the case of some block copolymer thin films, the morphology and orientation of nanostructure depend on the film thickness. Krausch and coworkers studied the phase behavior in cylinder-forming block copolymer thin films by both experiments and computer simulations.[7,8] Figure 1-3 shows the tapping mode scanning force microscopy (TM-SFM) phase images of two polystyrene-*block*-polyisobutadiene-*block*-polystyrene triblock copolymer thin films with gradients in film thickness and the result of simulation.[7] The distinct morphologies were observed as disordered phase, polystyrene (PS) cylinders oriented parallel and perpendicular to the substrate plane and perforated lamellar. The formation of their distinct phases required interplay between film surface and confinement effects.

The two different orientations of PS cylinders are given in thin films. For films with thinner thickness than two cylindrical diameter, cylinders orient normal to film surface. In contrast, parallel orientation of cylinders is formed in thicker regions.[9] The inverse

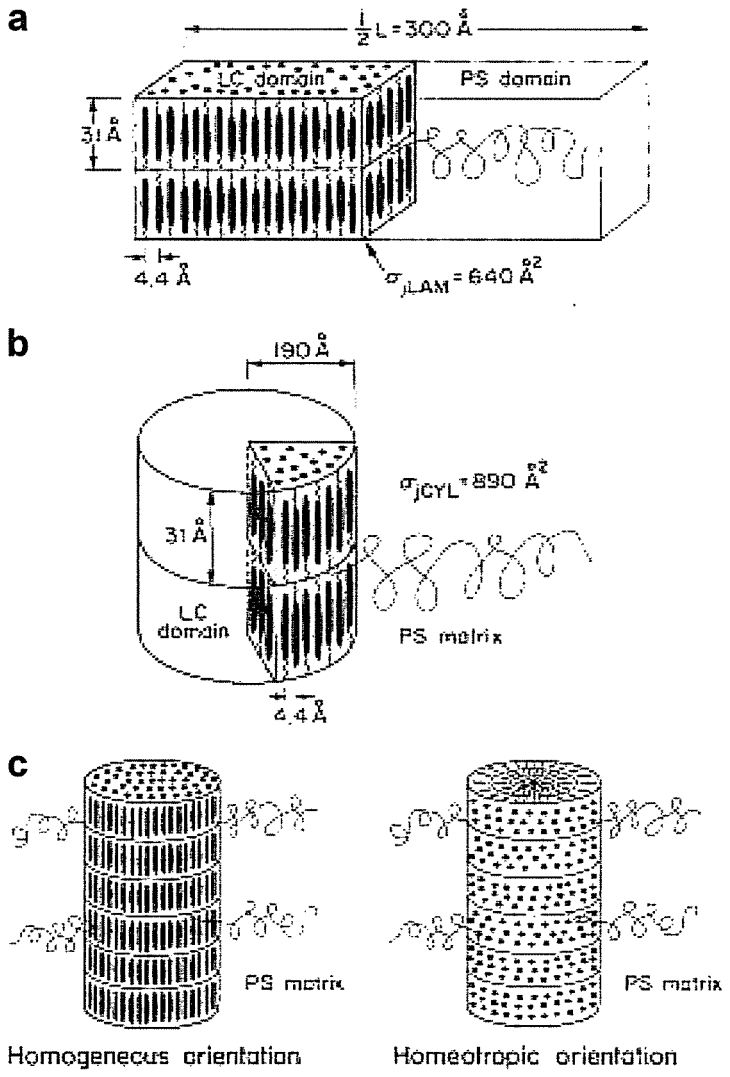

Figure 1-2 (**a**) Schematic illustration of lamellar structure of LC-segment-containing block copolymers. (**b** and **c**) cylinder structures (homogeneous and homeotropic orientation of mesogens to the IMDS). (taken from Ref. 4)

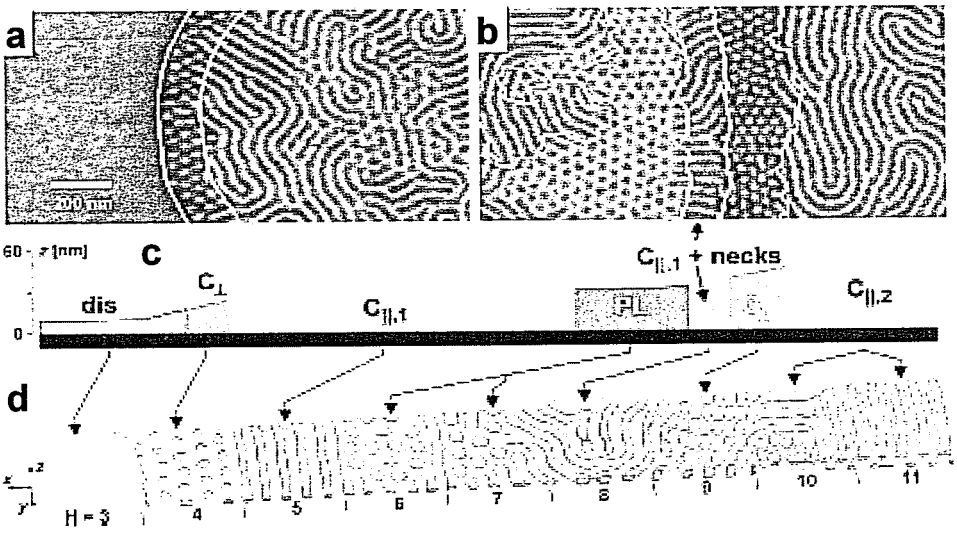

Figure 1-3 (**a** and **b**)TM-SFM phase images of a triblock copolymer film. (**c**) Schematic height profile of the phase images. (**d**) Simulation of an ABA triblock copolymer film. (taken from Ref. 7a)

state in relation to the cylinder orientation was reported by Krausch and co-workers.[10] The cylinders oriented horizontally for a film thickness of about one cylindrical diameter. In thicker regions, those exhibited normal orientations. Such phenomenon was also recognized lamellar-forming system.[11] For films that are thicker or thinner than the lamella period, lamellae oriented parallel or perpendicular to the substrate surface, respectively. In the case of thinner films, the formation of a surface-parallel lamellar phase will bring about entropic penalty because the polymer chains are subjected to compression effect.

1.3 Alignment control of nanostructures

The periodic nanoscale structures in block copolymer thin film have no preferred orientation and form a disordered fingerprint structure. Thus, macroscopic alignment control of nanostructures is essential for applications to high-density memory devices, nanoelectronics and optics, etc. The several methods for alignment control have been studied.[12] For example, topographically or chemically patterned substrates lead to macroscopic and patterned alignment of nanostructures. Also, application of external fields such as electric or magnetic field results in control of aligned nanodomains. Details on such methods are described as follows.

1.3.1 On topographically patterned substrates

The topographically patterned substrates obtained by top-down lithographic approach allow nanostructures to align self-assembly over long range. Kramer and co-workers demonstrated a graphoepitaxial strategy for creating epitaxial single crystal films of block copolymers over large areas of a topographically patterned substrate.[13] Sibener and co-workers reported macroscopic alignment guiding the trough edges in

grating substrate of cylindrical domains in PS-*block*-poly(ethylene-*alt*-propylene) (Figure 1-4).[14] At shorter annealing time, at most two cylinders align along the trough edges, and others orient perpendicular to the edges, i.e., along the direction of mass flow during a annealing process.[15] The alignment of cylinders in confined volumes is induced by the preferential wetting layer of PS on the vertical sidewalls of the trough. After enough annealing, the cylinders perfectly align parallel to the edges of the trough. It is necessary for this method to combine top-down and bottom-up approach. Besides, width of trough in topographically patterned substrates determines the rows in the arrays for the sphere forming diblock copolymer.[16]

On the other hand, a combination of topographically patterned substrates with thickness dependence of nanostructure alignment permits the patterning of out-of-plane alignment of cylinders in cylinder-forming diblock copolymer film.[17] The parallel and normal orientations of cylinders are obtained in thicker and thinner regions on the modified substrate, respectively.

1.3.2 On chemically patterned substrates

Chemically patterned substrates with length scales coincident to the natural periodicity of the block copolymer are capable of control of the nanodomains orientation.[18,19] The chemical affinity of the nanodomains to the patterned substrates plays important roles.

Nealey's group studied the effects of varying both the period of the surface pattern and chemical affinity on the periodic pattern of lamella forming block copolymer. The two-step process was used to prepare well-defined nanopattered surfaces (Figure 1-5).[18] Chemically patterned substrates were prepared by extreme ultraviolet interferometric lithography (EUV-IL) on self-assembled monolayer (SAM) of phenylethyltrichlorosila-

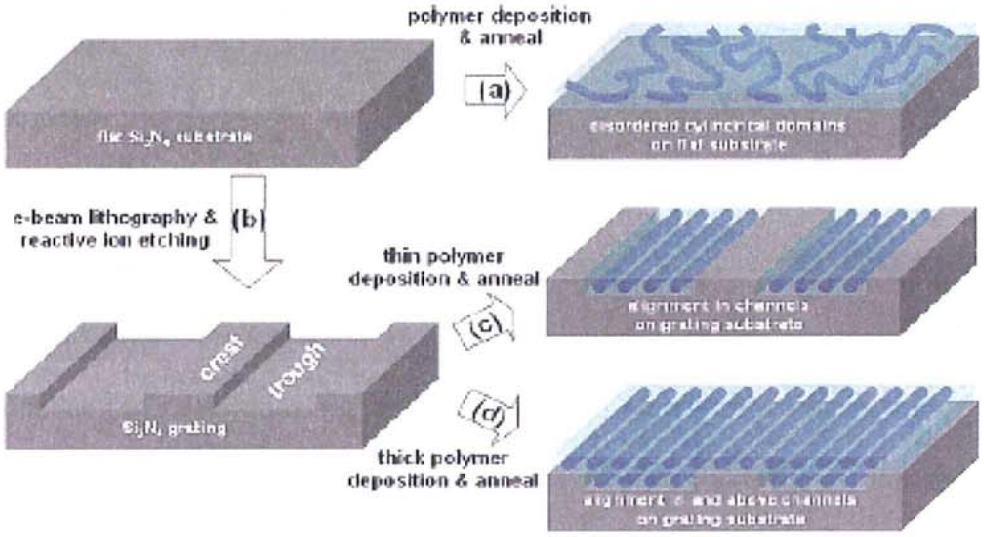

Figure 1-4 Schematic illustration of alignment control process of cylindical nanodomains by utilizing topographical patterned substrate. (taken from Ref. 14)

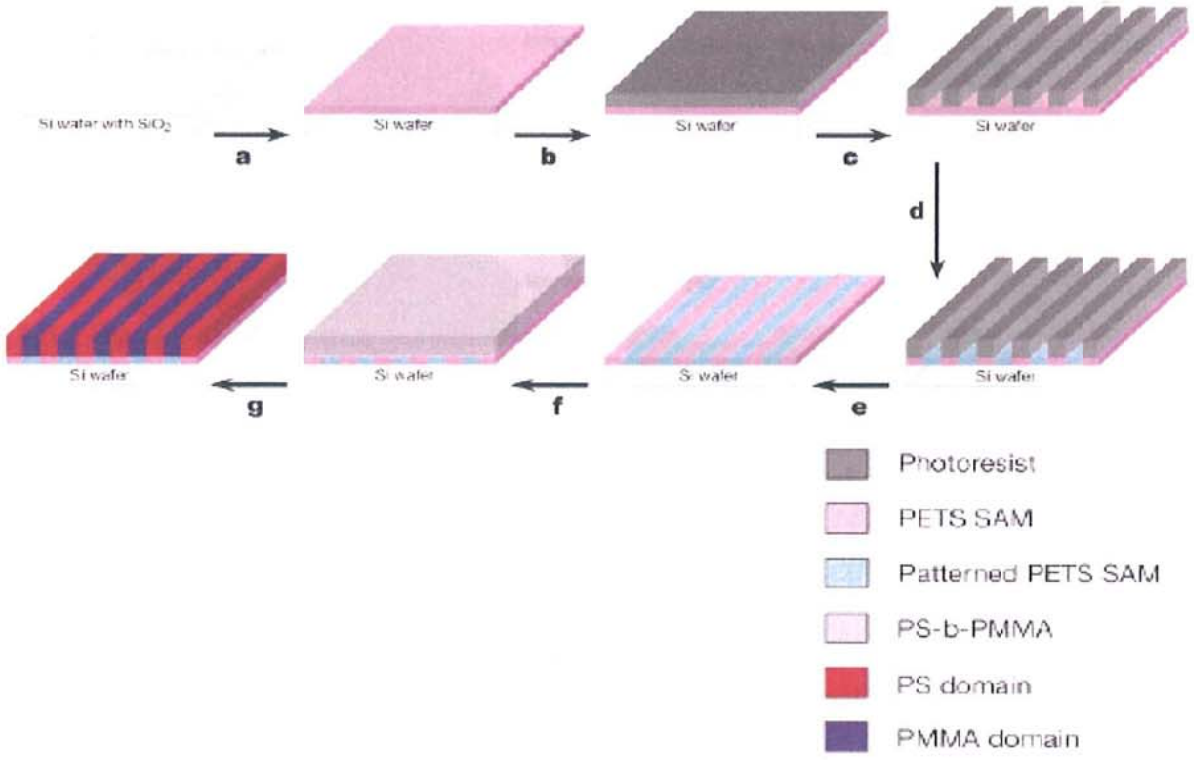

Figure 1-5 Schematic illustration of the strategy used to creat chemically patterned surfaces and investigate the epitaxial assembly of nanodomains. (taken from Ref. 18)

ne. Next, the film of the symmetric lamella forming PS-*block*-poly(methyl methacrylate) (PMMA) was obtained by spin-coating from toluene solutions on the chemically patterned surface and then was annealed. The PMMA block preferentially wet the regions where SAMs are decomposed by EUV-IL since those areas were chemically modified to contain polar groups. The other regions exhibited neutral wetting behavior by the PS block. Cylinder forming PS-*block*-PMMA thin films were also directed to assemble on chemically patterned surfaces consisting of alternating stripes that are preferentially wet by the two blocks of the copolymer as well as lamella systems.[20] The PMMA cylinders orient parallel to the film surface on the chemically modified regions for the above reason.

1.3.3 Applications of external fields

Electric fields

The electric fields allow nanodomains of block copolymers to align and switch the orientation. Since the differences in the dielectric constants of the blocks, the nanodomains prefer the parallel orientation in relation to the electric field vector. The both lamellar[21] and cylindrical nanostructures[22] in PS-*block*-PMMA melts, for example, are aligned in over large areas under an applied electric field. Figure 1-6 shows the experimental results reported by Russell's group.[22] Under an applied direct current (DC) electric field, the PS-*block*-PMMA films were then annealed above the glass temperature (T_g) for 24h and cooled to room temperature. The PMMA cylinders aligned parallel to the electric field lines after annealing (left area in (a) and (b)). When a film was annealed without an electric field present, in contrast, the cylinder orientation was random (c).

Applied alternating current (AC) electric fields make possible control of orientation

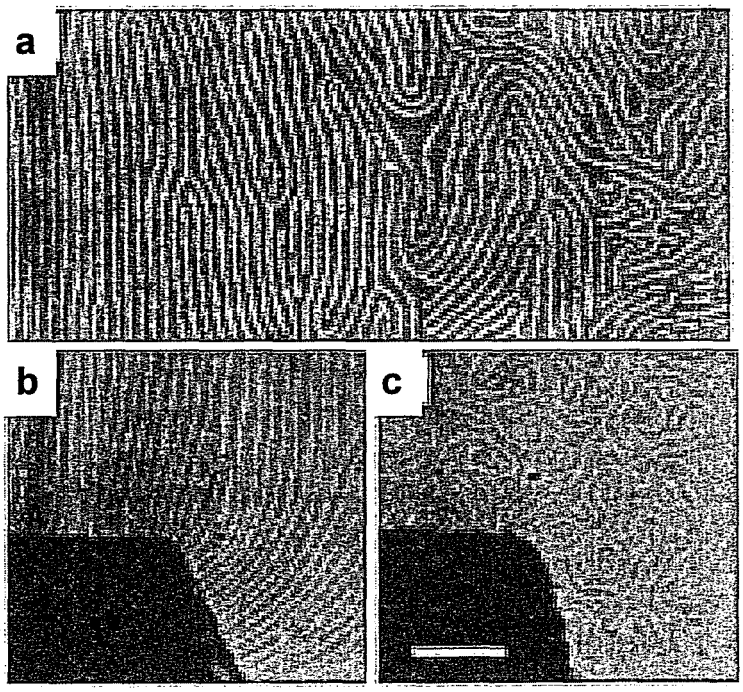

Figure 1-6 TEM micrographs of cylindrical nanodomains in the region between the electronodes in diblock copolymer films. (taken from Ref. 22)

of low-molecular-mass liquid crystals and side-chain LC polymers.[5] The orientation of LCs is determined by their dielectric anisotropy ($\Delta\varepsilon = \varepsilon_{//} - \varepsilon_{\infty}$) between the longitudinal permittivity ($\varepsilon_{//}$, the permittivity parallel to the molecular axis) and the lateral permittivity (ε_{∞}, the permittivity perpendicular to the molecular axis). When the $\Delta\varepsilon$ is positive or negative, mesogens align parallel or perpendicular to an AC field. Under an applied AC field at temperature below the order-disorder transition and above the T_g, alignment and orientational switching of mesogens and nanodomains are achieved in hydrogen-bonded side-chain LC block copolymers.

Magnetic fields

Alignment by the application of a magnetic field for LC mesogens is resulted from the collective anisotropy of the mesophase diamagnetic susceptibility, $\chi_a = \chi_{//} - \chi_{\perp}$, (where $\chi_{\perp}$ and $\chi_{//}$ denote the susceptibility perpendicular and parallel to the long axis direction of the LC mesogens, respectively). The positive anisotropy, $\chi_a > 0$, mesogens orient parallel to the direction of magnetic field. The negative anisotropy, $\chi_a < 0$, orthogonal orientation of mesogens is exhibited. For PS-*block*-poly(isoprene LC) diblock copolymer, under an applied magnetic field on appropriate temperature range, the both PS cylinders and mesogens aligned perpendicular to the direction of the applied field because of a homogeneous anchoring of the mesogens at the inter material deviding surface (IMDS).[23]

1.4 Applications as template for nanostructures

The morphological features such as stripes and dots can be utilized as the template of fine structures at several tens nanometer levels in block copolymer thin films. Stamm et. al. demonstrated the electroless deposition of metallic nanostructures by templating

the 2D stripe patterns (Figure 1-7).[24] Palladium metal ions coordinated selectively with 4-vinylpyridine (P4VP) blocks followed by reduction of palladium nanopartticles metal onto it blocks in PS-*block*-P4VP thin film.

Porous templates in which only one domain is selectively etched by deep UV and vacuum UV exposure, are useful for the formation of nanowire arrays and metallic nanoparticles. In the cylinder-forming diblock copolymer thin film, nanowires can be grown within the porous template obtained by removal of cylindrical domains.[25] The lamellar-forming diblock copolymer allows a process where the metallic nanoparticles are deposit within the photogenerated trough in thin films.[26]

1.5 Alignment control of Az chromophores

Azobenzene (Az) chromophores have been investigated for potential applications such as command surfaces to align LC, reversible data storage and diffractive optical elements, etc.[1,27-34] Under irradiation with UV and visible light, the Az chromophores are reversibly isomerized through *trans-cis-trans* cycles (Figure 1-8a). The *cis* isomer is also subjected the thermal backward isomerization to the *trans* isomer.

In Az polymer films, the in-plane orientation is controlled by LPL irradiation.[27] The optical transition moment of Az chromophore approximately coincide to long axis of this molecule. When the polarization direction of LPL is parallel to transition moments of Az chromophores, they effectively absorbs LPL, followed by *trans-cis* isomerization. When the directions of the polarization moment of LPL and the transition moment of Az chromophores are orthogonal to each other, Az chromophores hardly absorb the LPL, resulting in the inactive state. After many *trans-cis-trans* cycles, transition moments of most Az chromophores, i.e. the long axis of Az, are orthogonally oriented to the polari-

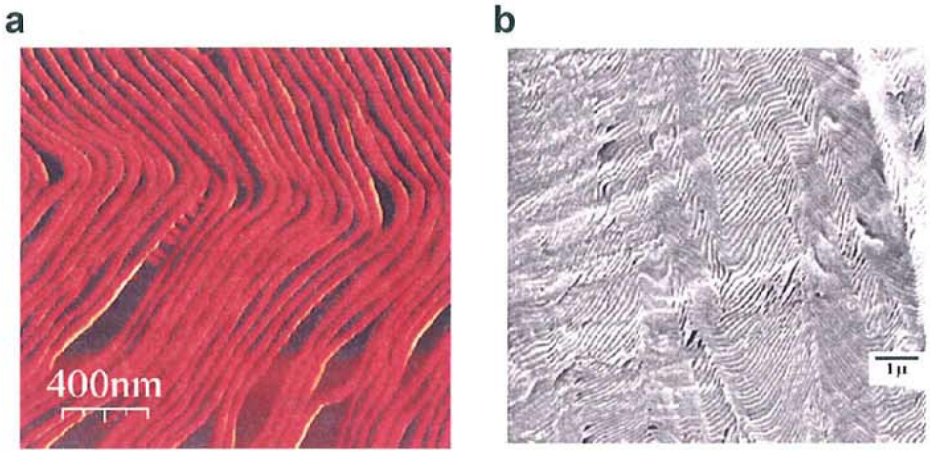

Figure 1-7 (**a**) AFM phase image of stripe morphological feature of a block copolymer film. (**b**) SEM micrograph showing selective deposition of Pd nanoparticles onto the stripe morphological feature after the metallization process. (taken from Ref. 24)

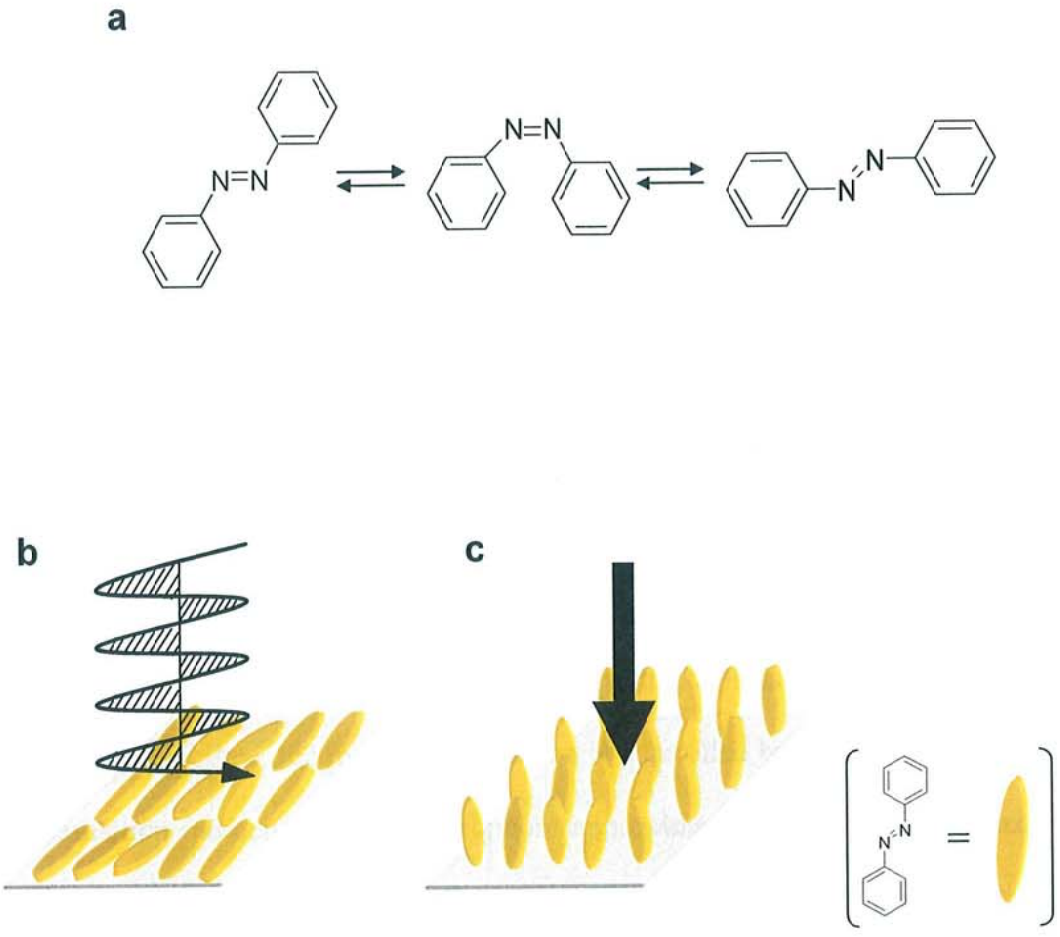

Figure 1-8 (a) Schematic illustration of photoisomerization of azobenzene. (b) In-plane alignment of Az by LPL irradiation. (c) Out-of-plane alignment of Az by non-LPL irradiation from the normal direction to the film surface.

zation direction of LPL (b). For the same reason, when non-polarized light expose from the normal direction to the film plane, the Az chromophores exhibit the out-of-plane perpendicular orientation, leading to the inactive state (c).

1.6 Photo-triggered mass migration on Az polymer films

Az polymers have been investigated as superior materials for holographic information storage. When thin films of Az polymers with various types of polymers including amorphous and liquid crystalline ones are exposed to interference LPL, mass transfer from irradiated regions to non-irradiated regions occurs, resulting in formation of surface relief structures with interference periodicity (Figure 1-9).[35-43] In block copolymer systems, however, the efficiency of the relief formation is very low compared with random copolymers or an Az-homopolymers due to the influence of microphase separation.[41,42] Therefore, attempts to develop surface relief formation system in block copolymer systems is subject of fascinating challenge. In this respect, our group showed that hybridization with a low-molecular-mass LC material drastically enhances the efficiency relief formation.[43] The timescale required for the relief formation is seconds to minutes. When suitable conditions are provided, the height from the top to valley becomes comparable to that of the initial film thickness. To explain the driving force for mass migration, a lot of efforts have been made. Some models such as pressure gradients based on the change of the free volume required in photoisomerization of chromophores, electric field gradients of LPL at the mass migration direction, phase transition from isotropic to LC phase in Az-containing LC polymer films are proposed. The significance of these processes is that the topographical relief patterns are formed in all-optical and single-step manners without

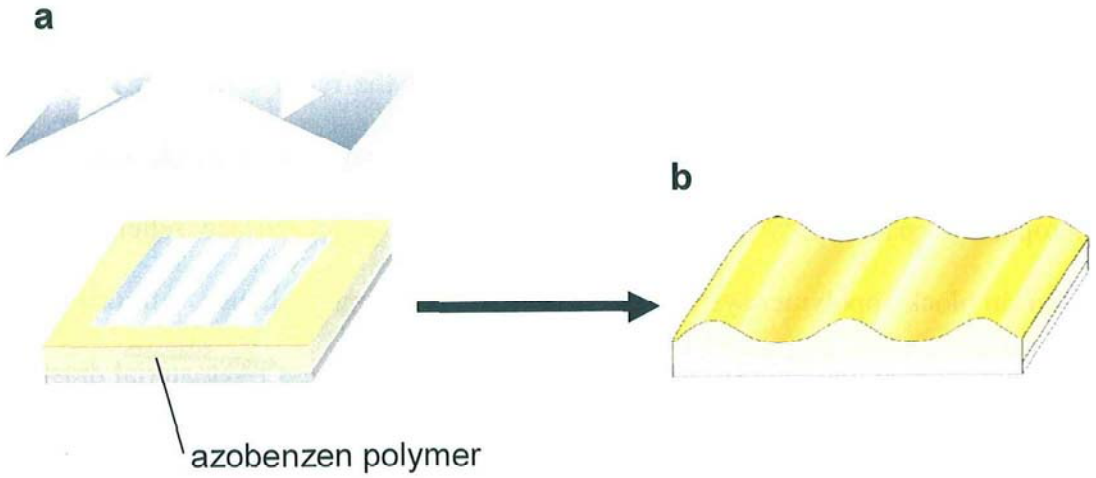

Figure 1-9 Schematic illustration of photo-triggered mass migration. (**a**) Interference exposure with LPL. (**b**) resulting surface relief structure.

development procedures.

1.7 Purpose of this work

The main target of this work is to achieve 3D photoalignment controls and patterning of nanostructures of Az-containing liquid crystalline diblock copolymer by applying photo-triggered processes. For attainment of this target, two kinds of diblock copolymers, poly(ethylene oxide)-*block*-poly(methacrylate) containing Az mesogenic group and polystyrene-*block*-poly(methacrylate) containing Az mesogenic group, are employed. The soft block component of poly(ethylene oxide) exhibiting low glass transition temperature (T_g) may enable a photoalignment of nanostructures based on high plasticity. The rigid PS-based block copolymer may be used to develop functional materials such as nanoporous templates through photodecomposition of one component.[25,26] For photoalignment control of hierarchical nanostructures, photoinduced orientational behavior of Az chromophores is of especially important. The surface relief formation via photo-triggered mass migration, therefore, has been utilized for patterning of the hierarchical structures alignment. It is expected that the combination of bottom-up approach as self-assemble nanostructure formation and top-down approach as pattern irradiation for surface relief formation will lead to development of novel methods for alignment control of hierarchical structures. The present thesis consists of the following chapters.

In chapter 2, the factors affecting the orientation of cylindrical nanodomains are described in thin films of cylinder-forming PEO-based diblock copolymers.

In chapter 3, the relief structure formation via photo-triggered mass migration in Az-containing PEO-based diblock copolymer films is demonstrated.

In chapter 4, on-demand 3D orientation control and patterning of nanocylinders are studied in thin films modulated by photo-triggered mass migration using PEO-based diblock copolymers.

In chapter 5, 3D photoalignment and reorientation of nanocylinders are described in thin films of polystyrene-based diblock copolymer.

In chapter 6, photoalignment is achieved for lamella-forming polystyrene-based block copolymers, and the memory effect to the orientation of the Az mesogenic groups within photoaligned lamellar structures is found.

Finally the overall summary of this work and outlook for the future are provided in chapter 7.

References

1. *Developments in Block Copolymer Science and Technology*; Hamley, I. W., Ed.; John Wiley & Sons, Ltd: West Sussex, 2004.
2. C. Park, J. Yoon, E. L. Thomas, *Polymer* **2003**, *44,* 6725.
3. K. Ichimura, *Chem. Rev.* **2000**, *100*, 1847.
4. G. Mao, J. Wang, S. R. Clingman, C. K. Ober, J. T. Chen, E. L. Thomas, *Macromolecules* **1997**, *30*, 2556.
5. C. Y. Chao, X. Li, C. K. Ober, C. Osuji and E. L. Thomas, *Adv. Funct. Mater.*, **2004**, *14*, 364.
6. M. Anthamatten, W. Y. Zheng, P. T. Hammond, *Macromolecules* **1999**, *32*, 4838.
7. (a) A. Knoll, A. Horvat, K. S. Lyakhova, G. Krausch, G. J. A. Sevink, A. V. Zvelindovsky, R. Magerle, *Phys. Rev. Lett.* **2002**, *89,* 035501. (b) A. Knoll, R. Magerle, G. Krausch, *J. Chem. Phys.*, **2004**, *120*, 1105. (c) S. Ludwigs, K. Schmidt, C. M. Stafford, E. J. Amis, M. J. Fasolka, A. Karim, R. Magerle, G. Krausch, *Macromolecules* **2005**, *38*, 1850.
8. S. Ludwigs, G. Krausch, R. Magerle, A. V. Zvelindovsky, G. J. A. Sevink, *Macromolecules* **2005**, *38*, 1859.
9. M. A. van Dijk, R. van den Berg, *Macromolecules* **1995**, *28*, 6773.
10. M. Konrad, A. Knoll, G. Krausch, R. Magerle, *Macromolecules* **2000**, *33*, 5518.
11. M. J. Fasolka, P. Banerjee, A. M. Mayes, G. Pickett, A. C. Balazs, *Macromolecules* **2000**, *33*, 5702.
12. J. Y. Cheng, C. A. Ross, H. I. Smith, E. L. Thomas, *Adv. Mater.*, **2006**, *18*, 2505.
13. R. A. Segalman, H. Yokoyama, E. J. Kramer, *Adv. Mater.* **2001**, *13*, 1152.
14. D. Sundrani, S. B. Darling, S. J. Sibener, *Nano. Lett.*, **2004**, *4*, 273.

15. D. Sundrani, S. J. Sibener, *Macromolecules* **2002**, *35*, 8531.

16. J. Y. Cheng, A. M. Mayes, C. A. Ross, *Nat. Mater.*, **2004**, *3*, 823.

17. C. Park, J. Y. Cheng, M. J. Fasolka, A. M. Mayes, C. A. Ross, E. L. Thomas, C. de Rosa, *Appl. Phys. Lett.*, **2001**, *79*, 848.

18. (a) S. O. Kim, H. H. Solak, M. P. Stoykovich, N. J. Ferrier, J. J. de Pablo, P. F. Nealey, *Nature* **2003**, *424*, 411. (b) E. W. Edwards, M. F. Montague, H. H. Solak, C. J. Hawker, P. F. Nealey, *Adv. Mater.*, **2004**, *16*, 1315.

19. M. P. Stoykovich, M. Müller, S. O. Kim, H. H. Solak, E. W. Edwards, J. J. de Pablo, P. F. Nealey, *Science* **2005**, *308*, 1442.

20. E. W. Edwards, M. P. Stoykovich, H. H. Solak, P. F. Nealey, *Macromolecules* **2006**, *39*, 3598.

21. J. Y. Wang, J. M. L. Belanger, J. D. Sievert, T. P. Russell, *Macromolecules* **2006**, *39*, 8487.

22. T. L. Morkved, M. Lu, A. M. Urbas, E. E. Ehrichs, H. M. Jaeger, P. Mansky, T. P. Russell, *Science* **1996**, *273*, 931.

23. C. Osuji, P. J. Ferreira, G. Mao, C. K. Ober, J. B. V. Sande, E. L. Thomas, *Macromolecules* **2004**, *37*, 9903.

24. A. W. Fahmi, M. Stamm, *Langmuir* **2005**, *21*, 1062.

25. T. T. Albrecht, J. Schotter, G. A. Kästle, N. Emley, T. Shibauchi, L. K. Elbaum, K. Guarini, C. T. Black, M. T. Tuominen, T. P. Russell, *Science* **2000**, *290*, 2126.

26. S. B. Darling, N. A. Yufa, A. L. Cisse, S. D. Bader, S. J. Sibener, *Adv. Mater.*, **2005**, *17*, 2446.

27. M. Han, S. Morino, K. Ichimura, *Macromolecules*, **2000**, *33*, 6360.

28. J. G. Meier, R. Ruhmann, J. Stumpe, *Macromolecules*, **2000**, *33*, 843.

29. T. Ikeda, *J. Mater. Chem.*, **2003**, *13*, 2037.

30. R. Rosenhauer, T. Fischer, J. Stumpe, R. Giménez, M. Piñol, J. L. Serrano, A. Viñuales, D. Broer, *Macromolecules* **2005**, *38*, 2213.

31. P. H. Rasmussen, P. S. Ramanujam, S. Hvilsted, R. H. Berg, *J. Am. Chem. Soc.*, **1999**, *121*, 4738.

32. K. Fukuda, T. Seki, K. Ichimura, *Macromolecules* **2002**, *35*, 1951.

33. L. Cui, Y. Zhao, A. Yavrian, T. Galstain, *Macromolecules* **2003**, *36*, 8246.

34. X. Tong, L. Cui, Y. Zhao, *Macromolecules* **2004**, *37*, 3101.

35. A. Natansohn, P. Rochon, *Chem. Rev.* **2002**, *102*, 4139.

36. (a) N. K. Viswanathan, D. Y. Kim, S. Bian, J. Williams, W. Liu, L. Li, L. Samuelson, J. Kumar and S. K. Tripathy, *J. Mater. Chem.* **1999**, *9*, 1941. (b) N. K. Viswanathan, S. Balasubramanian, L. Li, S. K. Tripathy, J. Kumar, *Jpn, J. Appl, Phys.*, **1999**, *38*, 5928.

37. (a) K. G. Yager, C. J. Barrett, *Curr. Opin. Solid State Mater. Sci.* **2001**, *5*, 487. (b) C. J. Barrett, A. L. Natansohn, P. L. Rochon, *J. Phys. Chem.*, **1996**, *100*, 8836.

38. R. H. Berg, S. Hvilsted, P. S. Ramanujam, *Nature* **1996**, *383*, 505.

39. A. Stracke, J. H. Wendorff, D. Goldman, D. Janietz, B. Stiller, *Adv. Mater.* **2000**, *12*, 282.

40. N. Zettsu, T. Ubukata, T. Seki, K. Ichimura, *Adv. Mater.* **2001**, *13*, 1693.

41. C. Frenz, A. Fuchs, H –W. Schmidt, U. Theissen, D. Haarer, *Macromol. Chem. Phys.* **2004**, *205*, 1246.

42. H. Yu, K. Okano, A. Shishido, T. Ikeda, K. Kamata, M. Komura, T. Iyoda, *Adv. Mater.* **2005**, *17*, 2184.

43. T, Ubukata, T. Seki, K. Ichimura, *Adv. Mater.* **2000**, *12*, 1675.

Chapter 2

Factors Affecting the Nanocylinder Orientation in Block Copolymer Thin Film

2.1 Introduction

Block copolymers form microphase separated nanostructures of typically lamellar, cylinder or sphere patterns through self-assembly.[1] Recently studies using thin films with varied thickness reveal that the forming nanostructures differ from those in the bulk state due to constrained geometry and surface energy of a planar substrate surface.[2-4] In cylinder forming systems, subtle changes in film thickness in the ultra thin regions typically below 100 nm lead to multifarious phases accompanying distinct alternations in the cylinder orientation.[5-7] On the other hand, Stamm et al. have reported that the polymer chains possessed LC mesogens in both main and side chains exhibit different orientations depending on the film thickness.[8] It is thus expected that the out-of-plane orientation of cylinder may be modulated according to the thickness dependent orientation of Az mesogens.

The orientation of nanostructures also depends on the chemical nature of substrate surfaces. In thin block copolymer film formed lamellar structure, the orientation of lamellar is known to orient normal and parallel to the substrate plane on the region of hydrophilic and hydrophobic surface, respectively.[9,10] Thus the renewed behavior of cylinder orientation is expected on the substrates with different chemical nature.

On the other hand, the in-plane alignment of photoisomerizable molecules in a liquid crystalline polymer film is controlled by linearly polarized light (LPL) irradiation. The long axis of azobenzene orients perpendicular to the electric field vector of the

polarized light.[11]

This chapter focuses onto the factors affecting the nanocylinder alignment in $p(EO_x\text{-}Az_x)$ thin films. The parameters such as film thickness, chemical nature of the substrate surface, and the direction of LPL are described. The nanocylinders and LC mesogens alignment are evaluated by AFM images and UV-visible absorption spectra, respectively.

2.2 Experiments

2.2.1 Materials

The diblock copolymers, $p(EO_x\text{-}Az_y)$, possessing the different unit numbers of PEO and poly(methacrylate) containing an Az mesogenic group were used in this chapter (Figure 2-1). Syntheses and characterizations of $p(EO_x\text{-}Az_y)$ were carried out according to same manner as described in the previous paper.[12] Table 2-1 shows the thermal phase properties and the results of polymerization of the polymers under investigation. It has been known that these polymers form hexagonally packed PEO cylinders aligned parallel to the long axis of Az mesogen in thin films.[12] Hexamethyldisilane (HMDS) and octadecyltriethoxysilane (OTS) as the silane coupling agents and other compounds were used without further purification.

2.2.2 Preparation of substrates of different chemical nature

Hydrophilic substrates were obtained by washing with a saturated potassium hydroxide ethanol solution, and pure water under ultrasonication. The typical value of the contact angle was ca. 5^{o}.

Hydrophobic substrates terminated silane coupling agent were prepared as follows

Solution deposition: The cleaned substrates were immersed in a 1 wt% solution of

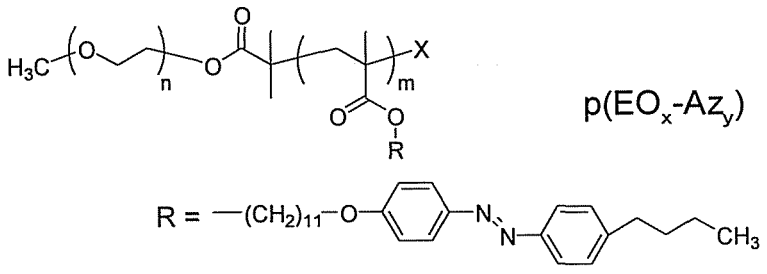

Figure 2-1 Chemical structure of p(EO$_x$-Az$_y$).

Table 2-1. Thermal transition properties and notation of the studied Az containing diblock copolymer (p(EO$_x$-Az$_y$)).

polymer	M_n[a]	M_w/M_n[b]	phase transition[c] (°C)	LC (wt%)
p(EO$_{114}$-Az$_{67}$)	38000	1.10	G 37 Sm$_X$ 67 Sm$_C$ 96 Sm$_A$ 119 I	87
p(EO$_{44}$-Az$_{40}$)	23600	1.11	G 40 Sm$_X$ 68 Sm$_C$ 95 Sm$_A$ 117 I	92

[a] M_n, number average molecular weight estimated by ^{1}H-NMR. [b] M_w/M_n, Polydispersity determined by GPC.

OTS for 40 h with 1 wt% concentrated HCl and subsequently rinsed for 20 min after dilution by 5 % with cyclohexane. After the substrates were removed from the solution, they were subjected to baking at 110 °C for 1 h and rinsed with cyclohexane under ultrasonication.[13]

Vapor phase deposition: The cleaned substrates were exposed to vapor of HMDS at room temperature for 2 days.

Typical values of the contact angle on the OTS and HMDS-terminated substrate surfaces were ca. 95 ° and 85 °, respectively.

2.2.3 Modification and patterning of chemical nature of OTS film surface

The surface modification of OTS films was achieved by exposure to UV light and O_3 gas in whole area of those in Filgen UV-O_3 cleaner. In a separate experiment, UV light and O_3 gas irradiation was achieved in a half area of OTS film with a mask on the OTS-covered substrate.

2.2.4 Preparation of p(EO_x-Az_y) thin films

p(EO_x-Az_y) thin films having different film thickness were prepared on a quartz substrate by spin-coating from chloroform solutions of various polymer concentrations. They were annealed at 110 °C for 2 h where the polymer adopts the Sm_A liquid crystalline phase. The annealed films were then exposed to saturated hexane vapor at 20 °C for 20 h.

2.2.5 Measurement of nanostructures orientation

The contact angles of pure water on various substrates were measured with Kyowa Interface FACE Contact Angle Meter (CA-X). The surface morphologies and film thickness of the films were evaluated by AFM using a Seiko Instrument SPA400/SPI3800N system in the dynamic force mode. UV-visible absorption spectra

were recorded on a Hewlett Packard 8452A diode array spectrometer. Lineally polarized visible light (LPL, 436 nm) irradiation was performed with a San-ei Supercure-202S. Polarized UV-visible absorption spectra were recorded on a Hewlett Packard 8452A diode array spectrometer equipped with a polarizer unit.

2.3 Results and Discussion

2.3.1 Orientation of nanocylinders and Az chromophores on Hydrophilic substrates

AFM observation

Figures 2-2a and 2d show the surface morphologies (1.0 x 1.0 μm) of $p(EO_{114}\text{-}Az_{67})$ thin films with film thickness of 20 nm (a), 60 nm (b) and 70 nm (c), after a post-treatment of annealing at 110 °C for 2 h and subsequent exposure to a hexane vapor for 20 h, evaluated by the phase mode AFM measurements. In the thinnest class of films (< 20 nm), featureless morphologies were seen, indicative of insufficient evolution of microphase separation (a). These indicate that the cylinder formation requires at least a film thickness of one period of cylindrical naodomains (the nearest-neighbor distance of the cylinder array was ca. 23 – 28 nm). In the thinner class of films (30 – 60 nm), line morphologies showing the laid (parallel to the substrate surface) cylinder orientation were observed (b). When the films became thicker than 70 nm, hexagonally arranged dot structures appeared, indicating that cylinders adopt normal orientation with respect to the substrate surface (c). The average nearest-neighbor distance between the dots observed at $p(EO_{114}\text{-}Az_{67})$ thicker film was ca. 23 nm.

Figures 2-3a and 3d display the AFM images (phase mode, 0.5 x 0.5 μm) of

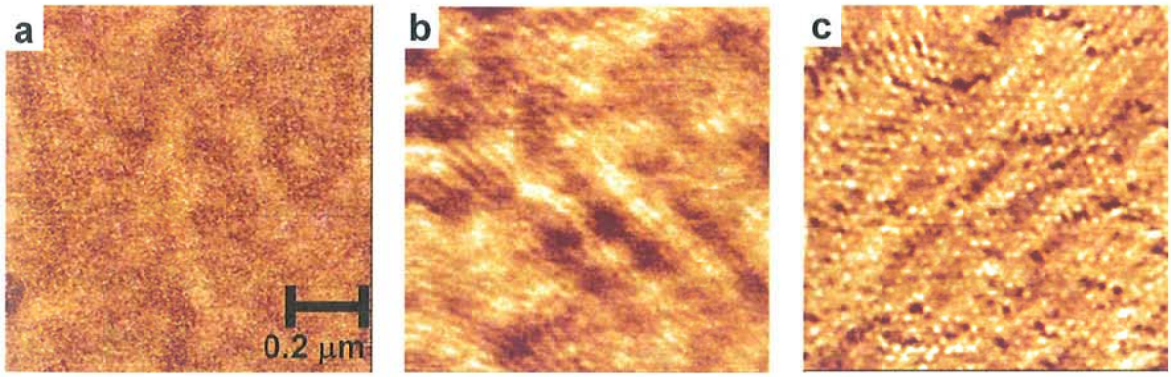

Figure 2-2. Phase-mode AFM images (1 μm x 1 μm) of the p(EO_{114}-Az_{67}) films with different film thickness: 20 nm (**a**), 60 nm (**b**) and 70 nm (**c**) after annealing.

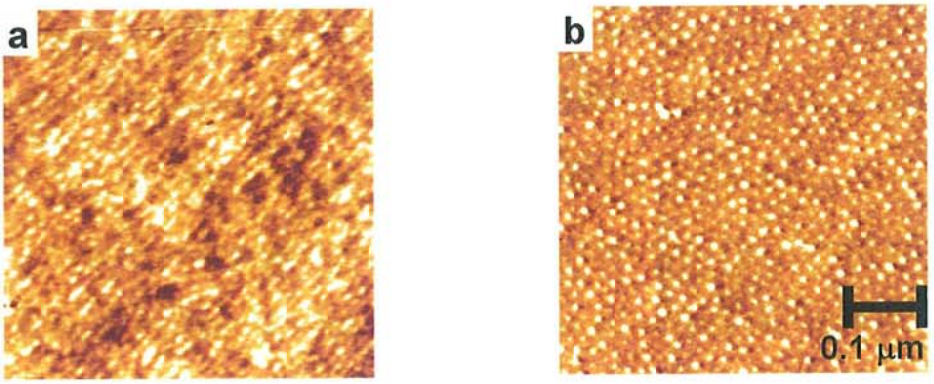

Figure 2-3. Phase-mode AFM images (0.5 μm x 0.5 μm) of the p(EO_{40}-Az_{44}) films with different film thickness: 60 nm (**a**) and 70 nm (**b**) after annealing.

$p(EO_{40}\text{-}Az_{44})$ thin films with film thickness of 60 nm (a) and 70 nm (b) after a post-treatment. The orientation direction of cylinders showed the same tendency as observed for $p(EO_{114}\text{-}Az_{67})$. The cylinder orientation changed drastically between 60 nm and 70 nm thickness, exhibiting strongly thickness dependence. The average nearest-neighbor distance between the dots observed at $p(EO_{40}\text{-}Az_{44})$ thicker film was ca. 16 nm in this case.

UV-visible absorption spectra measurements

Figures 2-4a and 4b show UV-visible absorption spectra of the corresponding $p(EO_{114}\text{-}Az_{67})$ films. The thinner films indicated essentially no change in the spectral shape before and after the annealing treatment (a). In contrast, the film having 70 nm thickness indicated large changes in the spectral shape before and after the annealing treatment (b). Absorbance of the π–π^* long axis transition band at 338 nm of the Az unit decreased significantly, indicating that the Az chromophores get oriented perpendicular to the substrate plane by the post-treatment. Furthermore, this film exhibited a blue shift due to H-aggregation. In the above manners, the orientation of Az chromophores after the post-treatment well coincided with that of the PEO cylinders, i.e., the long axis of Az and PEO cylinders are parallel with each other.

UV-visible absorption spectra of the corresponding $p(EO_{40}\text{-}Az_{44})$ films were displayed in Figures 2-5a and 5b. Those films had strong tendency to provide same spectral changes as mentioned above (Figures 2-4a and 4b). The Az chromophores oriented parallel or perpendicular to the substrate surface in the films having below 60 nm or above 70 nm thickness. The spectral data indicate that the cylinder alignment observed at the topmost surface by AFM is retained to the bottom of the film.

Following two aspects should be pointed out regarding the thickness dependence of

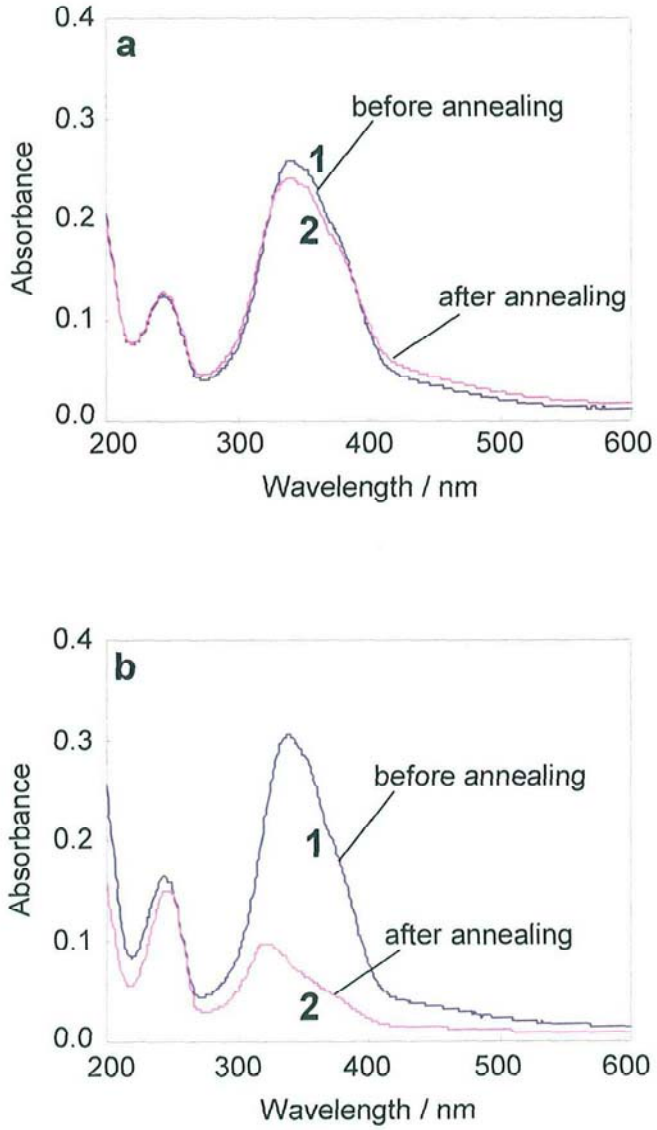

Figure 2-4. UV-visible absorption spectra of the corresponding p(EO_{114}-Az_{67}) films are shown: 60 nm (**a**) and 70nm thickness (**b**) for as-cast (**1**) and after annealing (**2**).

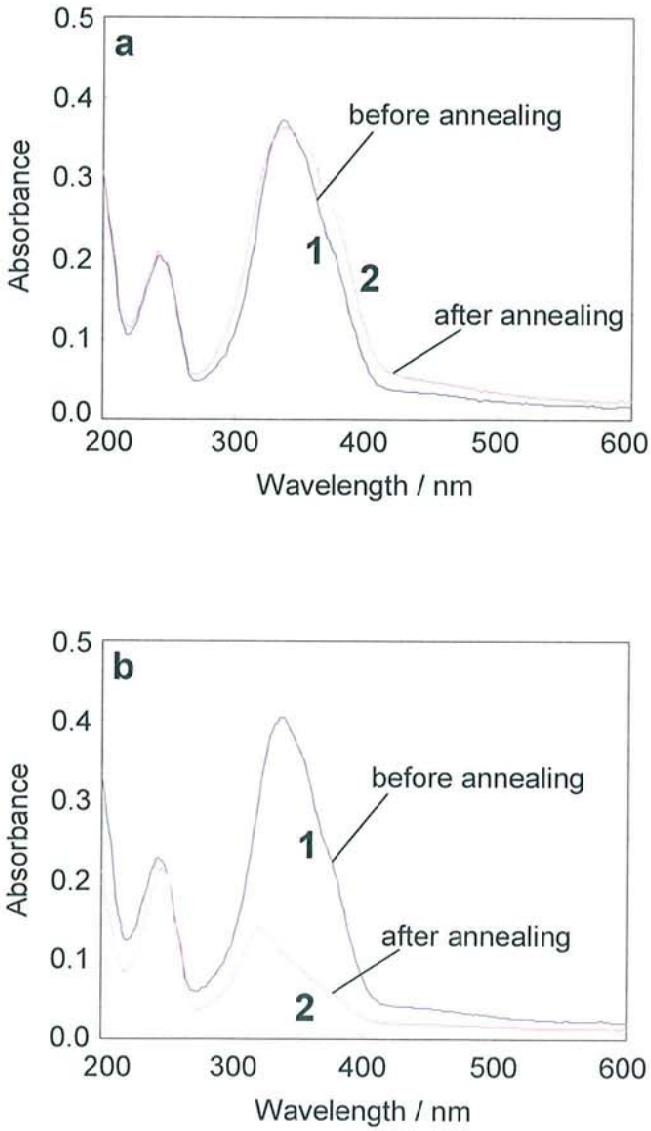

Figure 2-5. UV-visible absorption spectra of the corresponding $p(EO_{40}$-$Az_{44})$ films are shown: 60 nm (**a**) and 70nm thickness (**b**) for as-cast (**1**) and after annealing (**2**).

the nanocylinder orientation. First, the critical thickness that induces the change of cylinder orientation is constant independent of the degree of polymerization. This should suggest that the confinement by the surface plane should affect critically for the cylinder orientation. Second, the criterion thickness thus seems to be determined by the orientation of the Az mesogens. Stamm et al. indicated by X-ray analysis that a liquid crystalline polymer film exhibiting a smectic phase alters the orientation of mesogens around a thickness range of several ten nanometers, the orientation being normal and parallel to the substrate plane for the thicker and thinner films, respectively.[8] For the present block copolymer system, the same effect should be hold, which will be then govern the orientation of PEO cylinders. As a result, hierarchical orientation induction from Az mesogens to PEO cylinders should be obtained in diblock copolymer thin films.

2.3.2 Effects of humidity on the nanocylinder orientation

The film thickness undergoing the change of out-of-plane orientation was constant for both copolymer, p(EO_{114}-Az_{67}) and p(EO_{40}-Az_{44}) films bearing the different size feature of the microphase separated structure. As discussed in the previous section, this critical thickness is not dependent on the structure of polymers but the substrate nature is more influential. In thinner films, the orientation of Az mesogens and cylinders should be more sensitive to the surface characteristics (Figure 2-6). Because the cylinders tend to form from the surface to inner part of the films,[14] the orientation in the thicker films would be more strongly influenced by the interface of air side rather than the substrate side. This situation seems to lead to normal orientation of the cylinders. In this context, the morphological features of a thicker p(EO_{114}-Az_{67}) film annealed under a humidified atmosphere were examined. The annealing processes of the p(EO_{114}-Az_{67})

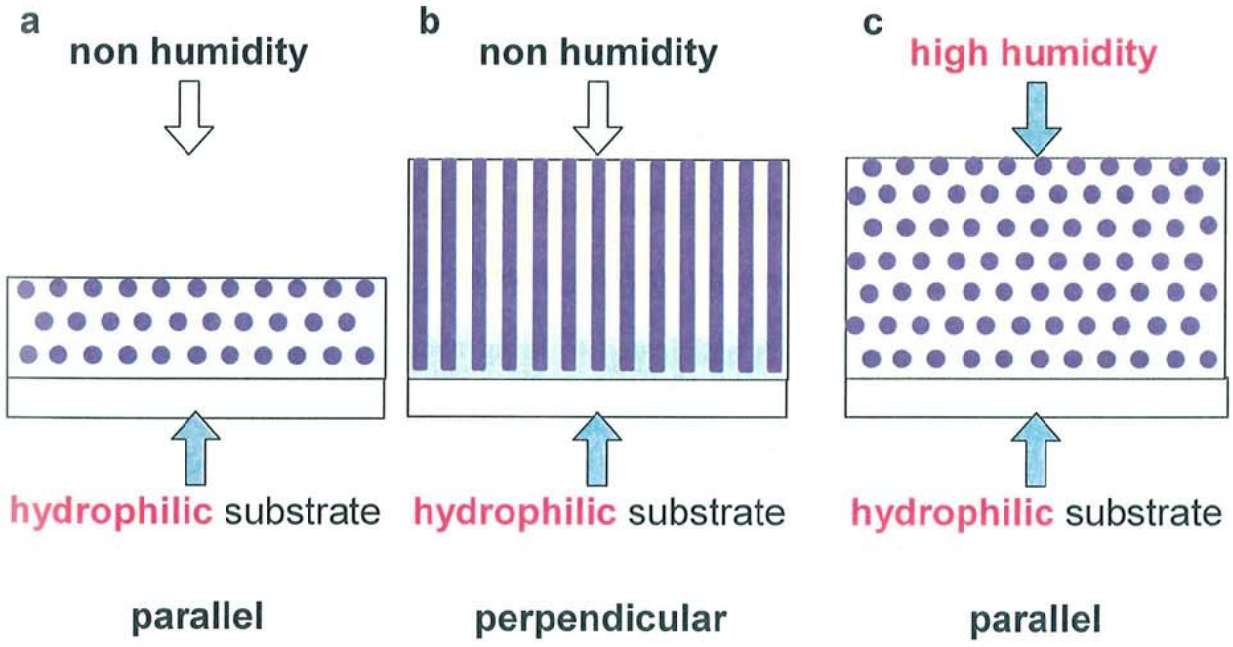

Figure 2-6. Schematic illustration of the relation between the direction of cylinder orientation and the annealing condition in the p(EO_{114}-Az_{67}) films with different thickness. (**a**) the cylinder orientation in thinner film after annealing under normal atmosphere. **b** and **c** the cylinder orientation in thicker film after annealing under normal or humidified atmosphere.

films under the different atmosphere, were followed with AFM images and UV-visible absorption spectra, and are shown Figures 2-7(a–f). Figure 2-7a is a schematic illustration of the annealing at an ambient atmosphere. As shown Figures 2-7b and 7c, the Az mesogens and cylinders both oriented perpendicular to the substrate plane in the film with 100 nm thickness after annealing at 110 °C for 2 h. Figure 2-7d displays a schematic illustration of the same procedure under humidified atmosphere. The cylinders in this case oriented parallel to the substrate plane even in the films having the same thickness (Figure 2-7e and 7f). Therefore, the annealing under humidified atmosphere crucially alters the cylinder orientation. The air side at the high atmosphere seems to act as if a hydrophilic substrate. (Figure 2-6).

2.3.3 Reorientation of cylinder under humidified atmosphere

The PEO and Az containing PMMA exhibit T_m's at ca. 65 °C and 120 °C, respectively. For the perpendicularly oriented structures, the annealing at above T_m under humidified atmosphere is anticipated to bring about disordered structures and then allow reorientation in the in-plane direction of the cylinders (Figure 2-8a). Figure 2-8b shows the morphological feature indicated normal oriented cylinders after annealing at 110 °C for 2 h and exposure to a hexane vapor for 20 h. This film was then subjected to annealing at 130 for 2 h under humidified atmosphere. Figure 2-8c shows the AFM image taken in the resulting film. In this feature, line morphologies showing the laid (parallel to the substrate surface) cylinder orientation were observed. Figure 2-8d displayed UV-visible absorption spectra measured at each process. These spectra indicate that the orientation of the Az mesogens coincide with that of PEO cylinders. Therefore, the reorientation of nanostructures was attained.

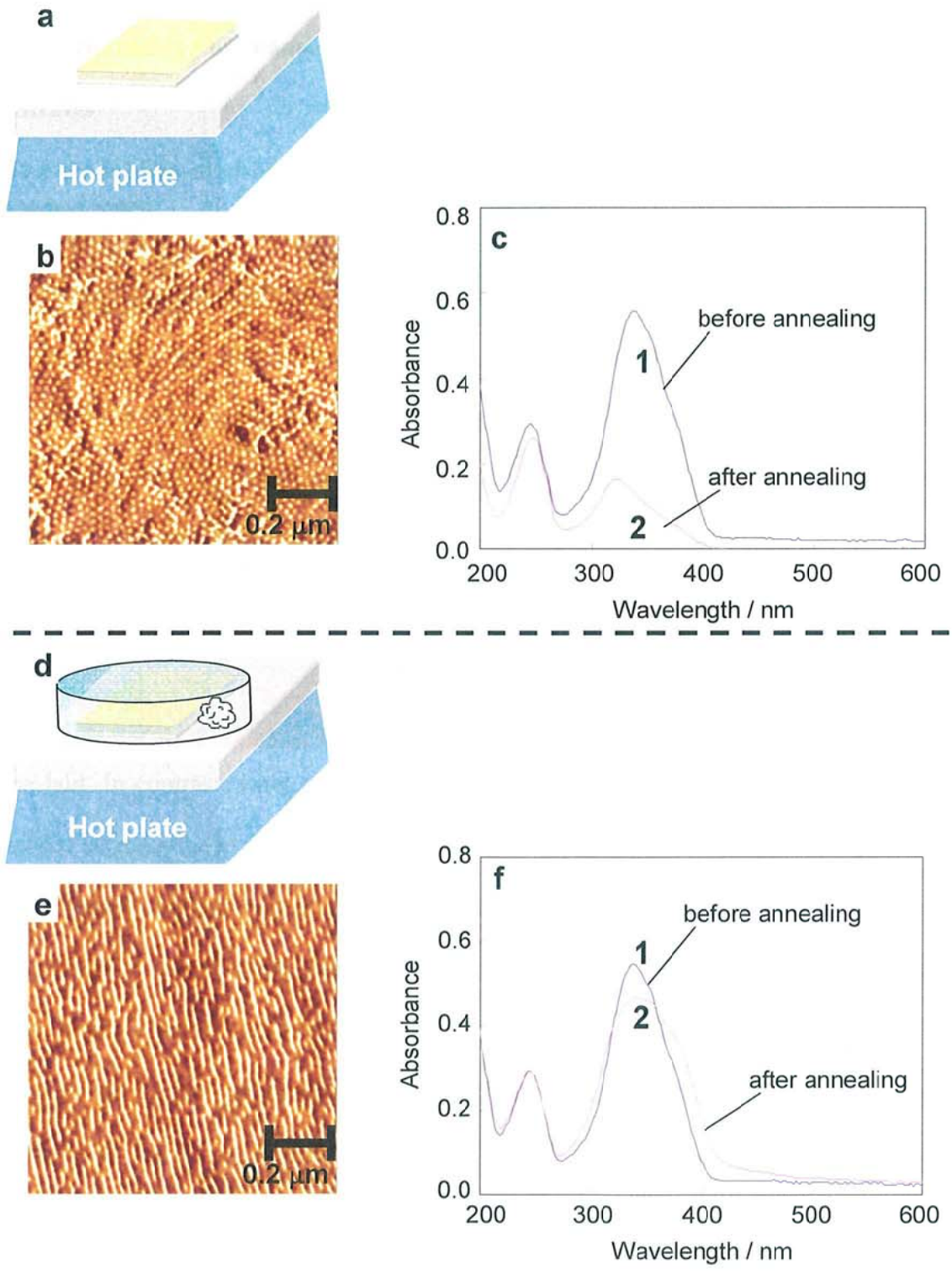

Figure 2-7. The orientation of Az mesogens and PEO cylinders of the p(EO_{114}-Az_{67}) films after annealing under normal atmosphere (**a-c**) and humidified atmosphere (**d-f**). **a** and **d**, Schematic illustration of the annealing processes. **b** and **e**, Phase-mode AFM images (1 μm x 1 μm) after annealing on different condition. **c** and **f**, UV-visible absorption spectra of the corresponding p(EO_{40}-Az_{44}) films for as-cast (**1**) and after annealing (**2**).

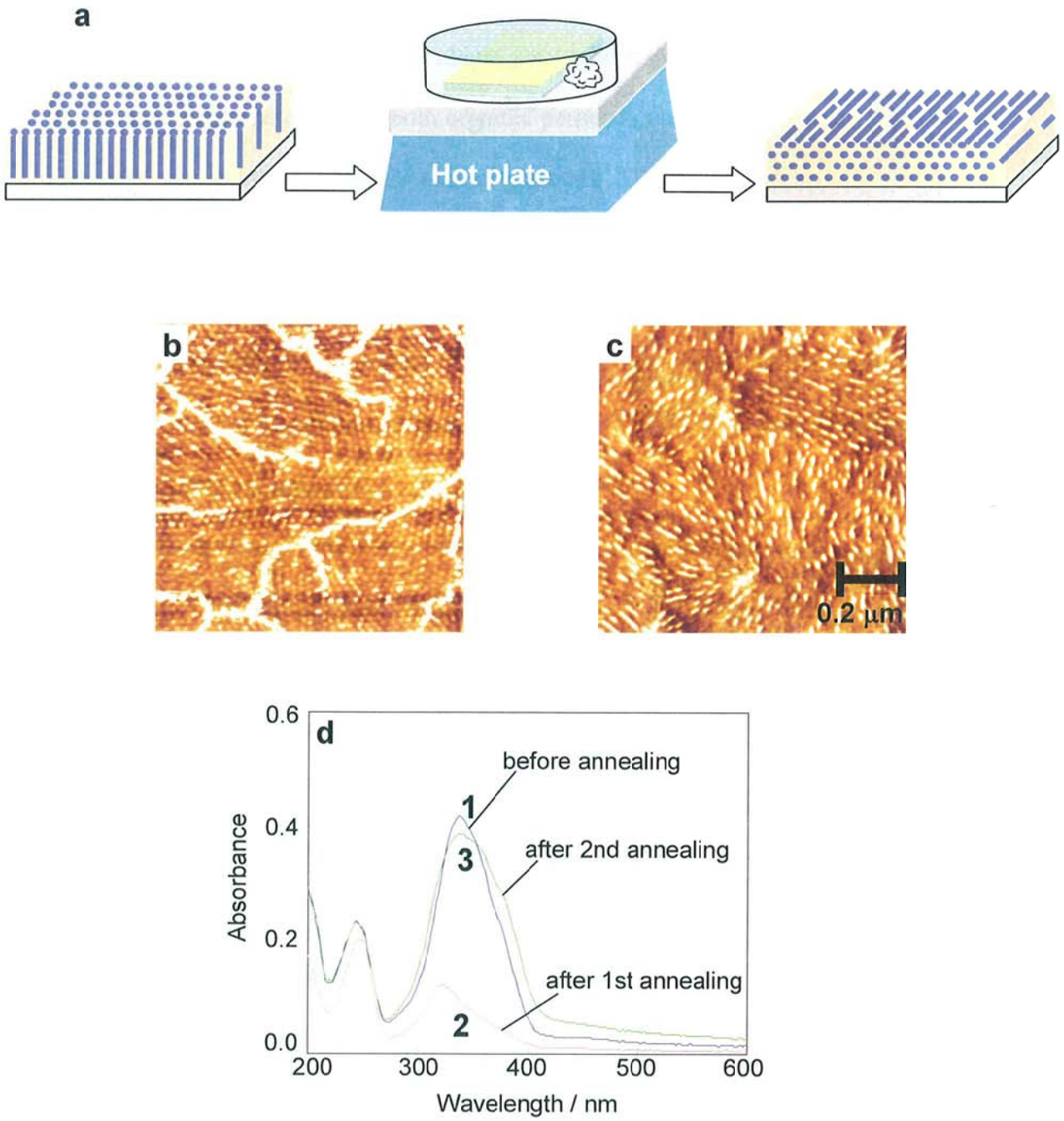

Figure 2-8. Schematic illustration of the reorientation of cylinders in the p(EO_{114}-Az_{67}) films after post-treatment. (**a**) The direction change process of vertical aligned cylinders by utilizing annealing. **b** and **c**, Phase-mode AFM images (1 μm x 1μm) of the p(EO_{114}-Az_{67}) films before and after annealing at 130 °C for 2 h under humidified atmosphere. (**d**) UV-visible absorption spectra of the corresponding p(EO_{40}-Az_{44}) films in each steps for as-cast (**1**), after post-treatment (**2**) and after annealing under humidified atmosphere.

2.3.4 Orientation of nanocylinders and Az chromophores on hydrophobic substrates

2.3.4.1 On HMDS-modified substrates

The $p(EO_{114}\text{-}Az_{67})$ films having 50 nm and 90 nm thickness were obtained by spin-coating from chloroform solutions on HMDS-modified substrates. Figures 2-9a and 9b display the surface morphologies (1.0 x 1.0 μm) of these films after a post-treatment of annealing at 110 °C for 2 h and subsequent exposure to hexane vapor for 20 h, evaluated by the phase mode AFM measurements. The dot morphologies are shown in both films, indicating that cylinders orient normal in the film. The cylinder orientation in thinner film gave the contrasting result from that on the hydrophilic substrate. This observation may be explained that the Az-containing PMMA segments are repulsed by the HMDS-modified substrate interface, preventing the PEO cylinders to be laid. In contrast, when the film thickness was above 70 nm, no difference was observed between the hydrophobic and hydrophilic substrates.

UV-visible absorption spectra of the corresponding $p(EO_{114}\text{-}Az_{67})$ films are shown in Figures 2-9c and 9d. Despite their film thickness, the both films indicated the same tendency characterized by large changes in the spectral shape due to perpendicular orientation of Az mesogens before (1) and after the annealing treatment (2). Absorbance of the π–π^* long axis transition band at 338 nm of the Az mesogens decreased significantly, furthermore, this film exhibited a blue shift due to H-aggregation. In the above manners, the orientation of Az mesogens after the post-treatment coincided with that of the PEO cylinder. The nanostructures were repulsed by substrate surfaces, resulting in normal orientation to the substrates.

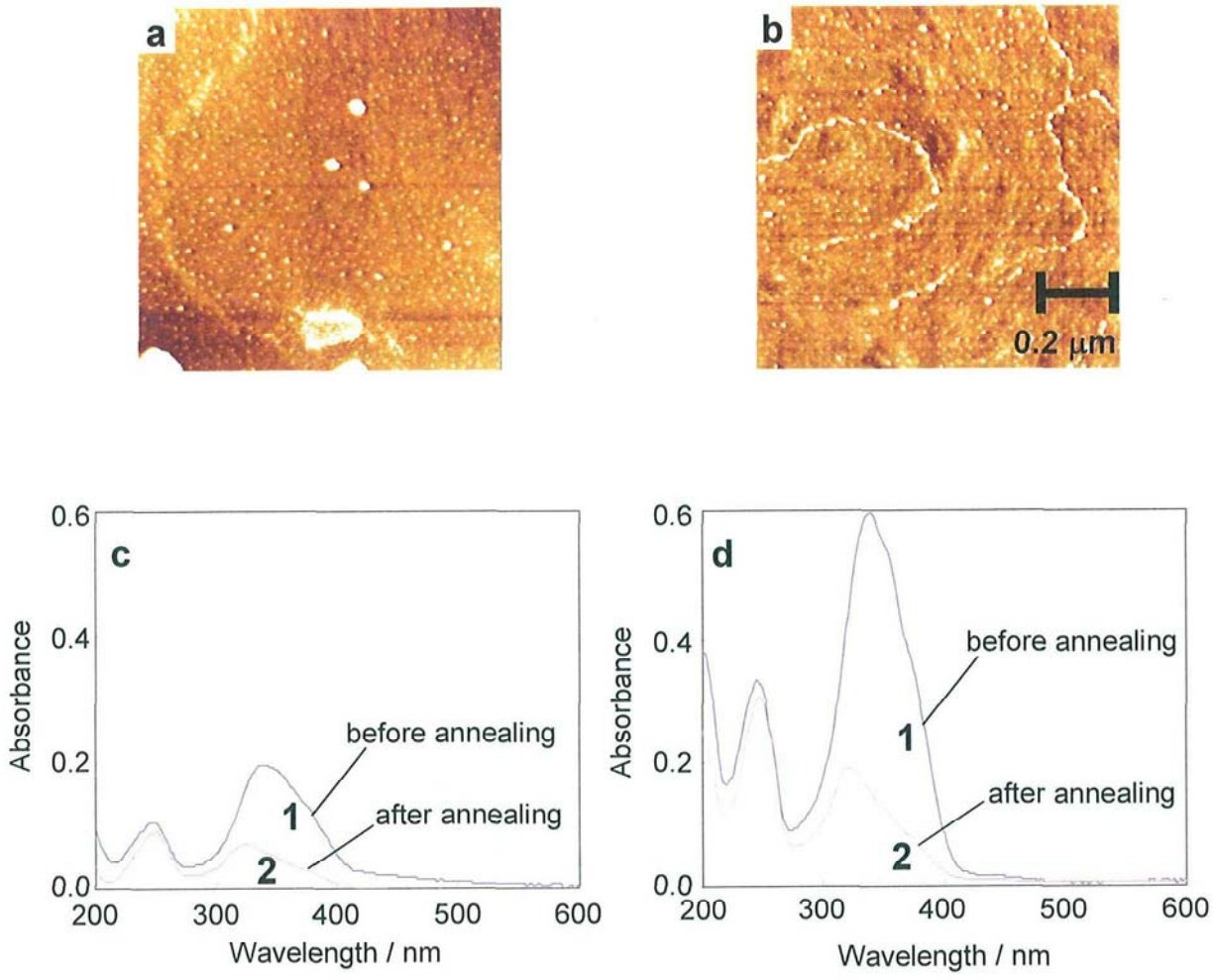

Figure 2-9. The orientation of PEO cylinders and Az mesogens in the p(EO_{114}-Az_{67}) films on HMDS-modified substrate surfaces. **a** and **b**, Phase-mode AFM images (1 μm x 1 μm) with different film thickness (**a**: 30 nm and **b**: 90 nm) after post-treatment. **c** and **d**, UV-visible absorption spectra of the corresponding films for as-cast (**1**) and after annealing (**2**).

2.3.4.2 On OTS-modified substrates

Long chain trialkoxysilane having higher silyl-functionality compared to monofunctional silane generally yields dense SAM and provides a more hydrophobic surface. $p(EO_{114}\text{-}Az_{67})$ films of 50 nm and 90 nm thickness were prepared onto an OTS-modified substrate by spin-coating. Figures 2-10a and 10b show the surface morphologies (1.0 x 1.0 μm) of these films observed by the phase mode AFM measurements after post-treatment. The dot morphologies showing the normal orientation of cylinders to the substrate plane were obtained in both films. This orientation behavior was similar to those on HMDS-modified substrates. Moreover, the similar tendency was also observed with respect to the orientation of Az mesogens, i.e., Az mesogens orient perpendicular to the substrate plane in all films bearing various thickness (Figures 2-10c and 10d). Consequently, it is clear that PEO cylinders and Az mesogens are parallel with each other and both orient only perpendicular to the substrate plane in the HMDS or OTS-terminated hydrophobic substrates.

2.3.5 Orientation of nanocylinders on modified hydrophobic substrates

In the $p(EO_{114}\text{-}Az_{67})$ films below 60 nm thickness, the direction of the cylinders is governed by chemical nature of substrates. On the other hands, it is known that substrates covered with an OTS monolayer can be photochemically modified by exposure to X-ray, deep UV and O_3 gas etc. These processes alter the initial alkyl-terminated surface into an oxygen-containing silanol surface, which means that the initially hydrophobic surface of OTS-modified substrates can be converted to a hydrophilic one. Thus, the exposed hydrophilic regions should alter the cylinders to be oriented parallel in the substrate. To confirm this, $p(EO_{114}\text{-}Az_{67})$ films were prepared onto an OTS-modified substrate exposed to UV light and O_3 atmosphere in the whole

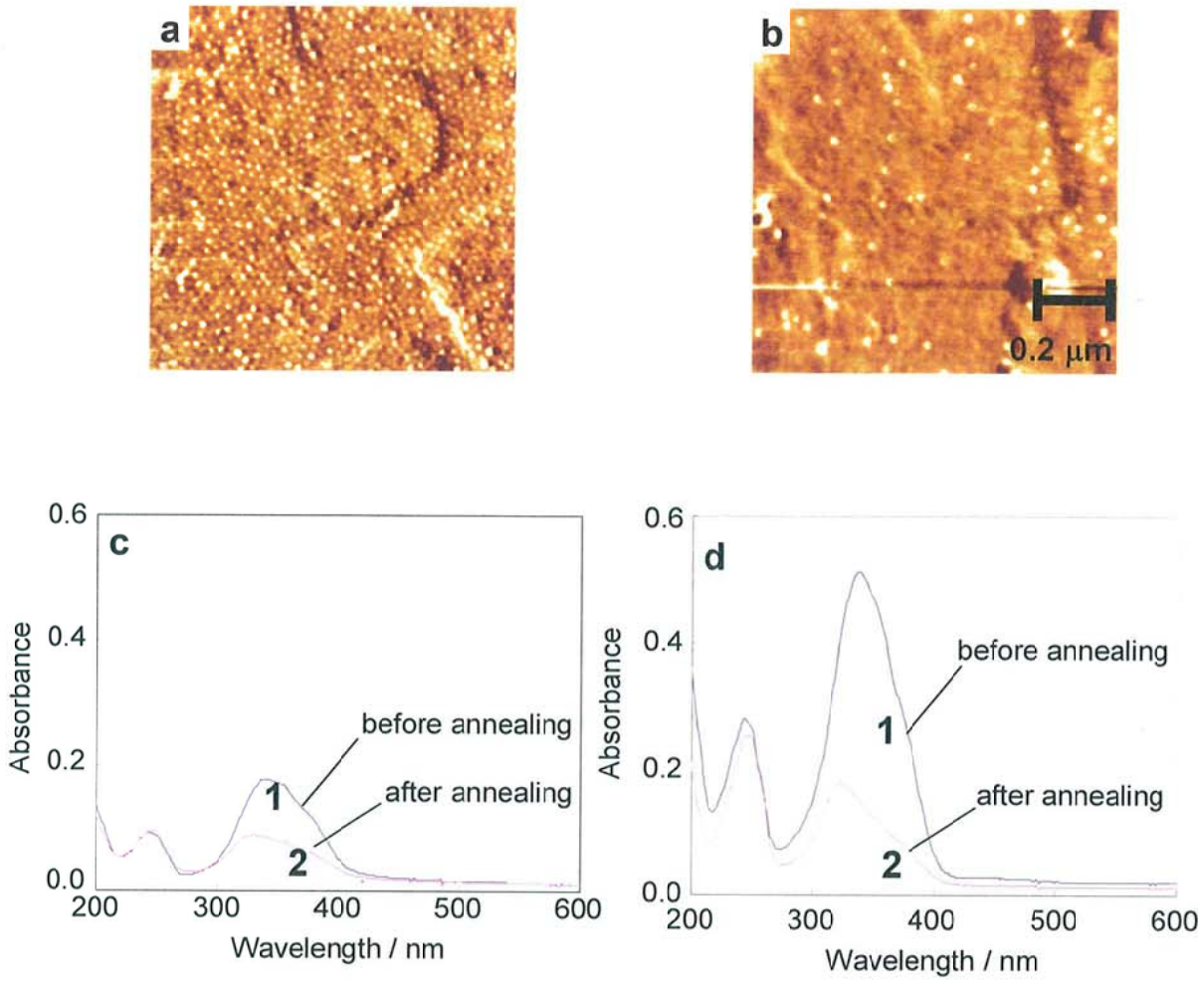

Figure 2-10. The orientation of PEO cylinders and Az mesogens in the $p(EO_{114}\text{-}Az_{67})$ films on OTS-modified substrate surfaces. **a** and **b**, Phase-mode AFM images (1 μm x 1 μm) with different film thickness (**a**: 50 nm and **b**: 90 nm) after post-treatment. **c** and **d**, UV-visible absorption spectra of the corresponding films for as-cast (**1**) and after annealing (**2**).

area. The contact angle of water on the phtochemically treated OTS-modified substrate was ca. 5°. Figures 2-11a and 11b display the AFM images in those films having 50 nm and 70 nm thickness after post-treatment. These morphological features, line and dot structures, indicate the laid and normal cylinder orientations in thinner and thicker films, respectively. Such behavior is just the same as that observed for the clean quartz substrate, As the result, the thickness dependence with respect to cylinder orientation was restored

The orientations of Az mesogens in the corresponding films were inspected by UV-visible absorption spectra measurements. The obtained spectra were shown in Figures 2-11c and 11d. In the thinner film (below 60 nm thickness) gave no change in the spectral shape, indicating that cylinders prefer parallel orientation to the modified OTS film surface. In the thicker film (above 70 nm), large change in the spectral shape was exhibited before (1) and after the annealing treatment (2) because of the alternation to the normal orientation of Az mesogens. Comparisons between the morphological features and the spectral data revealed the cooperative nature in the orientation of cylinders and the mesogens, providing the hierarchical structure from the molecules to the nanostructures. The phtochemically treated OTS-modified substrate as well as a cleaned one (cf. **2.3.1**) provided thickness dependence for the cylinder orientation.

2.3.6 Patterning of cylinder alignment on chemically patterned substrate

In above manners, two different cylinder orientations were observed in the block copolymer thin films of 50 nm thickness on substrates of different wettability. The PEO cylinders were oriented parallel and perpendicular to the substrate plane on the hydrophilic and hydrophobic substrate surfaces, respectively. These results lead to examine the possibility of the patterning of cylinder alignment in one flat films by

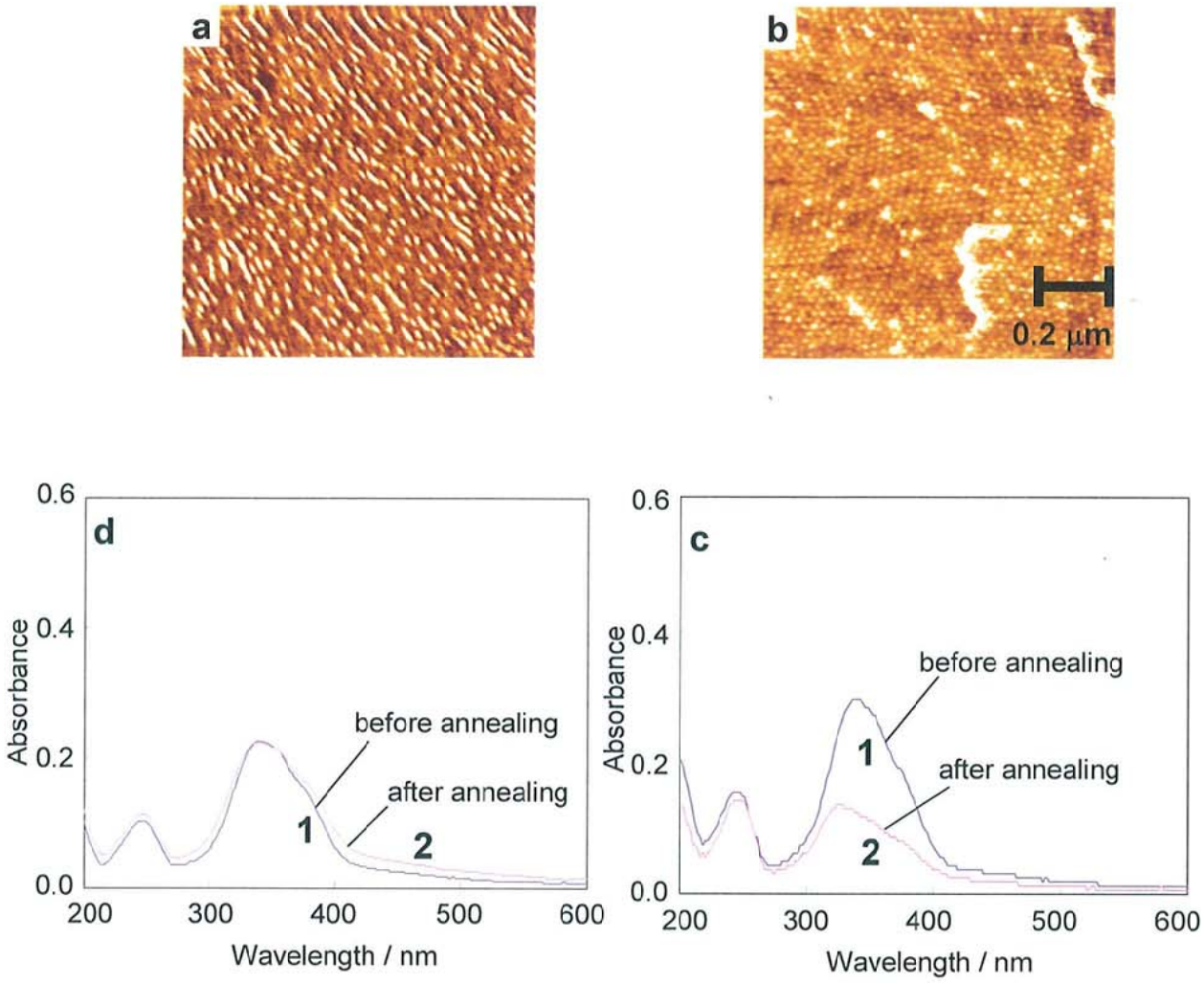

Figure 2-11. The orientation of PEO cylinders and Az mesogens in the p(EO_{114}-Az_{67}) films on OTS-modified substrate surfaces exposed to UV light and O_3 atmosphere . **a** and **b**, Phase-mode AFM images (1 μm x 1 μm) with different film thickness (**a**: 50 nm and **b**: 70 nm) after post-treatment. **c** and **d**, UV-visible absorption spectra of the corresponding films for as-cast (**1**) and after annealing (**2**).

photochemical patterning.

The experimental process for the photochemical patterning of the OTS-modified substrate surface providing the orientationally patterned cylinder is schematically illustrated in Figure 2-12. First, an OTS film was prepared on a cleaned quartz substrate by the solution deposition method (a). The OTS terminated substrate was subjected to UV light and O_3 atmosphere exposure through a mask (b). Onto this substrate a p(EO_{114}-Az_{67}) film of 50 nm thickness was prepared by spin-coating (c) and then annealed at 110 °C for 2h and exposed to a saturated hexane vapor for 20 h (d). The typical values of the contact angles on the non-irradiated and irradiated areas were ca. 95° and 5°, respectively. Figure 2-13 shows the morphological features and the spectral data in the diblock copolymer film after the post-treatment. As shown by the AFM images, the PEO cylinders were oriented perpendicular and parallel to the substrate plane at the areas of non-UV irradiation (a) and UV irradiation (b), i.e. the hydrophobic and hydrophilic areas. In addition, Az mesogens also displayed the same orientation as those of the cylinders. The non-irradiated area indicated large decrease and blue shift of absorbance at 338 nm due to π–π^* long axis transition band of Az unit. In the irradiated area, on the other side, essentially no change was observed. Thus, it is demonstrated that the patterning of cylinder alignment is possible in the chemically patterned substrate.

2.3.7 In-plane alignment control of nanocylinders

Next, optical in-pane alignment control was attempted for thin hybrid films below 60 nm thickness containing low-molecular mass liquid crystal (5CB). In Az polymer thin films, the in-plane alignment of the Az chromophores is controlled by LPL irradiation. The long axis of Az orients perpendicular to the electric field vector of the polarized light. Surface morphologies of the phase separated structure were observed

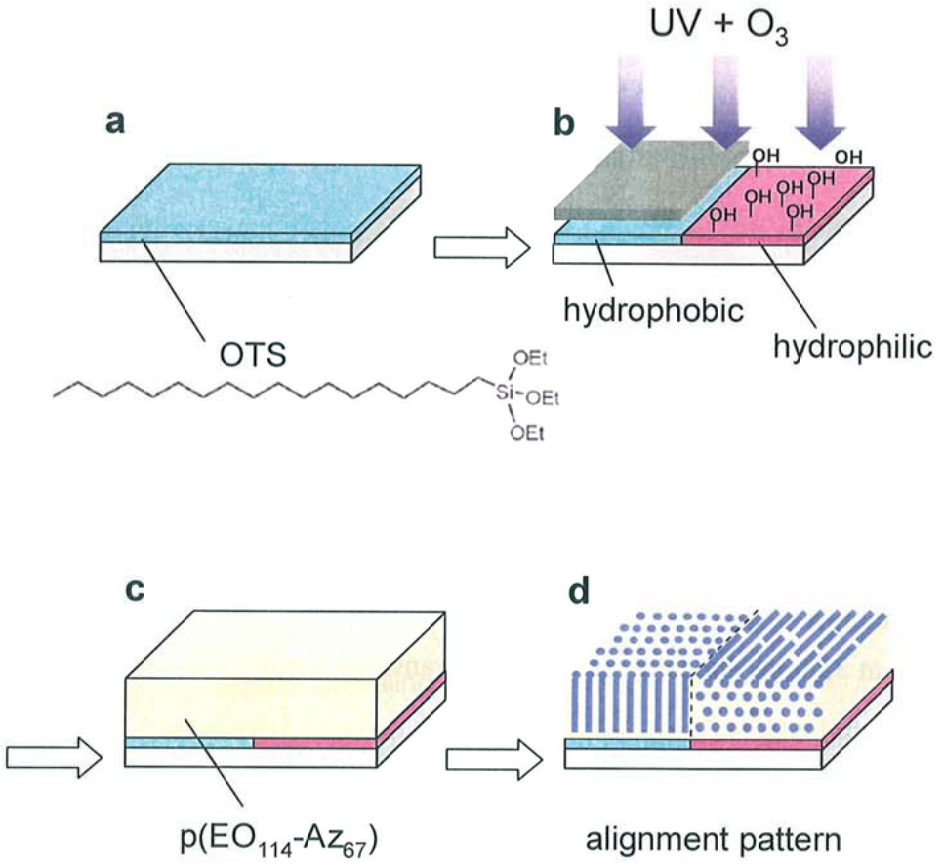

Figure 2-12. Schematic illustration of the strategy for patterning of chemically nature of OTS-modified substrate surface. (**a**) An OTS film on cleaned quarts glass substrate. (**b**) Exposure to UV light and O_3 atmosphere through a mask. (**c**) Spincoating of the p(EO114-Az67) film on a resulting substrate. (**d**) Alignment pattern of cylinders after post-treatment.

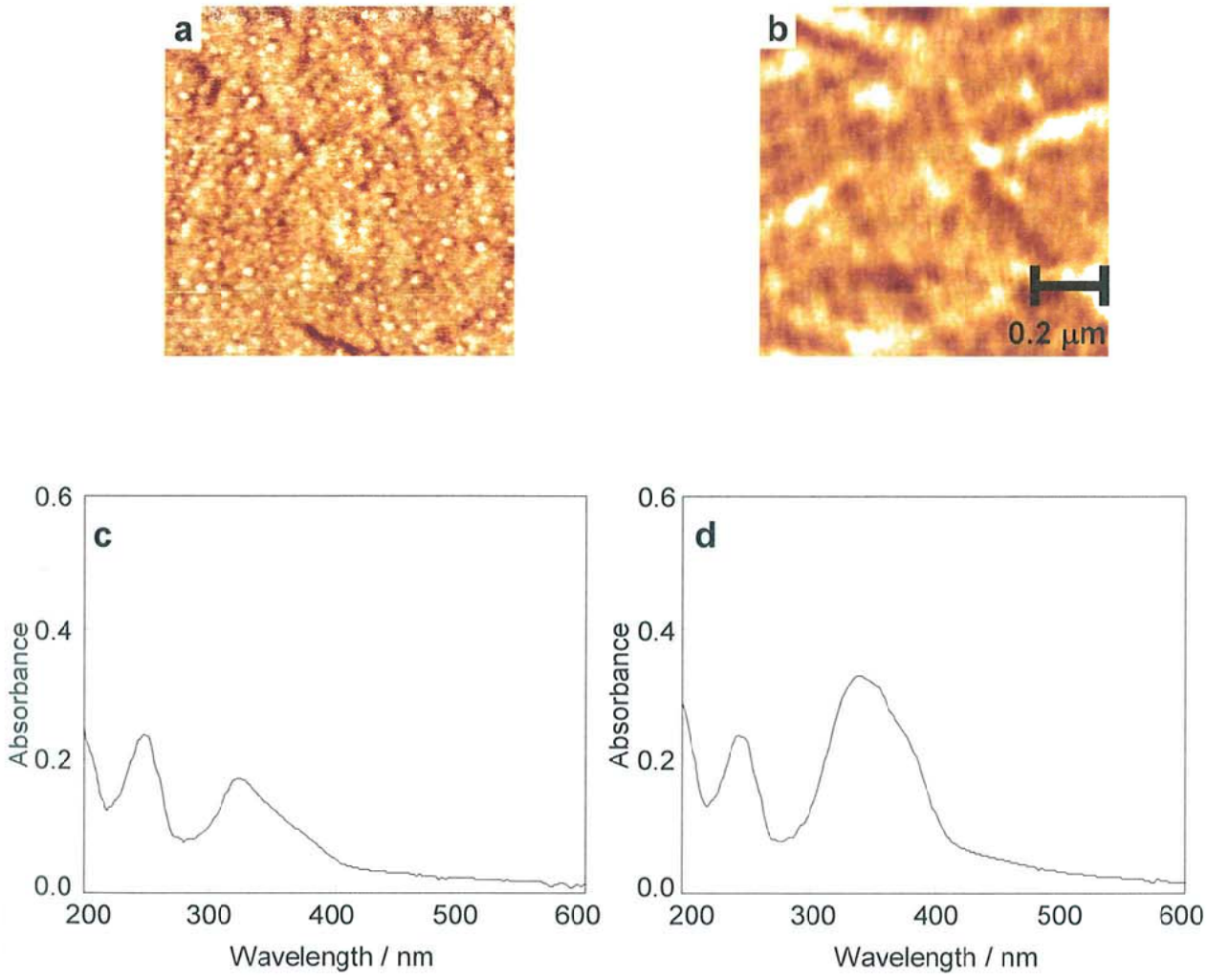

Figure 2-13. The orientation of PEO cylinders and Az mesogens in the p(EO_{114}-Az_{67}) films on chemically patterned substrate surfaces. **a** and **b**, Phase-mode AFM images (1 μm x 1 μm) at the areas of different chemically nature (**a**: non UV irradiated and **b**: UV irradiated) after post-treatment. **c** and **d**, UV-visible absorption spectra at the each area of the corresponding film.

in block copolymer thin films of 40 nm thickness after the exposure to LPL and annealing. The parallel oriented cylinders aligned perpendicular to the direction of LPL (Figure 2-14a). The orientation of Az groups agreed with that of cylinders as revealed by polarized UV-vis absorption spectra (Figure 2-14b). The absorbance at 338 nm became larger and smaller in the perpendicular ($A\perp$) and parallel ($A_{//}$) direction to the polarization direction of the irradiated LPL, respectively, showing that Az chromophores are highly oriented orthogonal to the electric field vector of LPL. The orientational order parameter (S) of the chromophore estimated by the equation $S = (A\perp - A_{//})/(A\perp + 2A_{//})$ (where $A\perp$ and $A_{//}$ denote the absorbance orthogonal and parallel to the irradiated LPL, respectively) was 0.57. The following scheme can be deduced. The LPL irradiation to the diblock copolymer thin films first brings about the in-plane alignment of Az in the direction perpendicular to the irradiated light. Second, the annealing induces the formation and the alignment control of PEO cylinders to the same direction as that of Az. As a result, hierarchical alignment induction from Az chromophores to PEO cylinders was achieved by the LPL irradiation onto the diblock copolymer thin films.

2.4 Conclusion

In this chapter, the factors affecting the cylinder orientation were investigated in detail. Three factors were found to be important, film thickness, surface energy of substrates and LPL irradiation. Film thickness and chemical nature of substrate surface controlled the out-of-plane alignment of cylinders and Az chromophores. LPL irradiation achieved in-plane alignment of nanostructures. The thinner films below 60 nm thickness provided parallel orientation of Az and cylinders on hydrophilic substrates

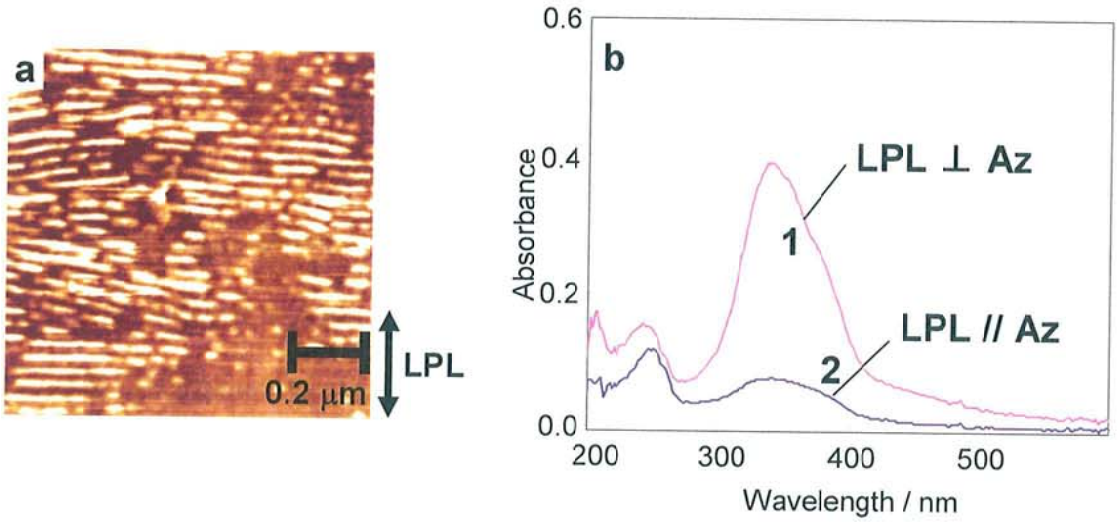

Figure 2-14. The orientation of PEO cylinders and Az mesogens in the p(EO_{114}-Az_{67}) films exposure to LPL and annealing. (**a**) Phase-mode AFM images (1 μm x 1 μm) exposure to LPL and annealing. (**b**) UV-visible absorption spectra of the corresponding filmsare shown after annealing taken with a probing beam perpendicular (**2**) and parallel (**3**) to the polarization direction of the actinic irradiating 436 nm light. An allow in (**a**) indicates the direction of the electric field vector of LPL.

In thicker films, the cylinders oriented normal to the substrate surface. In contrast, when hydrophobic substrates were used, perpendicular orientation to the substrate plane was always observed in spite of changes in the film thickness. In the thickness range below 60 nm, therefore, the cylinders were oriented parallel and perpendicular to the substrate plane on the hydrophilic and hydrophobic substrate surfaces, respectively, which then led to successful photopatterning. Finally, the LPL irradiation to thinner films provided in-plane alignment control of nanostructures.

References

1. *Developments in Block Copolymer Science and Technology*; Hamley, I. W., Ed.; John Wiley & Sons, Ltd: West Sussex, 2004.
2. C. Park, J. Yoon, E. L. Thomas, *Polymer* **2003,** *44,* 6725.
3. A. H. Anastasiadis, T. P. Russell, S. K. Satiji, C. F. Majkrzak, *Phys. Rev. Lett.* **1989,** *62,* 1852.
4. (a) R. A. Segalman, H. Yokoyama, E. J. Kramer, *Adv. Mater.* **2001,** *13,* 1152. (b) D. Sundrani, S. J. Silbener, *Macromolecules* **2002,** *35,* 8531. (c) J. Heier, E. J. Kramer, S. Walheim, G. Krausch, G. *Macromolecules* **1997,** *30,* 6610.
5. G. Krausch, *Mater. Sci. Eng.* **1995,** *14,* 1.
6. M. A. Van Dijk, R. van den Berg, *Macromolecules* **1995,** *28,* 6773.
7. A. Knoll, A. Horvat, K. S. Lyakhova, G. Krausch, G. J. A. Sevink, A. V. Zvelindovsky, R. Magerle, *Phys. Rev. Lett.* **2002,** *89,* 035501.
8. (a) H. Mensinger, M. Stamm, C. Boeffel, *J. Chem. Phys.* **1992,** *96,* 3183. (b) G. Henn, M. Stamm, M. Rücker, J. P. Rabe, *Physica* **1996,** B*221,* 174.
9. J. Heier, E. J. Kramer, S. Walheim, G. Krausch, *Macromolecules* **1997**, *30*, 6610.
10. J. Heier, J. Genzer, E. J. Kramer, F. S. Bates, S. Walheim, G, Krausch, *J. Chem. Phys.* **1999**, *111*, 11101.
11. Han, M.; Morino, S.; Ichimura, K. *Macromolecules* **2000**, *33*, 6360-6371.
12. (a) Y. –Q. Tian, K. Watanabe, X. Kong, J. Abe, T. Iyoda, *Macromolecules* **2002,** *35,* 3739. (b) K. Watanabe, Y. –Q. Tian, H. Yoshida, A. Asaoka, T. Iyoda, *Trans. Mater. Res. Soc. Jpn.* **2003**, *28*, 553.
13. U. Jonas, C. Krüger, *J. Supramol. Chem.*, **2002**, *2*, 255.
14. S. H. Kim, M. J. Misner, T. Xu, M. Kimura, T. P. Russell, *Adv. Mater.* **2004**, *16*, 226.

Chapter 3

Relief Formation in Liquid Crystalline Diblock Copolymer Thin Films via Photo-triggered Mass Migration

3.1 Introduction

Exposure to two interference coherent beams leads to a formation of surface relief structure with an interference pattern in the liquid crystalline Az monomer and the Az polymer including the side-chain and main-chain type.[1-4] Besides, photo-triggered mass migration using binary system with a liquid crystalline copolymer bearing Az side groups and a low-molecular-mass LC has been also studied as well as the single component system.[5] The markedly efficient mass transfer is performed due to the increased fluidity by addition of LC molecular and pre-irradiation with UV (365 nm) light onto the whole area of film which generate a cis-Az rich state.[5,6] Recently, the application of mass transportation to diblock copolymer bearing an Az segment has been investigated. Schmidt et al. have compared the mass transport behavior of a polystyrene polymer composed of Az polymer with that of a random copolymer or an Az-homopolymer.[7] The especial architecture of block copolymer and the polystyrene solid matrix severely impedes the mass migration motions despite the fact that the mass transport is induced for the random copolymer of the same composition. Yu et al. have obtained relief structure in poly(ethylene oxide) connected with liquid crystalline Az polymer.[8] For this system, the mass transport is actually induced by holographic irradiation, however, interference beam of relatively high intensity (50 mW cm^{-2}) is required. Furthermore, without annealing the surface relief modulation is at a few

percent level of the total film thickness.

This chapter describes the surface relief formation by holographic irradiation at low density (2 mW cm^{-2}) for hybrid films consisting of a low-molecular-mass liquid crystal, 4'-phenyl-4-cyanobiphenyl (5CB), and a diblock copolymer connecting poly(ethylene oxide) (PEO) and an Az-containing liquid crystalline polymer (Figure 2-1a). The influence of 5CB mixed with block copolymer on relief formation efficiency is estimated.

3.2 Experiments

3.2.1 Materials

The diblock copolymer, p(EO_{114}-Az_{67}), used in previous chapter was dealt in this chapter also. 5CB was obtained from Merck.

3.2.2 Preparation of hybrid thin films

The hybrid thin films containing p(EO_{114}-Az_{67}) and 5CB were spin-coated from chloroform solutions at a molar mixing ratio *f*, *f* being the molecular fraction of 5CB([5CB]/([Az unit]+[5CB])), onto hydrophilic quartz substrates and baked at 60 °C for 5 min to remove residual solvent. Quartz glass substrates were washed with a saturated potassium hydroxide ethanol solution, and pure water under ultrasonic wave treatment. The typical value of the contact angle was ca. 5 °. The films having different film thickness were prepared from chloroform solutions of various polymer concentrations on hydrophilic quartz glass substrates.

3.2.3 Formation of Surface Relief Structure

The set up for holographic recording experiment is sketched in Figure 3-1. In advance of holographic recording, UV light (365 nm) irradiation was performed with a

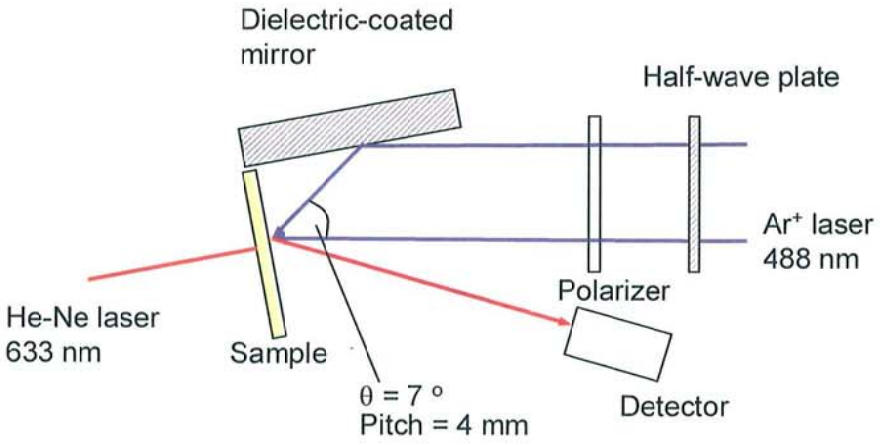

Figure 3-1 Schematic illustration of the experimental setup for the holographic recording by an argon ion laser beam.

San-ei Supercure-202S to induce photoisomerization to the cis-rich state. Onto this film the holographic irradiation was performed with a coherent argon ion (Ar^+) laser (Omnichrome 543R-AP-A01, 488 nm). The half wave plate was installed to rotate the plane of polarization of the coherent beam for selection of (*s*-: *s*-) or (*p*-: *p*-) modes. The half of the beam was reflected by a mirror. The interference state was made with direct beam and the reflected one at the film surface. Formation of surface relief structure was confirmed by intensity measurement of the first-order diffraction of a He-Ne laser beam (NEC GLC 5700) on the transmittance mode with an optical power meter (Advantest TQ82190). The topographic image was observed by AFM.

Visible light (436 nm) irradiation through a photomask was performed with a San-ei Supercure-202S.

3.2.4 Characterization of Surface Relief Structure

The film thickness of the films was measured by atomic microscopy (AFM, Nanopics 2100, Seiko Instruments.Inc). The film was scratched with a needle, and the height difference between the bare substrate surface and the film surface was estimated.

Differential scanning calorimetry (DSC) measurements were made on a Seiko DSC 200 (heating and cooling rates: 10 °C/min).

UV-visible absorption and transmission spectra were recorded on a Hewlett Packard 8452A diode array spectrometer.

3.3 Results and Discussion

3.3.1 Preparation and photoisomerization of hybrid films

The efficient surface relief formations of Az polymers hybridized with low-molecular-mass LC have been reported by Ubukata et al.[5] The mixed

low-molecular-mass LC can play a role of the plasticizer of the Az-containing polymers and decreases the phase transition temperature for the LC phase, which provides the efficient surface relief formation of Az-containing polymers. To evaluate the change of phase transition temperature, we measured thermal properties of the $p(EO_{114}\text{-}Az_{67})$/5CB system in bulk state by DSC. Figure 3-2 shows the DSC curves of mixture including various 5CB molar fractions. The absence of phase transition of the pure components for mixtures revealed full miscibility of the 5CB and $p(EO_{114}\text{-}Az_{67})$. The plasticization of $p(EO_{114}\text{-}Az_{67})$ by addition of 5CB resulted in the shift to lower temperature of its phase transition temperature. In the case of the systems containing high 5CB molecular fraction ($f > 0.3$), the formation of new LC phase were induced. For $p(EO_{114}\text{-}Az_{67})$ hybridized with 5CB, the LC phase appeared even at room temperature.

Furthermore, photoisomerization of the films of pure $p(EO_{114}\text{-}Az_{67})$ and $p(EO_{114}\text{-}Az_{67})$ with 5CB at $f = 0.5$ was examined by UV-visible absorption spectral measurement. Both films having film thickness of ca. 180 nm were prepared from chloroform solutions by spin coating. Figures 3-3a and 3b show the spectral changes of the pure $p(EO_{114}\text{-}Az_{67})$ film and the $p(EO_{114}\text{-}Az_{67})$/5CB hybrid film prepared on a quartz substrate before and after UV light exposure, respectively. The two absorption around 360 nm and 440 nm were assigned to the π-π^* and n-π^* transition band, respectively. In both cases, the π-π^* and n-π^* transition band was decreased and enhanced, respectively, indicative of the efficient proceeding of the trans-to-cis photoisomerization. The holographic irradiation described below was performed from the cis-rich photostationary state.

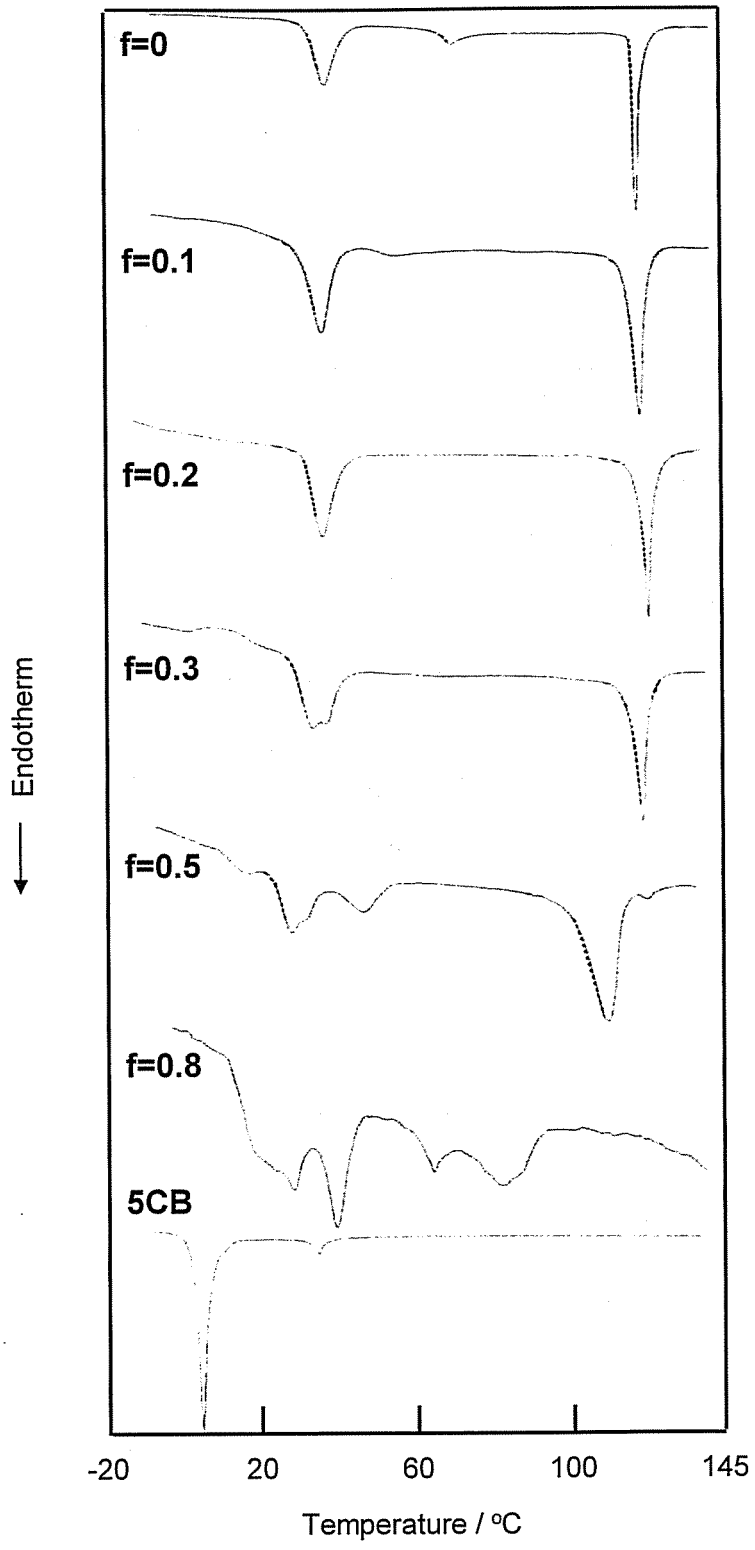

Figure 3-2 DSC curves of p(EO114-Az67)/5CB hybrids at various molar fractions of p(EO114-Az67) and 5CB (*f*).

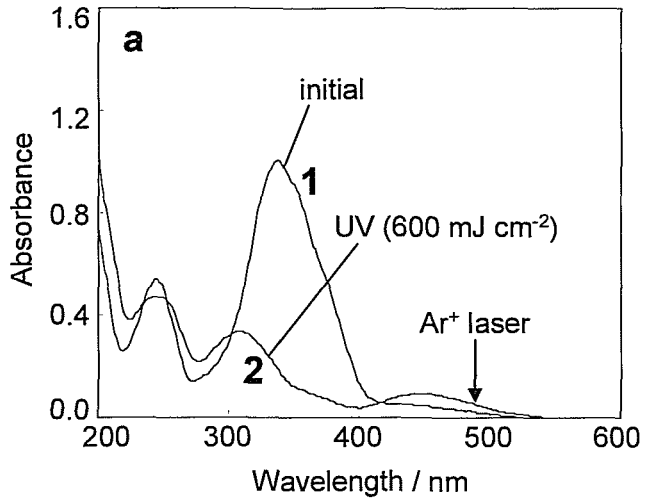

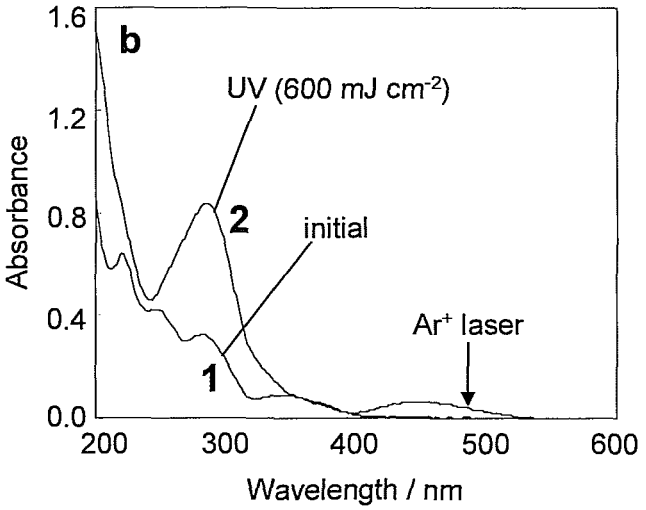

Figure 3-3 UV-visible absorption spectra. p(EO114-Az67) film (**a**) and the p(EO114-Az67)/5CB hybrid film (f = 0.5) (**b**) before (**1**) and after UV light exposure (**2**).

3.3.2 Effect of addition of liquid crystal molecule

The exposure to the interferometric Ar^+ beam was performed after pre-irradiation of UV light in the films of pure p(EO_{114}-Az_{67}) and p(EO_{114}-Az_{67}) with 5CB at f = 0.5. Figure 3-4 displays the enhancement of the first-order diffraction efficiency with exposure energy evaluated with a He-Ne laser beam, which monitors the surface relief structure formation. The effect of addition of 5CB was obvious. For the hybrid film (f = 0.5), diffraction efficiency reached up to 0.80 % at 220 mJ cm^{-2}, corresponding to 110 s exposure at 2.0 mW cm^{-2}. After this point the efficiency remained constant. In contrast, the enhancement of the diffraction efficiency for the film without 5CB was negligible (0.07 %).

Figures 3-5a and 5b show the topographical AFM images of the pure (EO_{114}-Az_{67}) film and in the hybrid film (f = 0.5) exposed with the interferometric Ar^+ laser beam at 2.0 mW cm^{-2} for 200 s. As shown, the pure film provided little undulation (a), and the hybrid one gave large undulation in accord with the interference periodicity (4 μm for this case) (b). The height from the top to valley reached 90 nm, clearly indicating that a very efficient mass transport took place seeing from the initial thickness of 180 nm. The marked enhancement of the mass transfer should be the result of strong synergy motions of the Az polymer and 5CB in the plasticized film.[5]

The fist-order diffraction efficiency (○) and surface modulation depth (■, Δh) of the films at various molar fractions (f) of 5CB were shown in Figure 3-6a. Starting from f = 0, the increase of 5CB content enhanced the diffraction efficiency. The maximum efficiency was obtained at f = 0.5 and above this point it was reduced. With respect to the undulation height (Δh), on the other hand, the maximum value was observed at f = 0.8. These results can be compared with those obtained for the random copolymer

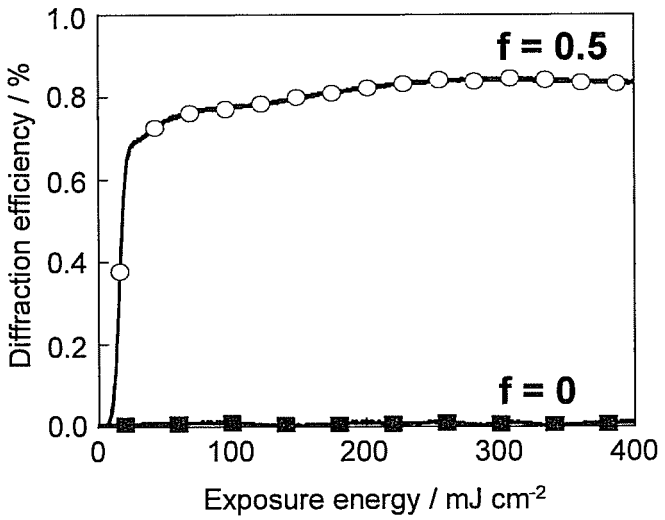

Figure 3-4 First-order diffraction efficiency of the p(EO114-Az67) film (■) and the p(EO114-Az67)/5CB hybrid film (*f* = 0.5) (○) vs exposure energy.

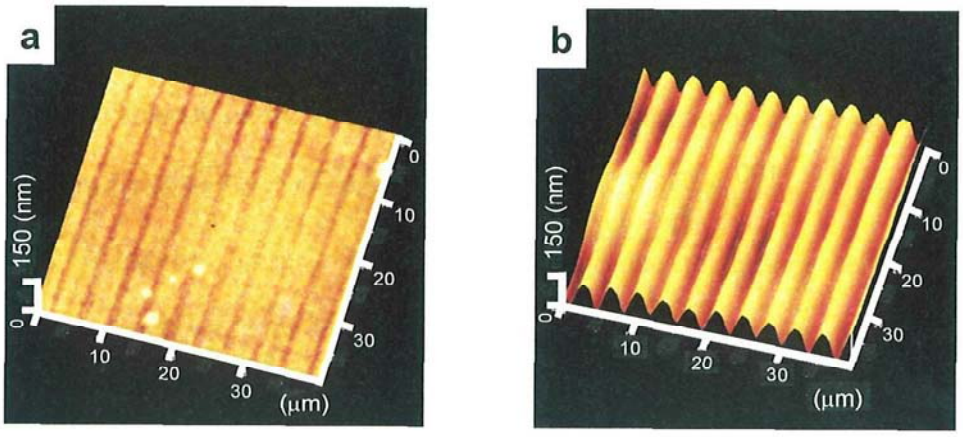

Figure 3-5 Topographic AFM images (40 x 40 mm) of photogenerated relief structure in (**a**) the pure p(EO114-Az67) film and (**b**) the p(EO114-Az67)/5CB hybrid film (f = 0.5).

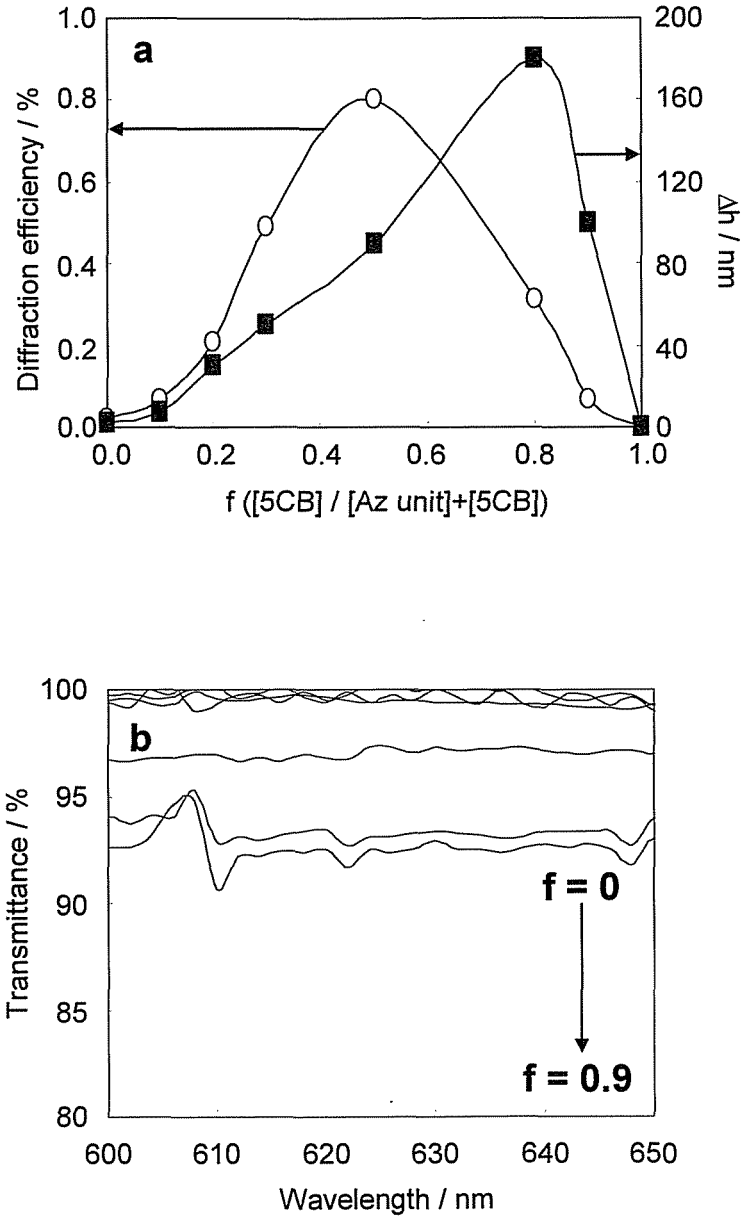

Figure 3-6 (**a**) The first-order diffraction efficiency (○) and surface modulation depth (■) of the p(EO114-Az67)/5CB hybrid films with various 5CB fractions (*f*). (**b**) Visible transmission spectra of the p(EO114-Az67)/5CB hybrid films with various 5CB fractions (*f*).

system, where both profiles of the diffraction efficiency and undulation height coincided with each other. At present, it turned out that this discrepancy is caused by light scattering of He-Ne laser beam in hybrid films. Figure 3-6b shows the transmission spectra of the hybrid films at 600 – 650 nm various fractions of 5CB. The transmittance of hybrid films decreased, i.e, the film became turbid with the increase of 5CB content. The light scattering can reduce the diffraction efficiency than the actual value. A phase separation of pure 5CB in the polymer matrix should occur at high *f*. Therefore, we regard that the optimal mixing ratio is $f = 0.5$, and this condition will be adopted for further investigation.

3.3.3 Polarization dependence of holographic grating

The strong polarization dependence of relief formation efficiency for amorphous or liquid crystalline Az polymers has been well known.[11,12] In this paragraph, a dependence of diffraction efficiency on the two different states of polarization of the probe light was investigated in hybrid films ($f = 0.5$) with 60 nm thickness. Figures 3-7a and 7b show the growth of the first order diffraction efficiency due to surface relief formation performed at 2.0 mW cm^{-2} for 2500 s under different polarization combinations; namely, the electric field vectors of the two beams were set parallel (a) and perpendicular (b) to the plane of incidence. The former and latter are denoted as (*p*-: *p*-) and (*s*-: *s*-) mode irradiation, respectively. Two diffraction efficient curves were almost exactly coincided with each other. The maximum efficiencies were 1.2 % and 1.1 %, and equilibrated ones were 1.1 % and 1.0 %. As shown in Figures 3-8a and 8b, the resulting relief structures were also similar in terms of grating pitch, depth and shape. In above manners, no polarization dependency was demonstrated for the relief formation.

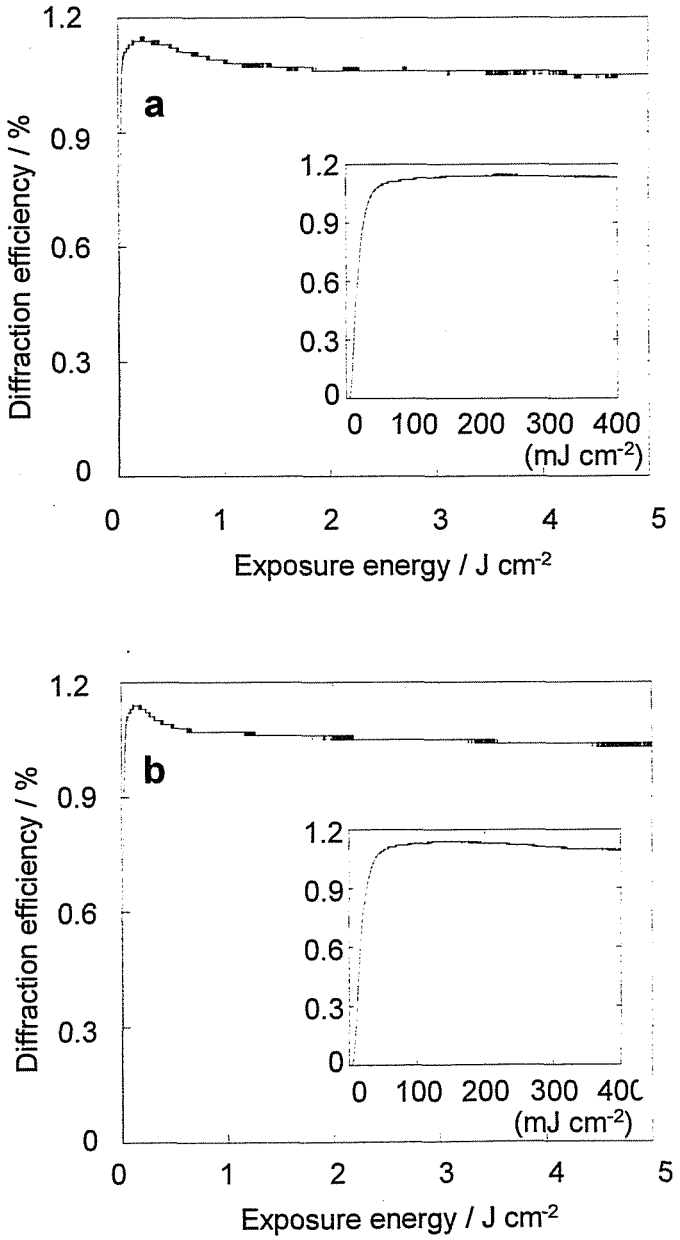

Figure 3-7 First-order diffraction efficiency of the p(EO_{114}-Az_{67})/5CB hybrid films resulted from (**a**) (*p*-: *p*-) mode or (**b**) (s-: s-) mode holographic irradiation.

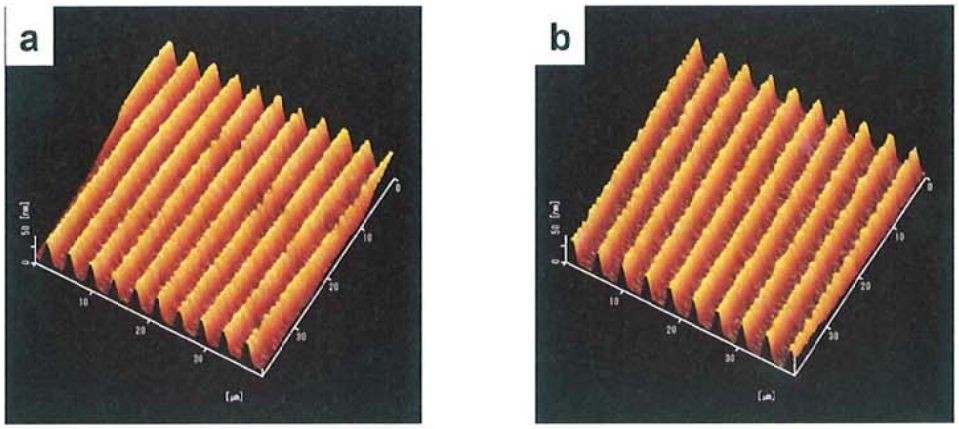

Figure 3-8 Topographic AFM images (40 x 40 mm) of photogenerated relief structure resulted from (**a**) (*p*-: *p*-) mode or (**b**) (s-: s-) mode holographic irradiation in the p(EO114-Az67)/5CB hybrid film (f = 0.5).

3.3.4 Relief formation by mask irradiation

Mass migration occurs from an area exposed to light to a non-irradiated one. The key of relief formation is the spatial modulation of light-intensity provided by the interference exposure. In addition to holographic irradiation process, photoirradiation through a photomask also produces a light intensity pattern which is expected to lead to formation of surface relief structures. The exposure to visible light was performed at 2.0 mW cm^{-2} for 2500 s after pre-irradiation of UV light to the $p(EO_{114}\text{-}Az_{67})$/5CB hybrid film ($f$ = 0.5). Figures 3-9a and 9b exhibit the microphotograph images of a line and space (10 μm period) photomask and the obtained relief in the hybrid film. In the corrugated films, the relief pitch coincided a pattern period of the photomask used.

3.4 Conclusion

In this chapter, the relief structure formation via photo-triggered mass migration in $p(EO_{114}\text{-}Az_{67})$ film was demonstrated. For a pure $p(EO_{114}\text{-}Az_{67})$ film, essentially no surface relief formation was admitted. When a low molecular mass liquid crystal, 5CB, is incorporated, highly efficient mass migration occurred by cooperative motions of the constituents. The full mass migration was attained at a dose of 220 mJ cm^{-2}, which is somewhat larger but almost comparable to the efficiency of the random copolymer system. By varying the molar fraction of 5CB, the optimal fraction was found to be f = 0.5. Based on the knowledge obtained here, mass migration leading to formation of topographical relief pattern will be applied for controls of microphase separation structure of the block copolymer film in the subsequent chapters.

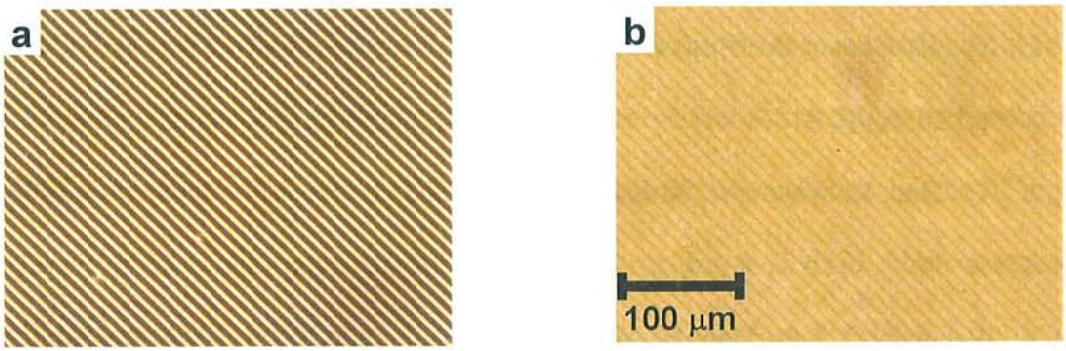

Figure 3-9 Microphotograph of a photomask (**a**) and the relief structure resulted from exposure to visible light through a photomask (**b**) in the p(EO114-Az67)/5CB hybrid film (f = 0.5).

References

1. A. Natansohn, P. Rochon, *Chem. Rev.* **2002**, *102*, 4139.
2. N. K. Viswanathan, D. Y. Kim, S. Bian, J. Williams, W. Liu, L. Li, L. Samuelson, J. Kumar, S. K. Tripathy, *J. Mater. Chem.* **1999**, *9*, 1941.
3. R. H. Berg, S. Hvilsted, P. S. Ramanujam, *Nature* **1996**, *383*, 505.
4. A. Stracke, J. H. Wendorff, D. Goldman, D. Janietz, B. Stiller, *Adv. Mater.* **2000**, *12*, 282.
5. T, Ubukata, T. Seki, K. Ichimura, *Adv. Mater.* **2000**, *12*, 1675.
6. N. Zettsu, T. Ubukata, T. Seki, K. Ichimura, *Adv. Mater.* **2001**, *13*, 1693.
7. C. Frenz, A. Fuchs, H –W. Schmidt, U. Theissen, D. Haarer, *Macromol. Chem. Phys.* **2004**, *205*, 1246.
8. H. Yu, K. Okano, A. Shishido, T. Ikeda, K. Kamata, M. Komura, T. Iyoda, *Adv. Mater.* **2005**, *17*, 2184.
9. Y. –Q. Tian, K. Watanabe, X. Kong, J. Abe and T. Iyoda, *Macromolecules* **2002**, *35*, 3739.
10. K. Watanabe, Y. –Q. Tian, H. Yoshida, A. Asaoka and T. Iyoda, *Trans. Mater. Res. Soc. Jpn.* **2003**, *28*, 553.
11. T. Seki, *Polym. J.* **2004**, *36*, 435.
12. N. K. Viswanathan, S. Balasubramanian, L. Li, S. K. Tripathy, J. Kumar, *Jpn. J. Appl. Phys.* **1999**, *38*, 5928.

Chapter 4

3D Optical Alignment of Nanostructures via Photo-triggered Mass Migration

4.1 Introduction

The determining factors of alignment of PEO cylinders and Az in block copolymer, p(EO_{114}-Az_{67}), thin films were described in Chapter 2. The out-of-plane alignment from the mesogens to the nanostructures was achieved by change in the film thickness. The in-plane alignment of those was controlled by the LPL irradiation for diblock copolymer thin films. Moreover, the nanocylinders were found to be oriented parallel and perpendicular to a hydrophilic and hydrophobic substrate surface, respectively, in ultra thin films. In Chapter 3, photo-triggered mass migration was successfully performed for block copolymer systems. The exposure to two interference coherent beams of argon ion laser let to a formation of surface relief structure in hybrid films composed p(EO_{114}-Az_{67}) containing 5CB.

This chapter proposes a new all optical 3D alignment control of nanocylinders of a diblock copolymer comprising liquid crystalline photoresponsive block chain and poly(ethylene oxide) (PEO) by applying the process of photo-triggered mass migration. This novel process is anticipated to achieve the out-of-plane and the in-plane alignment control based on film thickness and LPL direction upon illumination, respectively, at the same time.

4.2 Experiments

4.2.1 Materials

The diblock copolymer, $p(EO_{114}\text{-}Az_{67})$, used in previous chapter was also employed in this chapter. 5CB was obtained from Merck.

4.2.2 Preparation of hybrid thin films

The hybrid thin films containing $p(EO_{114}\text{-}Az_{67})$ and 5CB were prepared by spin-coating from chloroform solutions at a molar mixing ratio f =0.5 onto a hydrophilic quartz substrate and baked at 60 °C for 5 min to remove residual solvent. The films having different film thickness were prepared from chloroform solutions of various polymer concentrations on a hydrophilic quartz glass substrate.

4.2.3 Formation of Surface Relief Structure

For the surface relief formation, UV light (365 nm) irradiation was performed with a San-ei Supercure-202S in advance to allow photoisomerization to the cis-rich state. Onto this film the holographic irradiation was performed with a coherent argon ion laser beam (Omnichrome 543R-AP-A01, 488 nm) as reported in chapter 3. The setup for holographic recording experiment was sketched in Figure 3-1. The topographic image was observed by AFM.

4.2.4 Characterization of Surface Relief Structure

The relief inscribed films were then annealed at 100 °C for 2 h and exposure to a saturated hexane vapor for 8 h. AFM measurements were performed with a Seiko Instrument SPA400/SPI3800N system in the dynamic force mode (topographic and phase modes). The film thickness of the films was evaluated by AFM measurements. The film was scratched with a needle, and the height difference between the bare substrate surface and the film surface was estimated.

4.3 Results and Discussion

4.3.1 2D alignment of nanostructures (out-of-plane)

For the hybrid films of the diblock copolymer containing a low-molecular-mass liquid crystal, 5CB, pre-irradiation of UV light was first performed and the formation of corrugated relief structures was performed by irradiation with UV light followed by exposure to interferometic argon ion laser beam as discussed in Chapter 3. In the resulting relief structure with the film thickness at the crest and trough being above and below the level of 70 nm, it is expected that the out-of plane alignment control of cylinder array will be achieved because of the thickness dependence of cylinder alignment described in chapter 2.

So a surface relief whose thicknesses at the trough and crest were 30 nm and 70 nm, respectively, was obtained by the (*s*-: *s*-) mode holographic irradiation at 400 mJ cm^{-2}, corresponding to 200 s exposure at 2.0 mW cm^{-2}. This irradiated dose provided the in-plane alignment control of Az chromophores as $S = 0.44$. Figure 4-1 shows the AFM data after annealing followed by exposure to a hexane vapor. The initial relief structure was characterized by smooth sinusoidal curves, and after the hexane vapor exposure, in contrast, the surface became rough as indicated in the topographic image (a). The initial top-to-trough height difference was ca. 80 nm, which decreased by ca. 35 nm after the procedures of annealing and the hexane exposure. The thickness of the film at the trough and top of crest were ca. 35 nm and 70 nm, respectively. Figures 4-1b and 1c display 0.8 x 0.8 μm phase images taken at the trough and crest areas respectively. As clearly indicated, the orientations of the cylinder exhibited contrasting results in the two parts. The cylinders were oriented parallel and perpendicular to the substrate plane at the areas of trough and crest, respectively. The in-plane alignment of cylinders oriented

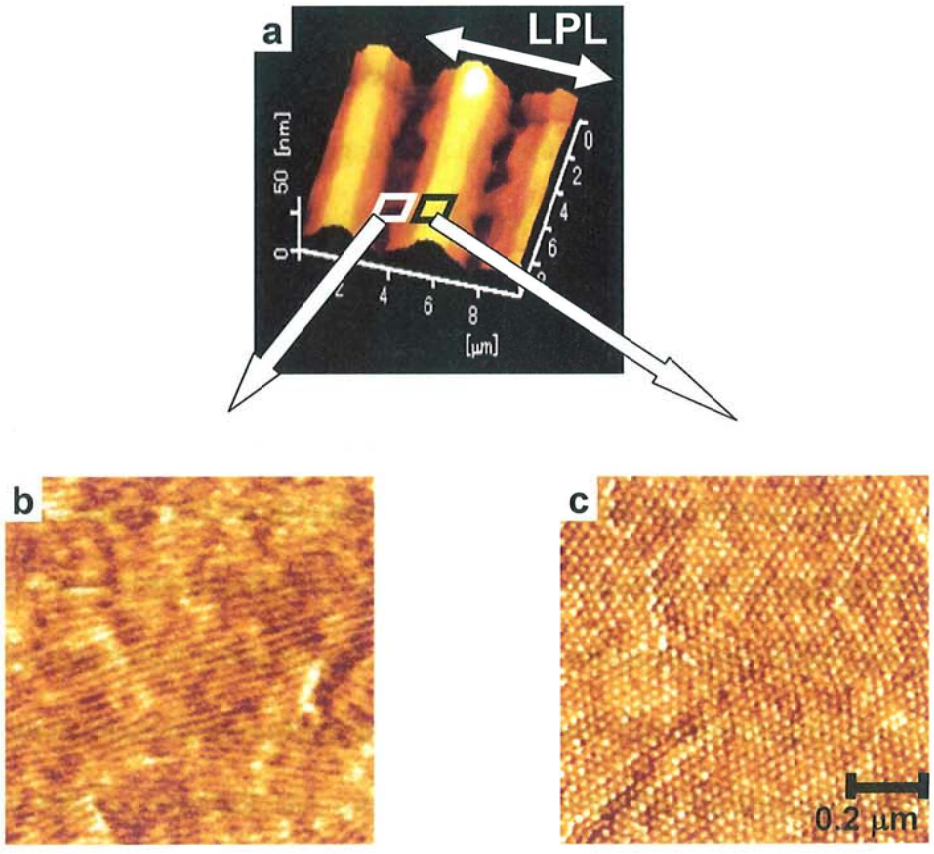

Figure 4-1. AFM images of surface relief structure of $p(EO_{114}\text{-}Az_{67})$ film after post-treatment. Topographic AFM image (10 x 10 μm) of a photogenerated relief (**a**), and corresponding magnified phase mode images (0.8 x 0.8 μm) at the trough (**b**) and crest (**c**) resulted from (*s*-: *s*-) mode holographic irradiation at 400 mJ cm^{-2} .

parallel to the substrate was not controlled at the trough area after irradiation at 400 mJ cm^{-2}.

4.3.2 3D alignment of nanostructures (out-of-plane and in-plane)

4.3.2.1 Holographic illumination with (*s*-: *s*-) mode

The holographic irradiation was performed in the (*s*-: *s*-) mode at prolonged irradiation. Here, a dose of LPL irradiation was increased to 5 J cm^{-2} (13 times as large as the condition adopted in the previous section), corresponding to 2500 s exposure at 2.0 mW cm^{-2}.In this condition, in-plane alignment control of azobenzene chromophores was achieved ($S = 0.53$). Figure 4-2 shows the AFM images of obtained relief structure in the hybrid thin film after the post-treatment. The initial relief structure was characterized by smooth sinusoidal curves, and after the annealing and hexane exposure, in contrast, the surface of the trough areas were flattened as indicated in the topographic image (a and e). Such surface deformation should be essential as will be discussed below. Also, the crest-to-trough height difference was reduced after the above-mentioned post-procedures from initial ca. 80 nm to ca. 40 nm. The resulting thickness of the film at the trough and crest were ca. 30 nm and 70 nm, respectively.

Figures 4-2(b – d) show the phase mode AFM images (1.0 x 1.0 μm) taken at the trough, boundary and crest areas of Fig. 4-2a inscribed by the (*s*-: *s*-) mode irradiation, respectively. The cylinders were oriented parallel and perpendicular to the substrate plane at the areas of trough and crest, respectively (b and d). Interestingly, the cylinder orientation changed critically with no graduation at the boundary region between the trough and crest (c). The parallel oriented (laid) cylinders at troughs aligned perpendicular to the undulation orientation, i.e., perpendicular to the electric field vector of polarized light of holographic recording (b). The flattened surface at the trough areas

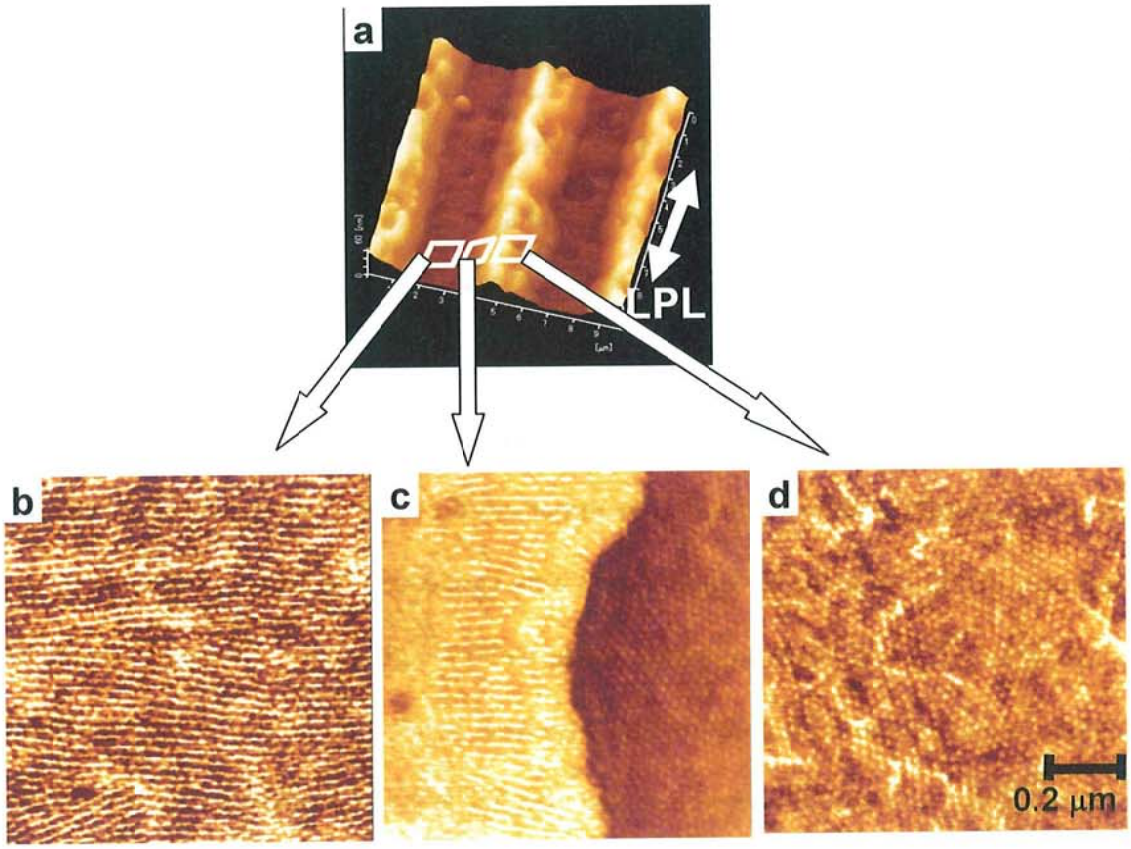

Figure 4-2. AFM images of the surface relief structure of the p(EO_{114}-Az_{67}) film after post-treatment. Topographic AFM image (10 x 10 μm) of a photogenerated relief (**a**), and corresponding magnified phase mode images (1.0 x 1.0 μm) at the trough (**b**), boundary region (**c**) and crest (**d**) resulted from the (*s*-: *s*-) mode holographic irradiation at 5 J cm^{-2} .

should be the consequence of laid orientation of the cylinders. The diameter of the core of PEO cylinder was 13 ± 1 nm in both areas. The average nearest-neighbor distance between the dots observed at the crest and that between the stripes at the trough were 23 ± 1 and 28 ± 2 nm, respectively. It is noteworthy that when a relief-inscribed film was thicker whose trough thickness exceeded 70 nm, all the cylinders adopt normal orientation regardless of the modulation shape. Therefore, the thickness control is of essence for the out-of-plane orientation discriminations.

4.3.2.2 Holographic illumination with (*p*-: *p*-) mode

Figure 4-3 shows the topographical and the similar phase mode images for the relief structure in the (*p*-: *p*-) mode irradiation. The cylinders were similarly oriented according to the corrugations. The only but essential discrepancy was the direction of in-plane alignment of the laid cylinders at the trough areas. The laid cylinders aligned uniformly along the edges of the crests, i.e., perpendicular (non-excitable direction) to the electric field vector of polarized light (b). Thus, the direction of the photo-oriented Az chromophore given by the linearly polarization of the laser beam obviously governs the orientations of PEO cylinders in the trough parts. The terrace was formed in the boundary area after post-treatment. As shown in (c), the same morphological feature as it in the trough area was observed in the terrace. The sharp inclination between the trough and the terrace exhibited featureless morphology. This observation indicates that the multiple layers of in-plane aligned cylinders are formed. It is clear that the height of the sharp inclination, i.e. terrace-to-trough height difference, coincides with the diameter of the cylinder (Figure 4-4). In the crest thicker than terrace, the cylinders oriented perpendicular to the substrate plane (d). In the above manners, by the combination of thickness modulation and polarized light-sensitive behavior, both

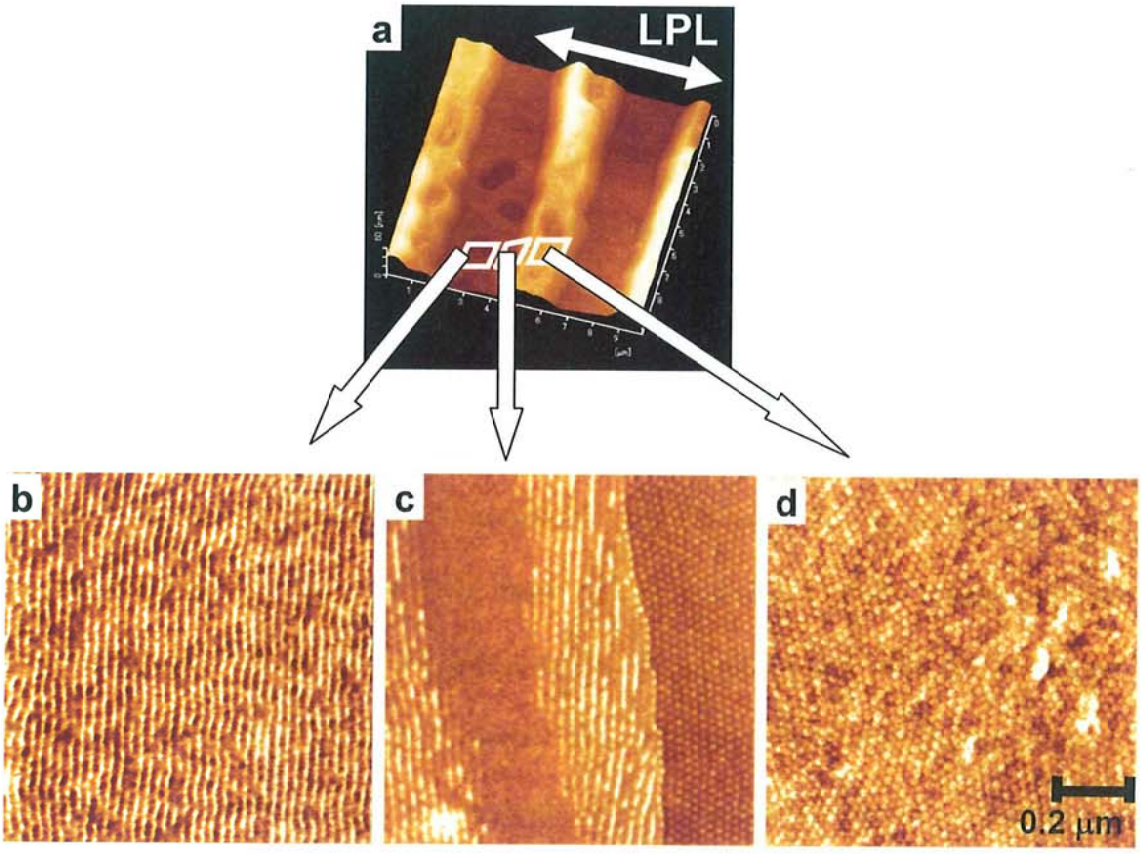

Figure 4-3. AFM images of the surface relief structure of the $p(EO_{114}\text{-}Az_{67})$ film after post-treatment. Topographic AFM image (10 x 10 μm) of a photogenerated relief (**a**), and corresponding magnified phase mode images (1.0 x 1.0 μm) at the trough (**b**), boundary region (**c**) and crest (**d**) resulted from the (*p*-: *p*-) mode holographic irradiation at 5 J cm^{-2} .

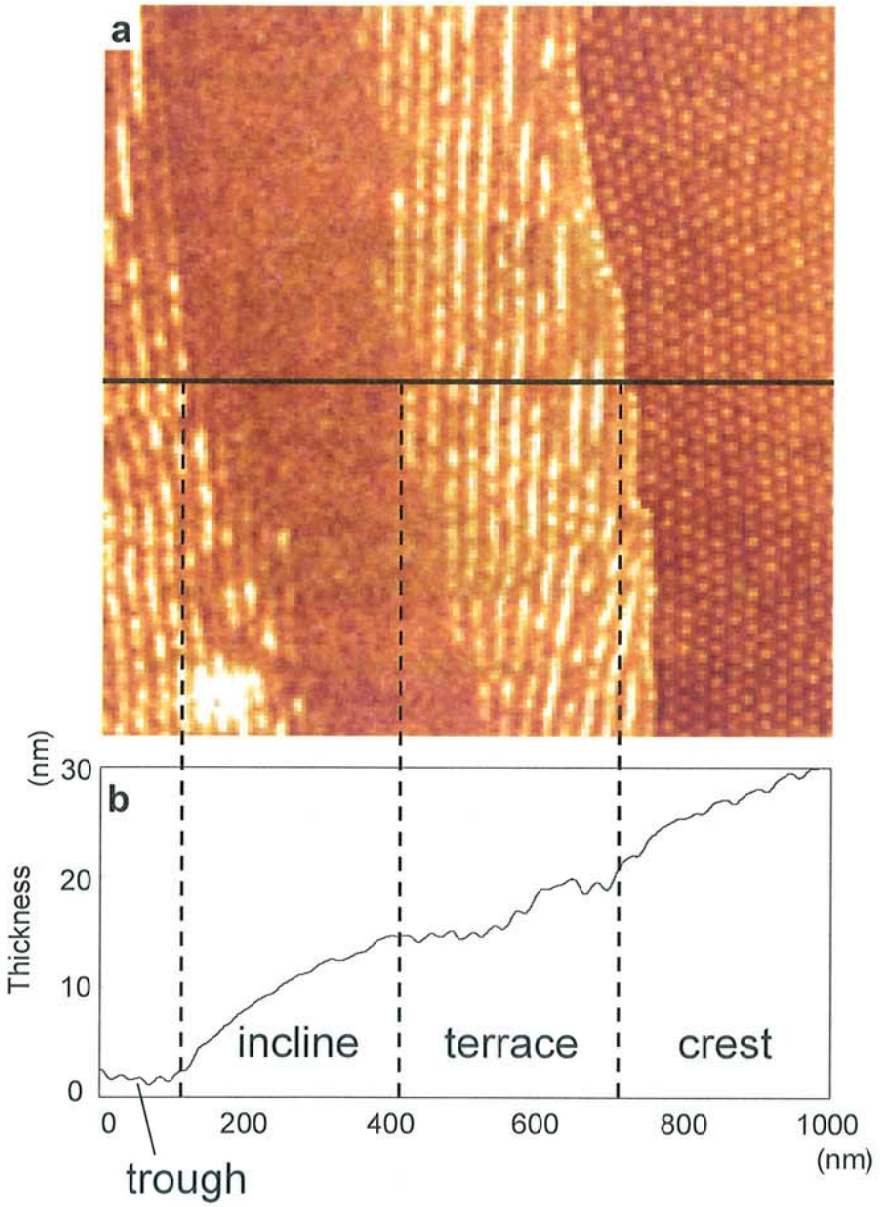

Figure 4-4. AFM data of the surface relief structure at the boundary region of the p(EO_{114}-Az_{67}) film after post-treatment. Phase mode AFM image (1 x 1 μm) of the photogenerated relief (**a**), and cross section of the topographic AFM image corresponding to the black line indicated in a (**b**).

out-of-plane and in-plane control of the hierarchical structure of the microphase separation were accomplished.

4.3.3 Cylinders alignment via photo-triggered mass migration in thicker film

When the thicknesses of the film at the trough and top of crest were above 70 nm in photo-generated relief structure, cylinders are expected to orient normal to the substrate plane in whole area of film on account of thickness dependence of cylinder alignment. Figure 4-5 displays the AFM data in a thicker relief film after post-treatment. The thickness of the film at the trough and crest were ca. 70 nm and 300 nm, respectively. Figures 4-5b and 5c show the phase images taken at the trough and crest area, respectively. The cylinders oriented perpendicular to the substrate plane at the both areas of trough and crest. In this way, 3D patterning of nanostructures alignment was not provided by surface relief formation in this thickness. This result confirms the importance of the thickness dependence on the cylinder alignment.

4.3.4 Cylinders alignment via photo-triggered mass migration on a hydrophobic substrate surface

The cylinders oriented perpendicular to the substrate plane on a hydrophobic substrate regardless of the thickness change (Chapter 2.3.4). The application of relief formation to the thin film on a hydrophobic substrate allows the preparation of a template where the cylinders orient normal to the film in the whole area of relief structure. Figure 4-6 displays the AFM data in the relief on a hydrophobic substrate after post-treatment. The thickness of the film at the trough and crest were ca. 30 nm and 70 nm, respectively. Figures 4-6b and 6c show the phase images taken at the trough and crest area in figure 4-6a, respectively. As shown, only dots morphology was observed in both AFM images. The cylinders were preferably oriented perpendicular to

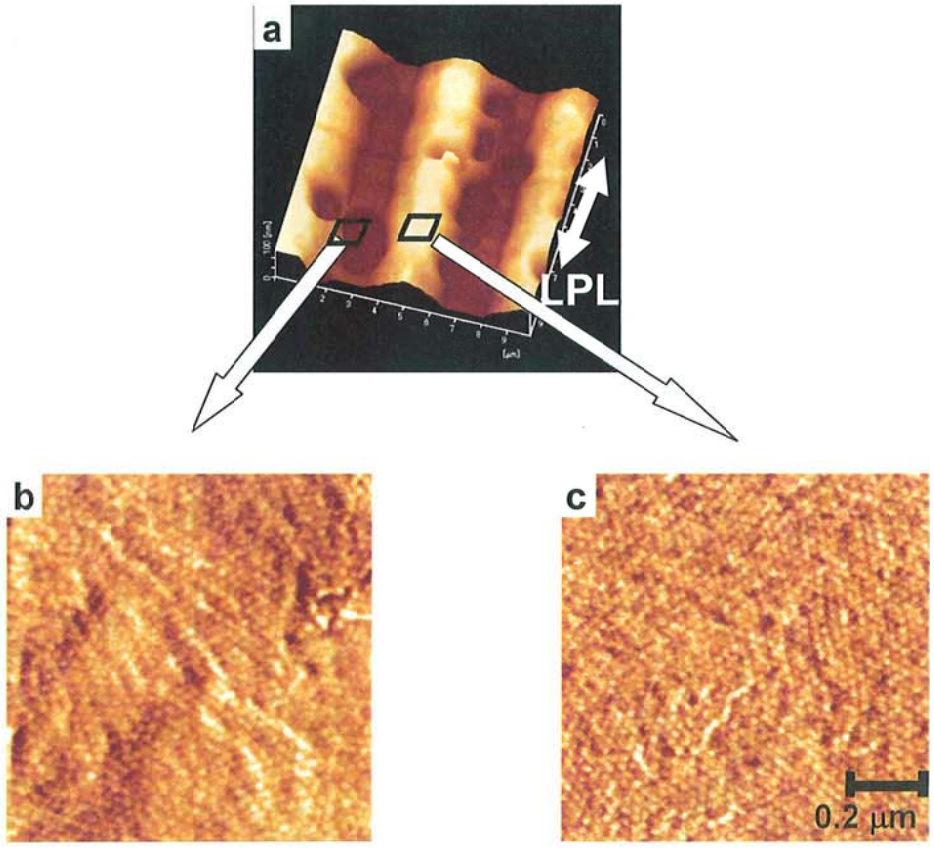

Figure 4-5. AFM images of the surface relief structure of the $p(EO_{114}\text{-}Az_{67})$ thick film after post-treatment. Topographic AFM image (10 x 10 μm) of the photogenerated relief (**a**), and corresponding magnified phase mode images (0.8 x 0.8 μm) at the trough (**b**) and crest (**c**) resulted from the (*s*-: *s*-) mode holographic irradiation at 400 mJ cm^{-2} .

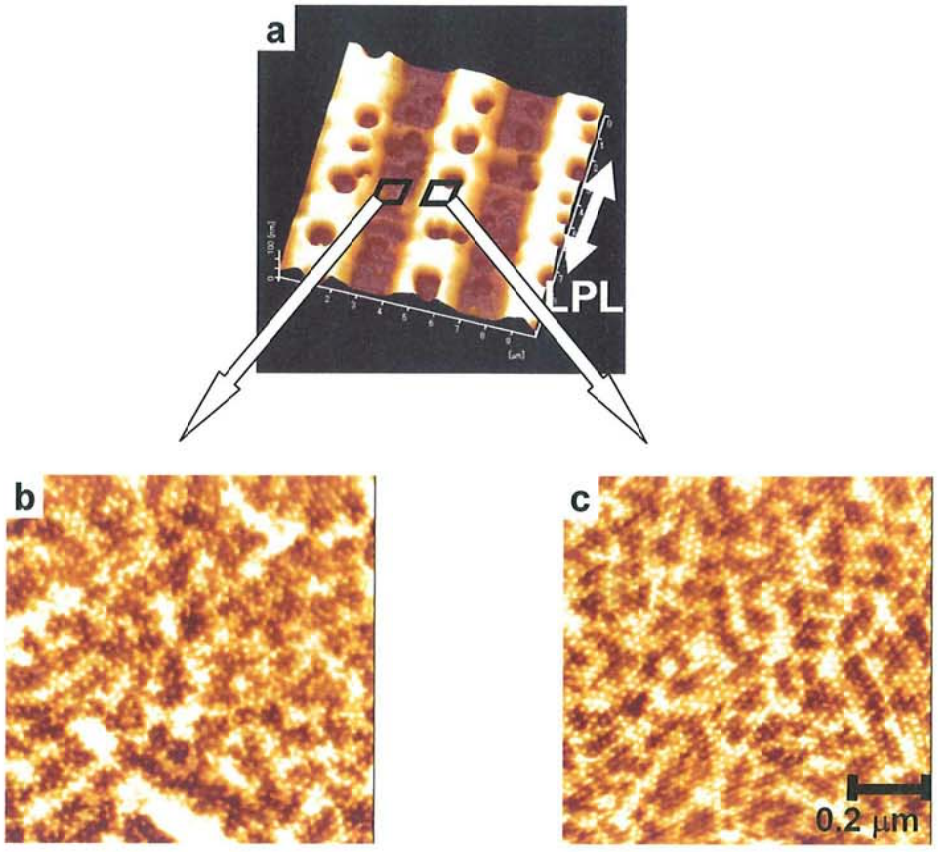

Figure 4-6. AFM images of the surface relief structure of the p(EO_{114}-Az_{67}) film on a hydrophobic substrate after post-treatment. Topographic AFM image (10 x 10 μm) of the photogenerated relief (**a**), and corresponding magnified phase mode images (1.0 x 1.0 μm) at the trough (**b**) and crest (**c**) resulted from the (*s*-: *s*-) mode holographic irradiation at 400 mJ cm^{-2} .

the substrate plane at both areas of trough and crest.

4.3.5 LPL irradiation through a photomask

The LPL irradiation was performed onto a hybrid thin film with 60 nm thickness through a photomask. Figure 4-7 presents AFM images of the resulting relief structure after the post-treatment. As indicated, large undulations in accord with the line and space (10 μm period) mask pattern (a) were obtained. The height difference from the top to trough reached 60 nm. The parallel and perpendicular orientation of cylinders were observed at the tough and crest areas, respectively (b and c). The trough area exhibited horizontally aligned cylinders with orientation at a tilt to the edges of the crests, i.e., perpendicular to the electric field vector of polarized light of mask irradiation. The direction of in-plane alignment of laid cylinders after this irradiation process can be freely installed, which is in contrast to the situation of the holographic irradiation process. The cylinders can be oriented at any directions, namely parallel, perpendicular, and tilted to the edges of the undulations relying on the angle between the mask pattern and the LPL direction.

4.4 Conclusion

The way of pattern irradiation of LPL and the resulting hierarchical pattern of cylinder alignment in the corrugated p(EO_{114}-Az_{67}) films are shown in Figure 4-8. Upon holographic irradiation to the p(EO_{114}-Az_{67})/5CB hybrid film, the film underwent efficient mass transfer to form a corrugated relief structure. When the film thicknesses at the crests and troughs range above and below the criterion level of 70 nm, the out-of plane control of cylinder arrays was achieved. The in-plane control for the laid cylinders was attained by selecting the polarization mode of holographic irradiation. The mask

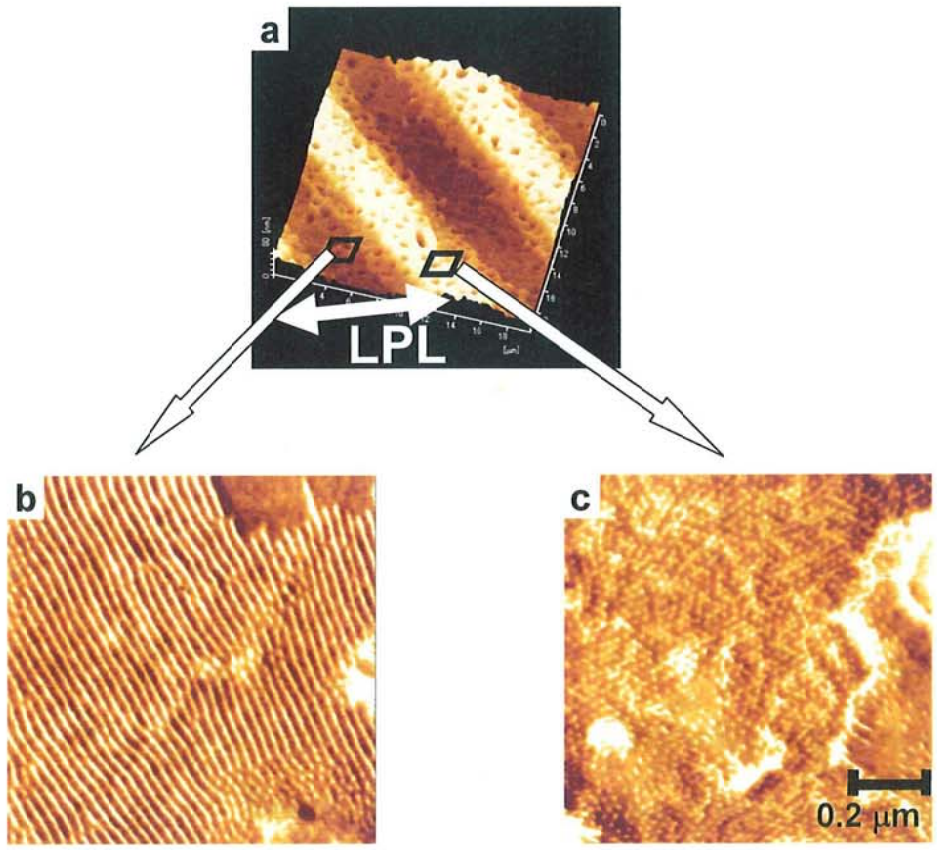

Figure 4-7. AFM images of the surface relief structure of the $p(EO_{114}\text{-}Az_{67})$ film after post-treatment. Topographic AFM image (10 x 10 μm) of a photogenerated relief (**a**), and corresponding magnified phase mode images (1.0 x 1.0 μm) at the trough (**b**) and crest (**c**) resulted from irradiation through a line and space phtomask at 5 J cm^{-2} .

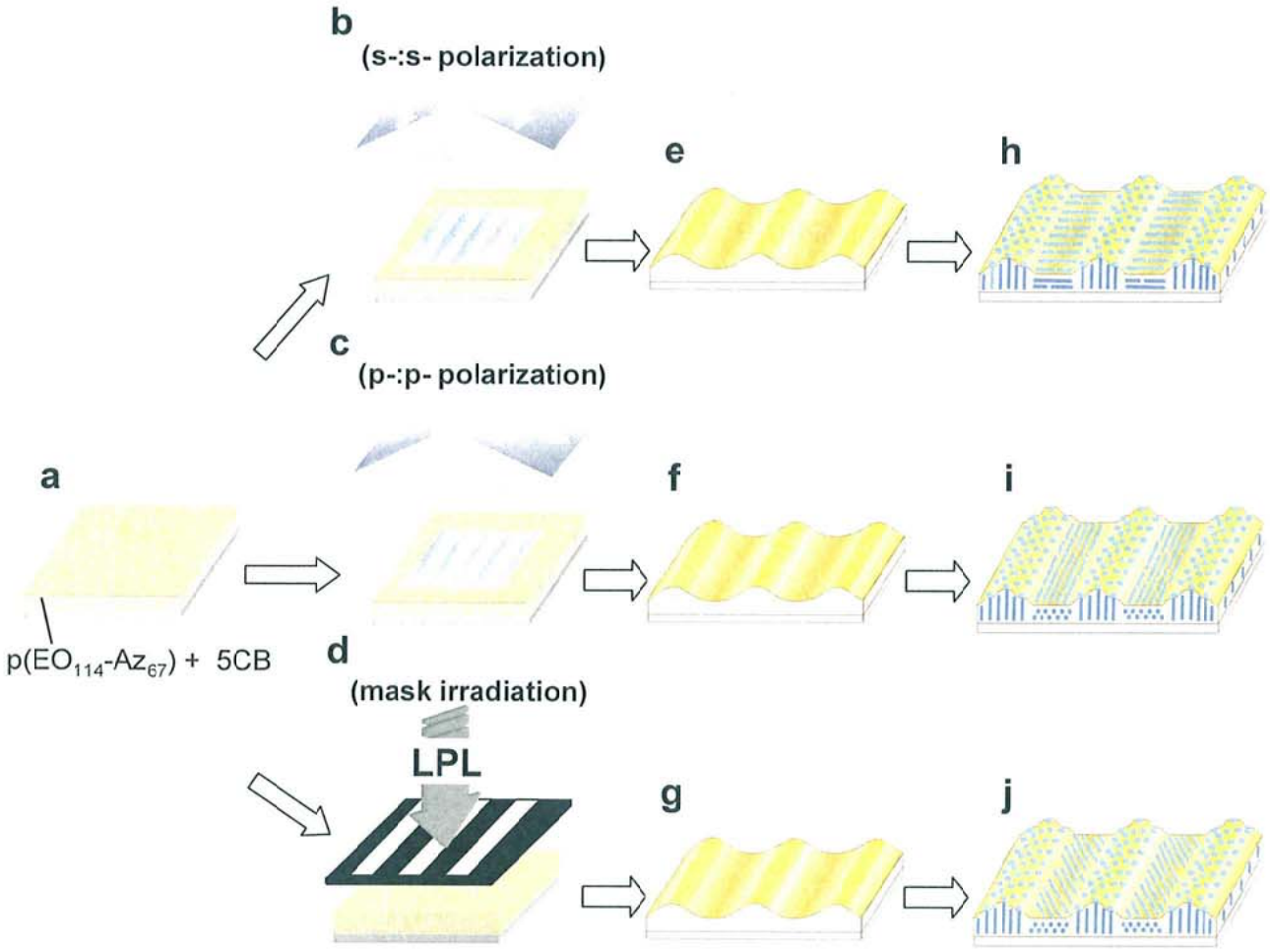

Figure 4-8. Schematic illustration of the strategy for the photo-patterning and alignment of nanostructure. (**a**): A hybrid film consisting of diblock copolymer and 5CB. **b** and **c**: Interference exposure of polarization beam of (*s*-: *s*-) (**b**) or (*p*-: *p*-) (**c**) mode holographic illumination of two beams of argon ion laser. The arrows indicate the direction of the electric field vector of linearly polarized light. (**d**): LPL irradiation through a photomask. **e** – **g**: Photogenerated relief structure with an interference or mask pattern. **h** – **j**: The resulting hierarchical structures where photoaligned PEO nanoscale cylinders are incorporated into the corrugated relief structure at a micrometer scale.

irradiation could be also applied to control the cylinders alignment as well as the above process. Here, the 3D alignment and patterning of nanostructures were attained by all optical procedures without any modifications of substrate[1,2] or mechanical manipulations.[3-5]

Reference

1. R. A. Segalman, H. Yokoyama, E. J. Kramer, *Adv. Mater.*, **2001**, *13*, 1152.
2. D. Sundrani, S. B. Darling, S. J. Sibener, *Nano. Lett.*, **2004**, *4*, 273.
3. S. O. Kim, H. H. Solak, M. P. Stoykovich, N. J. Ferrier, J. J. de Pablo, P. F. Nealey, *Nature* **2003**, *424*, 411.
4. M. P. Stoykovich, M. Müller, S. O. Kim, H. H. Solak, E. W. Edwards, J. J. de Pablo, P. F. Nealey, *Science* **2005**, *308*, 1442.
5. E. W. Edwards, M. P. Stoykovich, H. H. Solak, P. F. Nealey, *Macromolecules* **2006**, *39*, 3598.

Chapter 5

3D photoalignment and reorientation of nanostructures in PS-based block copolymer film

5.1 Introduction

In the previous chapters, 3D photoalignment and patterning of nanocylinders were achieved in diblock copolymer connecting PEO with Az polymer. For enhancement of thermal and mechanical stability, in this chapter, polystyrene-based block copolymers possessing higher T_g are of main target. The good physical properties of polystyrene (PS) should play an important role for nanotechnological applications such as the nanowires and nanotemplates, etc. The syntheses and characterizations of Az-containing block copolymer films have been investigated by several research groups. Ober's group first synthesized and characterized a series of diblock copolymers consisting of PS and Az-containing LC polymer derived from polyisoprene.[1] Schmidt and coworkers observed the microphase separated structure of a PS-based diblock copolymer connected with amorphous Az-containing polymer. They found that the photoinduced mass migration is highly hindered by the block architecture in comparison with the behavior of a statistical random copolymer of the same composition, and applications to photoaddressing for optical information are demonstrated.[2] Zhao and coworkers discussed the confinement effects on the photoalignment of liquid crystalline Az side chains within the microphase separated structures.[3]

This chapter demonstrates the 3D photoalignment and reorientation of the nanostructures in a PS-based block copolymer (Figure 5-1) thin film. The diblock

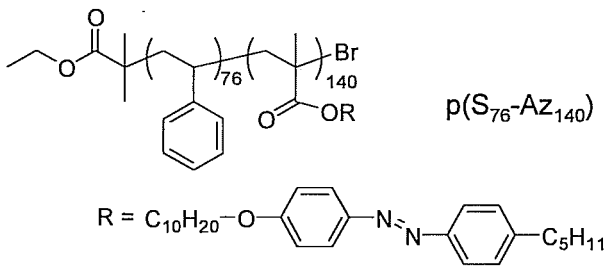

Figure 5-1 Chemical structure of $p(S_{76}\text{-}Az_{140})$.

Table 5-1. Thermal transition properties and notation of the studied Az containing diblock copolymer ($p(S_x\text{-}Az_y)$).

polymer	M_n[a]	M_w/M_n[b]	phase transition (°C)	LC (wt%)
$p(S_{76}\text{-}Az_{140})$	77000	1.21	G 43 Sm_X 90 Sm_A 118 I	92
$p(S_{226}\text{-}Az_{56})$	52000	1.22	G 43 Sm_X 60 Sm_A 115 I	54

[a] M_n, number average molecular weight estimated by ^{1}H-NMR. [b] M_w/M_n, Polydispersity determined by GPC.

copolymer used in this study is synthesized by atom transfer radical polymerization (ATRP) method. The orientation of nanostructures is estimated by AFM and UV-vis absorption spectral measurements.

5.2 Experiments

5.2.1 Synthesis of diblock copolymer

5.2.1.1 Materials

N, *N*'-Dimethyl formamide (DMF) as solvent was dehydrated by distillation from calcium hydride. Anisole and tetrahhydrofurane (THF) as solvents was distilled from sodium with benzophenone. Styrene was purified by distillation to remove inhibitor before use. Catalyst CuBr (Kanto Chem. Co., Japan) was washed with acetic acid containing a drop of HCl solution and diethyl ether for several times, and dried in vacuum. Other compounds were used without further purification.

5.2.1.2 Preparation of Macroinitiator Polystyrene-Br (PS-Br)

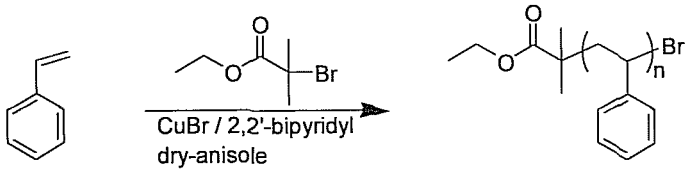

PS-Br

A flask was charged with 7.17 mg of CuBr, degassed and filled with N_2 gas. 3.12 g of styrene, 9.75 mg of 2-bromoisobutyric acid and 78.1 mg of 2,2'-bipyridyl in 1 ml of anisole were degassed, filled with N_2 gas and added through a syringe. The mixture was degassed by freeze-pump-thaw procedure and sealed under vacuum. The flask was placed in oil bath at 110 °C for 11 h. The reaction mixture was dissolved in THF and passed through alumina column to remove Cu catalyst. After being concentrated, The THF solution was poured to methanol to remove styrene monomer. The final product

was dried under vacuum. Yield: 350 mg (11.2 %). M_n = 8000 and M_w/M_n = 1.05.

5.2.1.3 Preparation of Az monomer

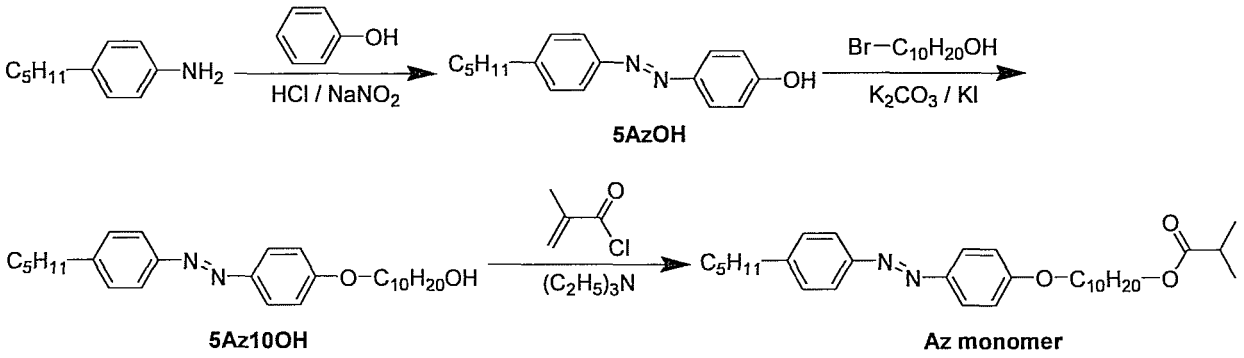

The synthesis of Az monomer was performed according to the above scheme.

4-[(4'-Pentylphenyl) azo] phenol (5AzOH)

4-Pentylaniline (25 g, 153 mmol) was dissolved in a mixture of concentrated hydrochloric acid (25 mL) and water (100 mL). Sodium nitrate (13.2 g, 191 mmol) in water (80 mL) was added dropwise to the above solution at 5 °C. An aqueous solution (800 mL) dissolving phenol (17.6 g, 187 mmol) and sodium hydroxide (9.42 g, 235 mmol) was then added dropwise under stirring. The solution was stirred for 2 h at 5 °C and 3 h at room temperature. After this solution was neutralized with a diluted hydrochloric acid aqueous solution, the precipitate was filtered off and dissolved in ethyl acetate. The solution was washed with water, sodium bicarbonate aqueous solution and water and NaCl aqueous solution, and then, dried over anhydrous magnesium sulfate. The precipitate was recrystallized from hexane twice to give yellow platelet crystals.

Yield: 24.9 g (60.6 %)

4-(10-Hydroxydecyloxy)-4'-pentylazobenzene (5Az10OH)

Potassium carbonate (25.7 g, 186 mmol) and catalytic amount of potassium iodide

were added to 5AzOH (10.0 g, 37.3 mmol) in dry DMF (90ml), and then mixture was stiired for 1 h at 60 °C. 10-Bromodecanol (15.9 g, 67.1 mmol) in dry DMF (10ml) was added dropwise to the solution. The solution was stirred for 4h at 60 °C. The reaction mixture was washed with water, sodium bicarbonate aqueous solution and NaCl aqueous solution, and then, dried over anhydrous magnesium sulfate. The solution was evaporated and separated out a solid. This product was recrystallized from methanol to give yellow solid.

Yield: 15.4 g (81.1 %).

4-(10-Methacryloydecyloxy)-4'-pentylazobenzene (Az monomer)

Trietylamine (7.16 g, 70.8 mmol) was added to 5Az10OH (15.0 g, 35.4 mmol) in dry THF solution. A dry THF solution of methacryloyl chloride (7.36 g, 70.8 mmol) was added dropwise to the solution at 0 °C. The mixture was stirred for 30 min at 0 °C and 12 h at room temperature. The reaction mixture was evaporated, and chloroform was added. The solution was washed with water, sodium bicarbonate aqueous solution and NaCl aqueous solution, and then, dried over anhydrous magnesium sulfate. The solvent was evaporated and the residue was recrystallized from methanol. Yellow solid was obtained.

Yield: 10.4 g (60.0 %).

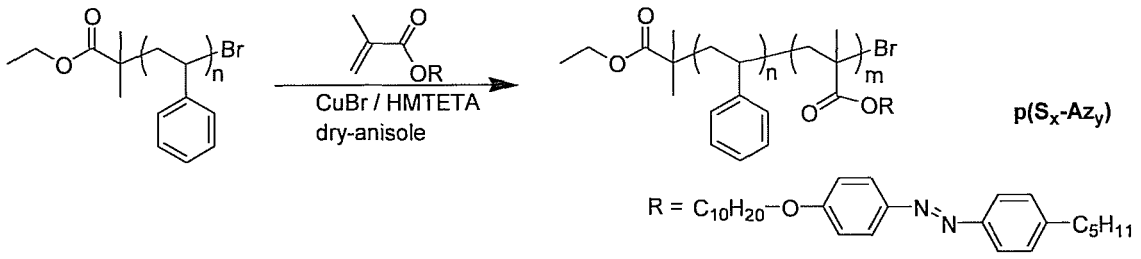

5.2.1.4 Preparation of Az-containing diblock copolymer ($p(S_x\text{-}Az_y)$)

A 10 ml ample tube was charged with 37.6 mg of PS-Br, 399 mg of Az monomer,

8.99 mg of HMTETA and 1 ml of THF. After several freeze-pump-thaw cycles, 5.59 mg of CuBr was immediately inserted in the ample tube. The mixture was degassed by freeze-pump-thaw procedure and sealed under vacuum. The flask was placed in 70 °C oil bath for 17 h. The solution was passed through alumina column with chloroform. The solution was concentrated and precipitated in hexane, methanol and finally in hot hexane (60 °C). The precipitation process in each solvent was repeated twice, respectively. The final product was dried under vacuum. Yield: 70 mg (16.0 %). M_n = 77000 and M_w/M_n = 1.21. Thermal phase properties for Az polymer block: Sm_X-90 °C-Sm_A-118 °C-I, Tg of polystyrene = 102 °C.

5.2.2 Characterizations of p(S_x-Az_y)

Molecular weight and polydispersity were measured by gel permeation chromatography (GPC) using a liquid chromatograph (Shodex UV-41) with an appropriate combination of columns (Shodex KF-803L and Shodex KF-805L). THF was used as eluent, and polystyrene standards were used for calibration. ^{1}H-NMR spectrum was recorded on a JEOL 270GXS instrument spectrometer (270 MHz). Phase transition temperatures were measured with a Seiko Instrument DSC6200/EXSTAR6000 (heating and cooling rates: 10 °C/min).

5.2.3 Preparation of p(S_{76}-Az_{140}) thin films

The p(S_x-Az_y) thin films having film thickness of ca. 100 nm were spin-coated from chloroform solutions on hydrophilic quartz substrates. They were annealed at 107 °C, above T_g of PS block and below the transition temperature of Sm_A to isotropic transition of the Az polymer block, for 12 h.

5.2.4 Estimation of nanostructures orientation

The surface morphologies and film thickness of the films were evaluated by AFM

using a Seiko Instrument SPA400/SPI3800N system in the dynamic force mode. UV-visible absorption spectra were recorded on a Hewlett Packard 8452A diode array spectrometer. Polarized UV-visible absorption spectra were recorded on that spectrometer equipped with a polarizer unit. LPL and non-LPL (436 nm) irradiation were performed at 2.0 mW cm^{-2} for 50 min at 130 °C, followed by gradual cooling at 2 °C min^{-1} to 30 °C with a San-ei Supercure-202S.

5.3 Results and Discussion

5.3.1 Orientation of nanocylinders in p(S_{76}-Az_{140}) thin film

The diblock copolymer consisting of polystyrene and Az polymer was synthesized by ATRP method. The GPC, ^{1}H-NMR, DSC and notation of PS-based block copolymers dealt with in the below chapters are summarized in Table 5-1. The polymer used in this chapter is denoted as p(S_{76}-Az_{140}), where the indices indicate the number of each unit. The polymerization degree of that was determined by GPC chart (Figure 5-2) and ^{1}H-NMR spectrum (Figure 5-3) of p(S_{76}-Az_{140}). The weight fraction of Az polymer was 0.92. This polymer had two T_g's at 43 °C and 102 °C, for the Az polymer block and PS block, respectively, indicating that the system is microphase-separated (Figure 5-4). The p(S_{76}-Az_{140}) thin film exhibited a cylinder morphology with PS cylinders placed in a Az matrix. AFM measurement revealed obvious oriented PS cylinders with an orthogonal orientation to the substrate after annealing (Figure 5-5a). UV-vis absorption spectra indicated that Az mesogens oriented orthogonal to the substrate, which oriented homogeneously to the cylinders in the corresponding film.

5.3.2 Photoalignment and reorientation of nanocylinders

The hierarchical alignment induction from Az mesogens to PS cylinders was

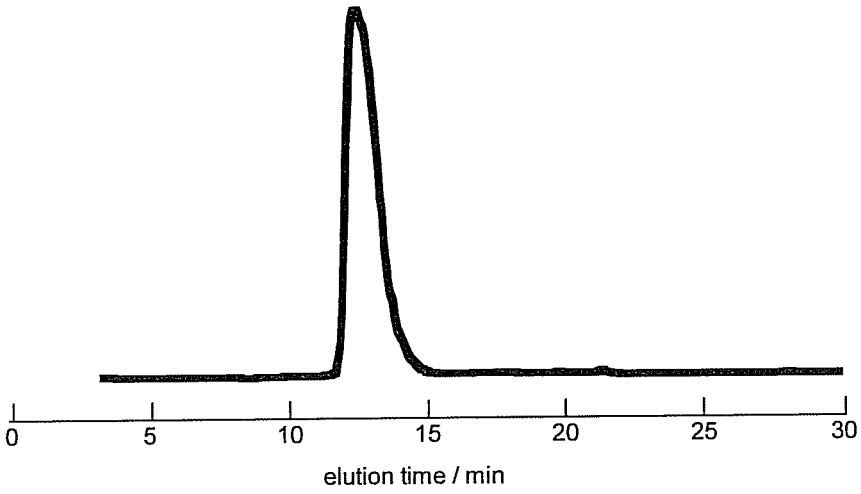

Figure 5-2 GPC chart of $p(S_{76}\text{-}Az_{140})$.

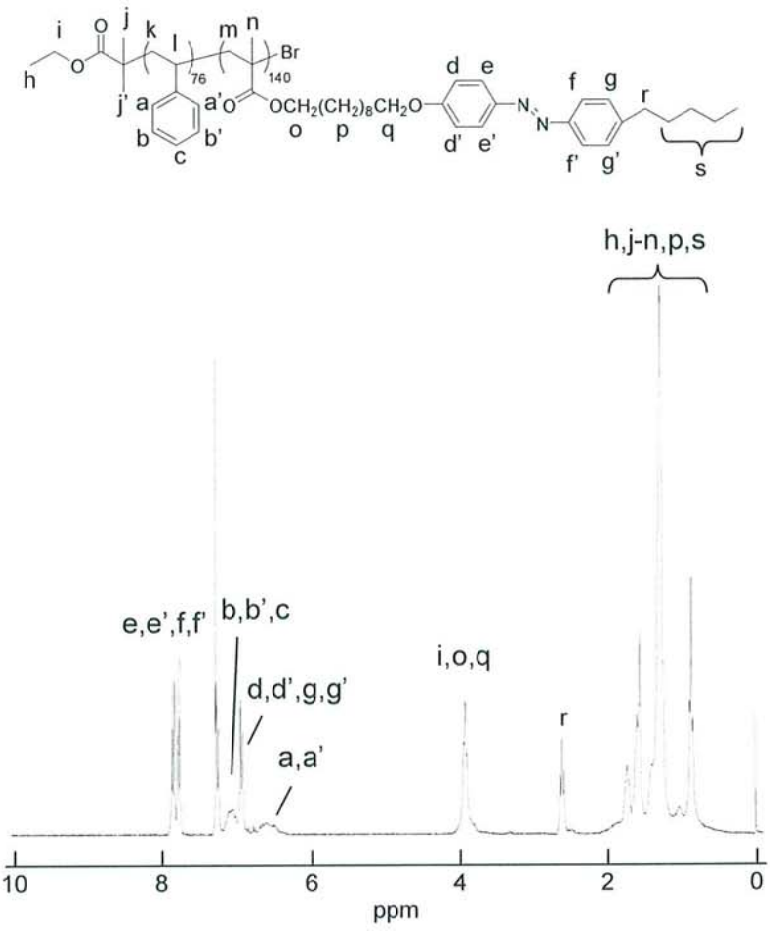

Figure 5-3 ^{1}H-NMR spectrum of p(S_{76}-Az_{140}).

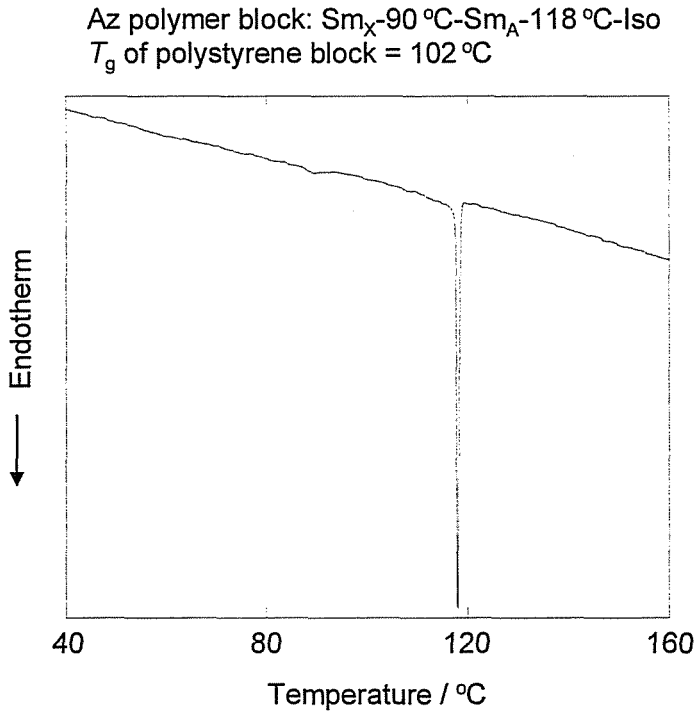

Figure 5-4 DSC chart of the $p(S_{76}\text{-}Az_{140})$ in a heating process. Heating rate: 10 °C/min.

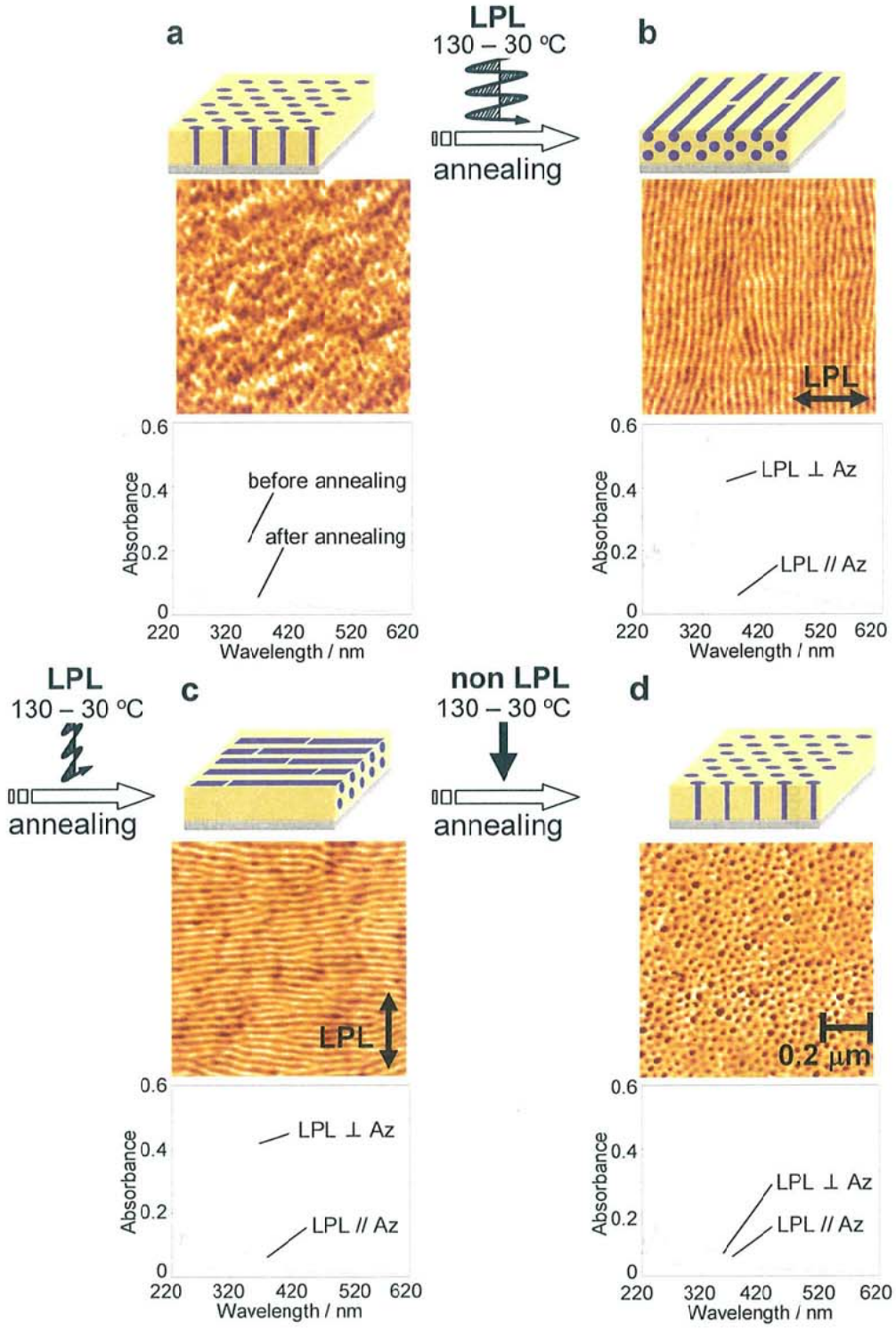

Figure 5-5 A series of optical controls of orientations of Az and PS cylinder in p(S_{76}-Az_{140}) film evaluated by phase mode AFM and polarized UV-vis absorption spectroscopy. (**a**) The initial state. The annealing induces the perpendicular orientation to the substrate for both Az and PS cylinder. (**b**) After irradiation with LPL (436 nm) followed by annealing. (**c**) Successive irradiation with LPL (436 nm) at different polarization angle by 90° followed by annealing. (**d**) After irradiation with non-polarized light (436 nm) followed by annealing.

attempted by a photoprocess for diblock copolymer thin film. As shown in Figure 5-5, obvious photoalignment and reorientation of hierarchical structure were confirmed.

Figure 5-5 displays the surface morphologies (3.0 x 3.0 μm) and UV-visible absorption spectra of light-irradiated p(S_{76}-Az_{140}) films of ca. 100 nm thickness. For the irradiated film, the LPL exposure (436 nm) was performed at 2.0 mW cm^{-2} for 50 min at 130 °C, followed by gradual cooling at 2 °C min^{-1} to 30 °C. For evolution of nanostructure, the films were successively annealed at 107 °C, slightly above T_g of polystyrene block and below the Sm_A transition to isotropic transition of the Az polymer block, for 12 h. Non-irradiated film provided PS cilynders in the upright orientation (a) after annealing. The spectral data also indicates that the annealing induces the Az orientation normal to the substrate plane. The reduction of absorbance of π–π^* band whose transition moment is along the long axis of Az peaking at 338 nm indicated this fact. The diameter of the cylinder was 14 ± 1 nm with average cylinder to cylinder distance of 32 nm. After LPL irradiation, a line morphology whose direction highly aligned orthogonal to the direction of LPL (b) was obtained. The average line to line distance was 32 nm, which agrees with that evaluated above. Also, the Az chromophores showed a strong in-plane anisotropy with the orientational order parameter S = 0.68. The same procedure was successively performed using LPL set at another angle, orthogonal to the previous irradiation (c). Essentially the same results on the line morphology and spectral data were obtained except for the direction of molecular orientation (S = 0.68) and line morphology. The cylinders aligned in the in-plane direction were again reverted to the out-of-plane (normal) mode by irradiation of non-polarized light irradiation in the normal direction (d). Az chromophores were also reoriented normal to the substrate plane, resulting in disappearance of in-plane

anisotropy. The state shown in the final state virtually corresponded to the initial state (a). These facts unequivocally indicate that 3D alignment, namely both in-plane and out-of-plane orientational control, and reorientation of PS cylinders are achieved by light.

When the LPL irradiation was performed at room temperature, the morphological feature of cylinders was unaltered, and only the orientation of Az mesogens was photoaligned. This result indicates that the alignment control of cylinders can be achieved on optimized thermal conditions in the photoprocess. In the process of cooling from 130 °C to 30 °C, the cylinders exhibit a random orientation in the isotropic state of the Az polymer block at above 118 °C. And subsequently, in the LC state of the Az polymer at below 118 °C, the cylinders seem to be oriented in the same direction as one of the Az mesogens. As the consequence, the cylinders and Az mesogens are both aligned cooperatively.

5.3.3 Photopatterning of nanocylinders

Photopatterning of cylinder orientation was examined by utilizing reorientation process of aligned cylinders (Figure 5-6). The LPL irradiation was performed onto a horizontally aligned film (a) through a line and space (10 μm period) photomask followed by annealing. The topographical image of the resulting film indicated that the surface was flat within 4 nm. The phase mode images (c – e) clearly indicated the patterned orientation of the nanocylinders. The LPL-irradiated area exhibited the in-plane orientation of the cylinders orthogonal to the direction of LPL (c). The perpendicular orientation of cylinders once changes to the isotropic state and then again reverted to normal orientation via self-assembly in non-irradiated area (e). The observation of the boundary region indicated that there was no gradient region between

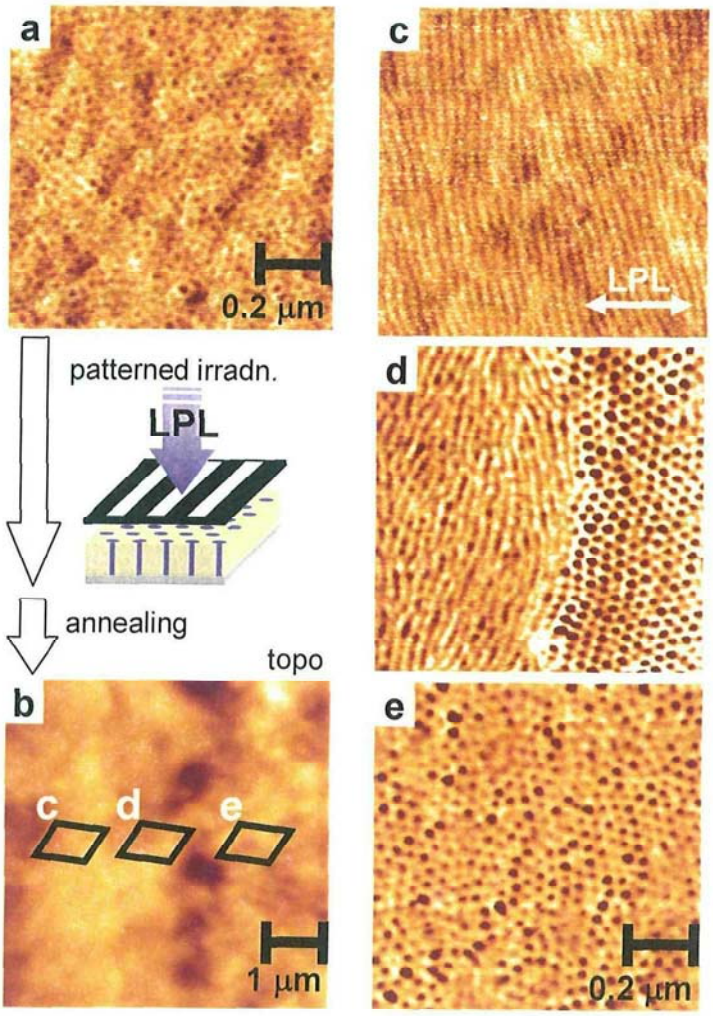

Figure 5-6 Orientational control of PS cylinder by patterned irradiation of LPL (436 nm) in p(S76-Az140) film (thickness = ca. 100 nm). (**a**) The initial state where all cylinders were in the perpendicular orientation. (**b**) Topographical AFM image after patterned irradiation with LPL. (**c** – **e**) Phase mode AFM images taken at the irradiated area (**c**), boundary region (**d**), and non-irradiated area (**e**).

the two oriented area (d). These morphological features suggested that on-demand 3D photoalignment and patterning were attained. Without modulation of film surface, the photo micropattern of cylinder orientation was obtained in a flat film.

5.4 Conclusion

In this chapter, the PS-based diblock copolymer possessed higher T_g than the PEO block was dealt with. The both in-plane and out-of-plane alignment of nanostructures were controlled in this thin film by light illumination while heating. For the PS cylinders having orthogonal orientation, the LPL exposure gave in-plane alignment of those with orientation orthogonal to the direction of LPL. The following in-plane alignment orienting another direction and initial alignment state in which cylinders were oriented perpendicular to the substrates were obtained by additional LPL and non-LPL exposure, respectively. These photoorientation behaviors allowed the on-demand 3D photopatterning of the cylinders.

Reference

1. G. Mao, J. Wang, S. R. Clingman, C. K. Ober, J. T. Chen, E. L. Thomas, *Macromolecules* **1997**, *30*, 2556.
2. (a) C. Frenz, A. Fuchs, H. –W. Schmidt, U. Theissen, D. Haarer, *Macromol. Chem. Phys.* **2004**, *205*, 1246. (b) M. Häckel, L. Kador, D. Kropp, C. Frenz, H. –W. Schmidt, *Adv. Func. Mater.* **2005**, *15*, 1722.
3. X. Tong, L. Cui, Y. Zhao, *Macromolecules* **2004**, *37*, 3101.
4. C. –Y. Chao, X. Lie, C. K. Over, C. Osuji, E. L. Thomas, *Adv. Func. Mater.* **2004**, *14*, 364.

Chapter 6

Memory Effect of Liquid Crystalline Phase in Hierarchical Structure of Diblock Copolymer

6.1 Introduction

The previous chapter dealt with photoalignment of the "cylinder" forming nanodomains. In this chapter, the photoalignment of the "lamellar" structure in a diblock copolymer of the similar polystyrene-based diblock copolymer with different block lengths is described. Moreover, due to the fixed nature of the PS domains, it is expect that different photoaligning behavior would be observed. It is found here that an obvious memory effect in the alignment of LC mesogens is observed resisting to the subsequent photo-reorientation. The diblock copolymer used in this study is denoted as p(S_{226}-Az_{56}), where the indices indicate the number of each unit (Figure 6-1). Due to the larger volume fraction of the PS block, this polymer adopts a lamellar structure. The morphological features and molecular orientation of LC mesogens are studied by AFM observations and wide angle x-ray scattering (WAXS) measurements, respectively.

6.2 Experiments

6.2.1 Materials

The diblock copolymer, p(S_{226}-Az_{56}), was prepared by the same process as synthesis procedure reported in Chapter 5.2.1. 5CB was obtained from Merck.

6.2.2 Preparation of pure p(S_{226}-Az_{56}) and hybrid p(S_{226}-Az_{56})/5CB films

The pure p(S_{226}-Az_{56}) films having film thickness of ca. 300 nm were spin-coated

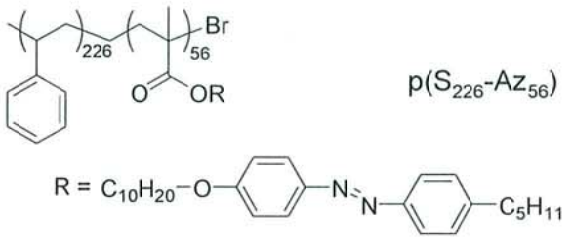

Figure 6-1 Chemical structure of $p(S_{226}\text{-}Az_{56})$.

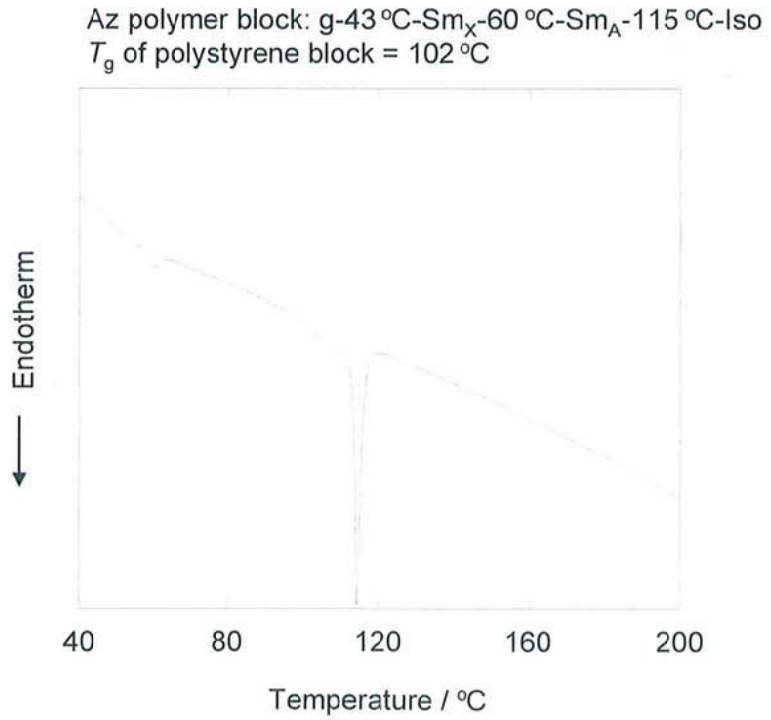

Figure 6-2 DSC chart of the $p(S_{226}\text{-}Az_{56})$ in a heating process. Heating rate: 10 °C/min.

from chloroform solutions on hydrophilic quartz substrates. The hybrid $p(S_{226}\text{-}Az_{56})$/5CB film with ca. 100 nm thickness was spin-coated from chloroform solutions at a molar mixing ratio f =0.8, f being the molecular fraction of 5CB([5CB]/([Az unit]+[5CB])), onto a hydrophilic quartz substrate.

6.2.3 Formation of Surface Relief Structure

The experimental setup for the holographic recording has been described in Chapter 3.2.3. UV light (365 nm) irradiation was first performed to undergo the photoisomerization to the cis-rich state with a San-ei Supercure-202S. Onto this film the holographic irradiation was performed with a coherent argon ion laser (Omnichrome 543R-AP-A01, 488 nm). The topographic image was observed by AFM.

6.2.4 Evaluations of nanostructure and molecular orientation

The surface morphologies and film thickness of the films were evaluated by AFM using a Seiko Instrument SPA400/SPI3800N system in the dynamic force mode. UV-visible absorption spectra were recorded on a Hewlett Packard 8452A diode array spectrometer. Polarized UV-visible absorption spectra were recorded on this spectrometer equipped with a polarizer unit. Wide angle x-ray scattering (WAXS) measurements were performed with a Rigaku FR-E using CuK_α radiation (λ = 0.154 nm) at 45 kV. The diffraction patterns were taken on an imaging plate. LPL and non-LPL (436 nm) irradiation were performed at 2.0 mW cm^{-2} for 50 min at 130 °C, followed by gradual cooling at 2 °C min^{-1} to 30 °C with a San-ei Supercure-202S.

6.3 Results and Discussion

6.3.1 Characterization of $p(S_{226}\text{-}Az_{56})$

The block copolymer, $p(S_{226}\text{-}Az_{56})$, was synthesized according to the atom transfer

radical polymerization (ATRP) method. As shown in Table 5-1, the resulting polymer possessed the unit numbers of PS and Az polymer of 226 and 56, respectively, with polydispersity of 1.22 based on the GPC and NMR measurements. The weight fraction of Az polymer was 0.54. The almost equivalent weight fractions of two polymer blocks support that lamellar structure is formed in diblock copolymer film.[1,2] Figure 6-2 shows a DSC chart of the p(S_{226}-Az_{56}). This polymer exhibited the glass transition temperatures (T_g's) at 43 °C and 102 °C for the Az polymer block and polystyrene block, respectively. The transition temperatures of the Az-containing polymer were 60 °C (Sm_X-to-Sm_A) and 115 °C (Sm_A-to-iso).

6.3.2 Photoalignment of nanostructures in p(S_{226}-Az_{56}) thin film

Two film samples of p(S_{226}-Az_{56}) possessing ca. 300 nm thickness were prepared by spin-coating. The LPL exposure (436 nm) was performed at 2.0 mW cm^{-2} for 50 min at 130 °C, followed by gradual cooling at 2 °C min^{-1} to 30 °C. One of the irradiated films was annealed at 100 °C, below both T_g of PS block and the transition temperature of Sm_A to isotropic of the Az polymer block, for 12 h.[3] The other film was annealed at 107 °C above T_g of PS block and below the transition temperature of Sm_A to isotropic transition of the Az polymer block, in the same manner.

Figures 6-3a and 3b display the surface morphologies (3.0 x 3.0 μm) of the p(S_{226}-Az_{56}) thin films evaluated by the phase mode AFM measurements. Both films gave the periodic surface-perpendicular lamellae spaced at an equilibrium period, L_0 = 80 nm. The film annealed at 100 °C provided a same similar morphology but exhibited a randomly arranged fingerprint-like nanoscale periodic structure as the film prepared without exposure to LPL (a). When the film was irradiated with LPL at 107 °C, the periodic nanostructure was preferentially oriented orthogonal to the electric field vector

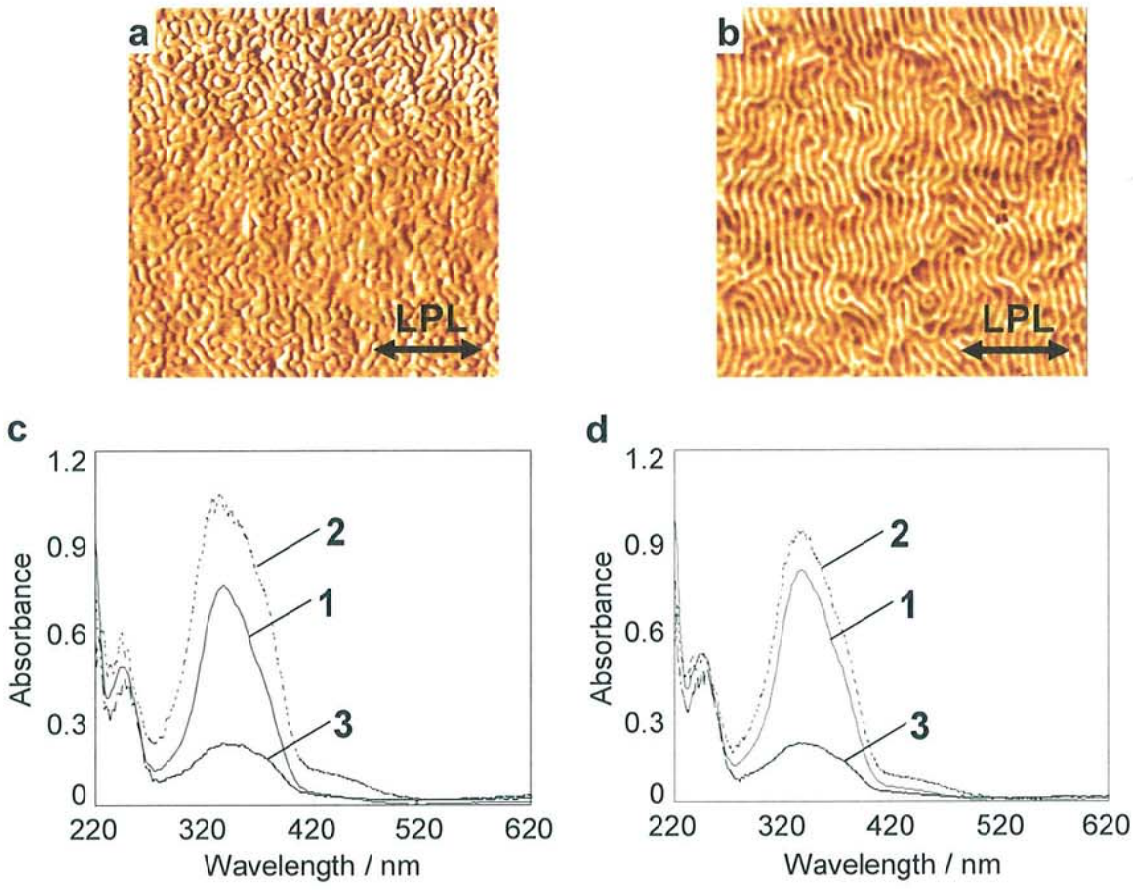

Figure 6-3 Phase mode AFM images (3.0 x 3.0 μm) of the LPL irradiated p(S_{226}-Az_{56}) films after annealing at 100 °C (**a**) and 107 °C (**b**). **c** and **d**, UV-vis absorption spectra of the corresponding films after annealing at 100 °C (**c**) and 107 °C (**d**). Spectrum **1**; as–cast film. **2** and **3** display polarized spectra taken with probing beam perpendicular and parallel to the polarization direction of the actinic irradiating 436 nm light.

of LPL (b).

Figures 6-3c and 3d show UV-visible absorption spectra of the corresponding films annealed at 100 °C and at 107 °C, respectively. Both LPL-irradiated films after annealing exhibited large in-plane anisotropy of Az mesogenic groups. The absorption band peaking at 338 nm became larger and smaller when observed with polarized light in orthogonal ($A\perp$, 2) and parallel ($A_{//}$, 3) to the polarization direction of the pre-irradiated LPL, respectively, showing that Az chromophores are highly oriented orthogonal to the electric field vector of LPL. The orientational order parameters (S) were 0.57 and 0.54 estimated from the spectra shown in Figures 6-3c and 3d, respectively.

As shown, the annealing at 107 °C above T_g of polystyrene and in Sm_A phase of the Az polymer was required for the evolution of photoalignement of hierarchical structure from LC mesogens to periodic nanostructures. These results indicate that sufficient segmental motions in polystyrene are of essence for the modulations of nanostructures. Comparisons with the spectral data and morphologies in Figure 6-3 leads to important conclusions that the photoorientation of the Az mesogens by LPL irradiation is readily attained, but that the alignment of microphase separated structure of the larger hierarchical size is only attained when the light-inert polymer segment has sufficient flexibility above T_g.

6.3.3 Memory effect of liquid crystalline orientation in hierarchical structure

6.3.3.1 Memory effect in the out-of-plane direction

For the pre-photoaligned film (Figure 6-3b), reorientation behaviors of Az mesogens and microphase separated nanostructures were examined. The orientation of nanostructures was confirmed by AFM measurements. The molecular orientation was

evaluated by WAXS measurements with grazing incidence as schematically illustrated in Figure 6-4a. The incident x-ray beam was set orthogonal (I) or parallel (II) to the orientation direction of the aligned microphase separated lamella structure of the photooriented p(S_{226}-Az_{56}) film. Figures 6-4 (b – f) display the obtained morphological features and WAXS patterns. In b, the initial state is depicted. The lamellar structure has aligned in one direction. In the WAXS pattern, two spots corresponding to a smectic *d* spacing of 3.5 nm (shown by arrows) were observed only in the beam direction I, clearly indicating the in-plane Az molecular orientation in parallel to the lamellar structure. An intense comet-tail-like image running along the out-of-plane direction is an artifact originated from a specular reflection.

This film was first subjected to non-polarized 436 nm light exposure from the normal direction to the film plane during the gradual cooling from 130 to 30 °C. Due to the angular-selected photoreaction, this procedure induces out-of-plane perpendicular orientation of Az units, and thus the smectic layer structure should orient parallel to the substrate plane. Appearance of clear arc images of 3.5 nm spacing in the out-of-plane direction in WAXS patterns in both beam directions in c instead of disappearance of the in-plane spots in b (I) implies the reorientation of the LC Az smectic layers as stated above. The morphological features of the microphase separated structures were unchanged in this procedure. The reoriented film was then subjected to UV (365 nm) light exposure at 5.0 mW cm^{-2} for 200 s at 70 °C, and held at this temperature for 30 min. The trans-to-cis photoisomerization of Az brings about an LC phase to isotropic transition, and thus the photoinduced molecular orientation will be lost. During the following adaptation at 70 °C, the thermal cis-to-trans back reaction occurs. The obtained WAXS patterns (d) were almost identical to the initial ones (b). Thus, the LC

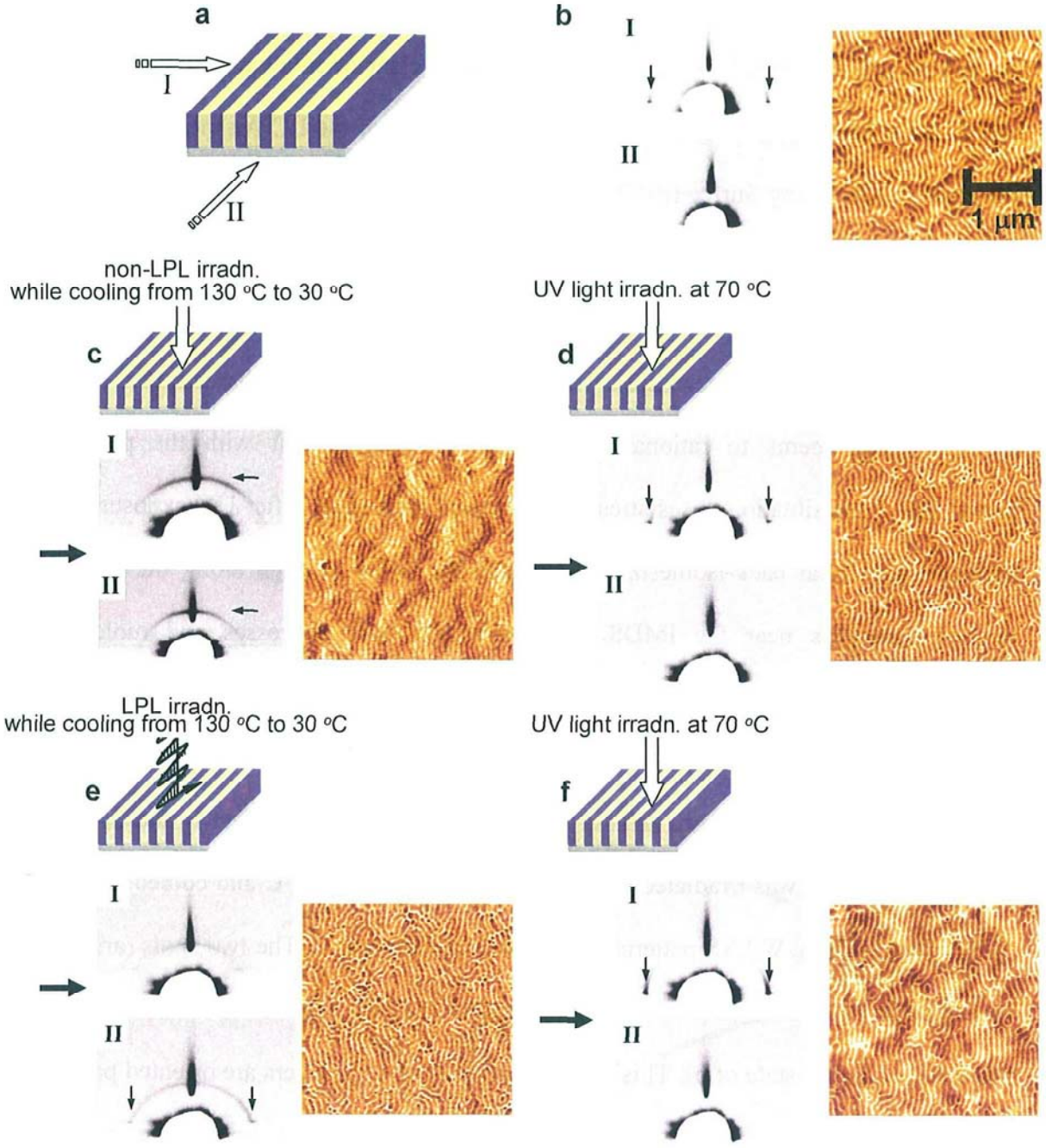

Figure 6-4 Phase mode AFM and GI-WAXS measurements of the initial and light-irradiated films. In **a**, Scheme of the direction of incident x-ray beam is shown. The strips in the film represents the direction of lamella sturucture. In **b** – **f**, Phase mode AFM images (3.0 x 3.0 μm) and GI-WAXS patterns were shown. The initially photoaligned p(S_{226}-Az_{56}) film (**b**), after non-polarized light irradiation (436 nm) with normal incidence while cooling from 130 °C to 30 °C for out-of-plane orientation (**c**), after UV light irradiation followed by annealing (**d**), after LPL irradiation, with the polarization beam parallel to the MPS structure while gradual cooling from 130 °C to 30 °C for attainment of another in-plane orientation (**e**), after UV light irradiation followed by annealing (**f**). The numbers, I and II, in the insets indicate incident direction of x-ray-beam displayed in **a**.

Az groups self-assembled into the initial state. This clear orientational memory effect should stem from the homogeneous (parallel) anchoring of the LC Az mesogens at the Intermaterial Deviding Surfce (IMDS). Here, the anisotropic morphology of the lamella structure and thus the state of IMDS was unchanged. So the mesogens arranged in the vicinity of the IMDS will have an initial orientation even after the subsequent out-of-plane orientation is generated. The insufficient reorientation characterized by the arc diffraction seems to rationalize this aspect, in agreement with the previous knowledge. This situation poses stress to reoriented mesogens. After UV exposure and subsequent thermal back-isomerization releases the stress to align along the initially aligned mesogens near the IMDS. The series of these processes and molecular orientations are shown as the upper route in Figure 6-5.

6.3.3.2 Memory effect in the in-plane direction

The same procedures were achieved to examine the memory effect in the in-plane direction. The film was irradiated with 436 nm LPL light at 130 °C and cooled down to 30 °C. The resulting WAXS patterns of the film are shown in e. The two spots (arrows), corresponding to a *d* spacing of 3.5 nm, were observed only with incident beam of II in this case (cf. initial state of b). This result shows that smectic layers are oriented parallel to the lamella domains in block copolymer thin film. It is also noteworthy that obtained diffraction pattern was less clear and arc-shaped. The orientational order parameter (*S*) evaluated with UV/VIS polarized absorption spectra was 0.40 lower than that ($S = 0.57$) at the initial state of b (Figure 6-6). Thus, also in this in-plane reorientation, motional freedom of the mesogens is suppressed to some extent. For the relaxation of the orientation of the mesogenic groups, the film was irradiated with UV light followed by annealing at 70 °C (f). The initial state was almost fully recovered again. These

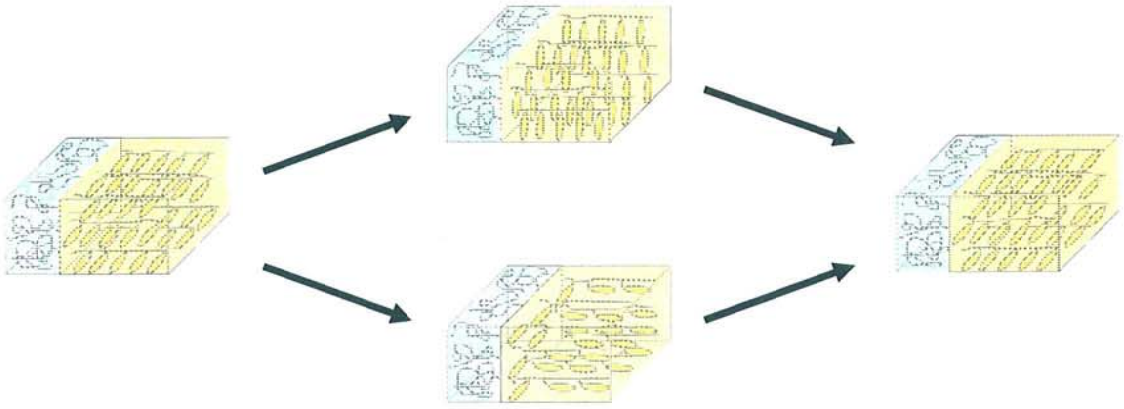

Figure 6-5 Schematic illustration of the orientation of mesogenic Az group confined in lamellar structure of $p(S_{226}\text{-}Az_{56})$ film in the series of irradiation processes indicated in Figure 6-3. The upper and lower routes show the out-of-plane and in-plane photoinduced reorientation of the LC block, respectively.

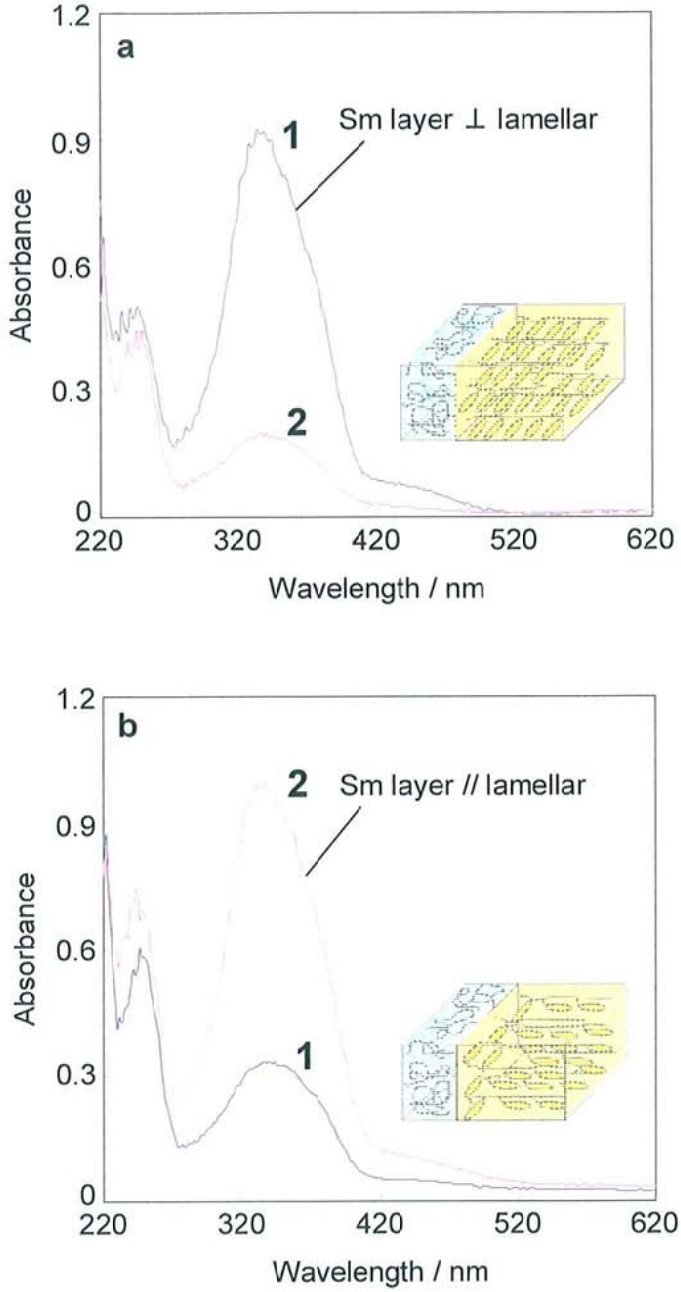

Figure 6-6 UV-vis absorption spectra of the initial (**a**) and subseruently LPL-irradiated (**b**) films. **1** and **2** display polarized spectra taken with probing beam parallel and perpendicular to the direction of the lamellar structure. Schematic illustrations of the corresponding hierarchical structures are inserted in **a** and **b**.

processes of the in-plane reorientation and recovery are schematically shown as the lower route of Figure 6-5.

In addition, the reorientation and memory effect of the mesogens were also brought about by a pure photoprocess without heating. Figures 6-7 (b – f) show the resulting morphological features and WAXS patterns in this process. Unfortunately, however, the diffraction pattern was less clear and arc-shaped (c and e). This fact suggests that a certain amount of Az mesogens remain confined due to the lack of the segmental relaxation induced by heating.

In the above manners both out-of-plane and in-plane acquired reorientations of the mesogens are retracted to the original pre-oriented state by relaxation procedures. Since the homopolymers[4] or statistical random copolymer systems[5] do not show such behaviors, the strong memory effect obviously stems from the oriented hierarchical structure. Interestingly, the metastable acquired state is fully frozen at room temperature. No orientational recovery was admitted at least for two months at ambient temperature.

6.3.4 Surface relief formation in p(S_{226}-Az_{56}) thin film

Next, the surface relief formation was attempted for p(S_{226}-Az_{56}). Since the polymer contains rigid PS block, the mass transport of the film of p(S_{226}-Az_{56}) was examined by hybridization with 5CB. In Chapter 3, effectiveness of this method has been described for PEO-based block copolymer films. A spincast film of ca. 100 nm thickness was prepared for a mixture of p(S_{226}-Az_{56}) and 5CB at $f = 0.8$, and holographic irradiation was performed as mentioned in Chapter 3. Here, the interferometric Ar^+ laser beam was subjected to the film at 2 mW cm^{-2} for 2500 s. The electric field vector of the irradiated beam was parallel to the plane of incidence ((*p*-, *p*-) mode). As shown in Figure 6-8a, the hybrid film provided clear undulations in accord with the interference periodicity (4

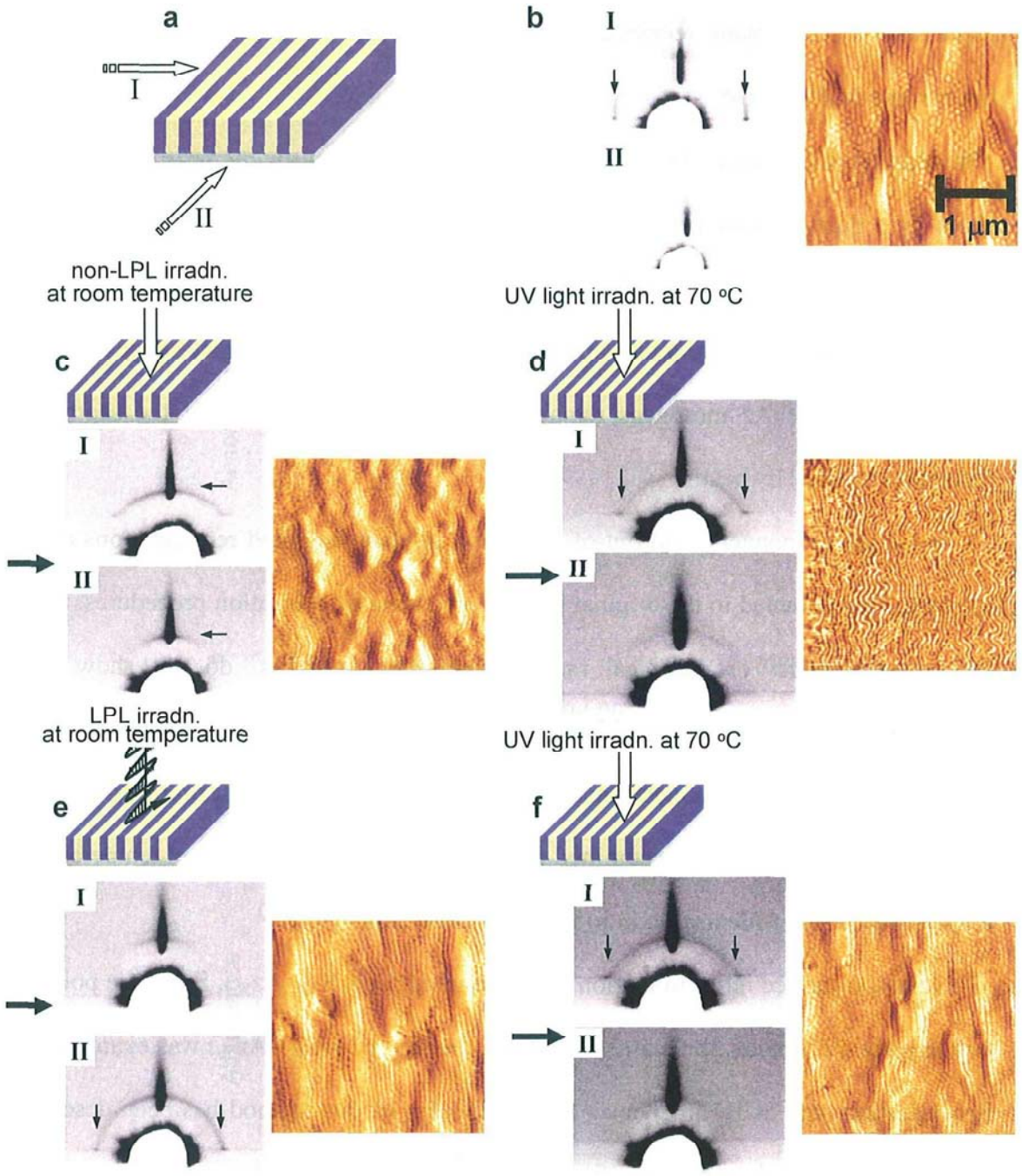

Figure 6-7 Phase mode AFM and GI-WAXS measurements of the initial and light-irradiated films. In **a**, Scheme of the direction of incident x-ray beam is shown. The strips in the film represents the direction of lamella sturucture. In **b** – **f**, Phase mode AFM images (3.0 x 3.0 μm) and GI-WAXS patterns were shown. The initially photoaligned p(S_{226}-Az_{56}) film (**b**), after non-polarized light irradiation (436 nm) with normal incidence at room temperature for out-of-plane orientation (**c**), after UV light irradiation followed by annealing (**d**), after LPL irradiation, with the polarization beam parallel to the MPS structure at room temperature for attainment of another in-plane orientation (**e**), after UV light irradiation followed by annealing (**f**). The numbers, I and II, in the insets indicate incident direction of x-ray-beam displayed in **a**.

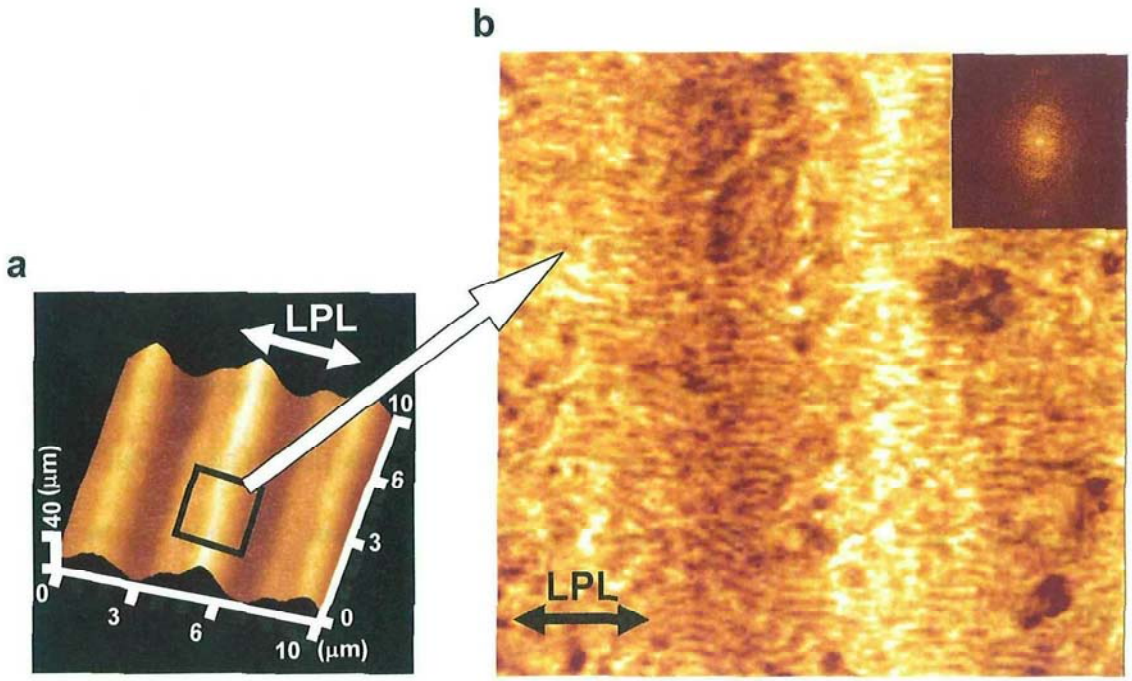

Figure 6-8 AFM image of the p(S_{226}-Az_{56}) film after interferometric irradiation with (*p*-: *p*-) mode Ar^+ laser beam. Topographic AFM image (**a**, 10 x 10 μm) of a photogenerated relief and a magnified phase mode image (**b**, 3.0 x 3.0 μm) of hill to valley slope area. Fast Fourier transform spectrum is shown in **b**.

μm for this case). The crest-to-trough height difference was 35 nm.

Figure 6-8b show the phase-mode AFM images (3.0 μm x 3.0 μm) taken at the slope area from a crest to trough. The microphase separated nanostructures tended to be aligned perpendicular to the undulated structure of the micrometer level. Contrary to expectation, the direction of the microphase separated structure was aligned parallel to the polarization direction of irradiated LPL, which is in contrast the result shown in Figure 6-3b. This contradicting data should suggest that the mass flow induces the orientation of nanostructures in this case. Yokoyama et al. reported the macroscopic orientation of cylindrical nanodomains in relief structure of poly(ethylene propyrene)-*block*-polystyrene film obtained by soft molding method[6] The microphase separated cylinders of this polymer were aligned after pressing a grating patterned poly(dimethylsiloxane) (PDMS) mold followed by annealing above T_g of this polymer. The nanocylinders were aligned perpendicular to the edge of crest. This phenomenon can be interpreted as the consequence of pressure induced flow of the film mass during the pressing. In this case, the same flow induced orientation effect seems to be observed, aligning the microphase separated structure along the mass flow. The present system is unique in that the mass flow is caused by light irradiation, and not by mechanical pressure.

6.4 Conclusion

In this chapter, the photoalignment behavior was focused onto the lamellar nanostructure of $p(S_{226}\text{-}Az_{56})$. The nanostructure can be photoaligned in the conditions that the LPL irradiation is achieved at temperature above T_g of PS block and below the transition temperature of Sm_A to isotropic of the Az polymer block. The photoaligned

lamellar structures gave strong memory effect to the orientation of the azobenzene mesogenic groups, i.e., the acquired reoriented state by successive light irradiation in both out-of-plane and in-plane mode is retracted to the original one after treatment for relaxations. This effect is ascribed to the aligned lamellar structure of rigid PS possessing relatively high T_g. The photo-triggered mass migration was also attempted for this polymer by hybridization with a low-molecular-mass LC molecule. The lamellar structures are governed by the flow induced orientation in this case and not by the electric field of the actinic LPL in the hybrid film.

Reference

1. X. Tong, L. Tue, Y. Zhao, *Macromolecules*, **2004**, *37*, 3101.
2. L. Cui, Y. Zhao, A. Yavrian, T. Galstian, *Macromolecules*, **2003**, *36*, 8246.
3. C. Y. Chao, X. Li, C. K. Ober, C. Osuji and E. L. Thomas, *Adv. Funct. Mater.*, **2004**, *14*, 364.
4. M. Han, S. Morino, K. Ichimura, *Macromolecules*, **2000**, *33*, 6360.
5. J. G. Meier, R. Ruhmann, J. Stumpe, *Macromolecules*, **2000**, *33*, 843.
6. L. Li and H. Yokoyama, *Adv. Mater.*, **2005**, *17*, 1432.

Chapter 7

Summary and Scope

In this doctoral thesis, the novel concept for alignment control and patterning of nanodomains in block copolymer thin films was demonstrated. The self-assembled block copolymer thin films have been attracting increasing attention due to their ability to form periodic microphase separated structures in nanometer levels. To control the disordered fingerprint orientation provided in thin films, the templated self-assembly methods produced by the bottom-up self-assembly combined with the top-down lithographic patterned templates have been reported by many research groups. The alignment control of nanostructures have been performed by utilizing topographically or chemically patterned substrates and introducing external fields such as electric or magnetic fields until now. Nevertheless, these methods require multiple and tedious processes. Contrary to this trend, this work has attempted to develop simple but powerful photoprocesses for alignment control of nanostructures in thin films. Consequently, herein on-demand 3D alignment control and patterning was successfully achieved in thin films of cylinder-forming diblock copolymer possessing Az mesogenic groups without any modification of the substrates.

In Chapter 2, the factors affecting the orientation behavior of nanocylinders in thin films of LC diblock copolymer consisting of PEO and Az polymer were described. The cylinders oriented parallel and perpendicular to the substrate surface in thinner (below 60 nm) and thicker (above 70 nm) films, respectively, on hydrophilic substrates. The LPL irradiation to thinner films gave the in-plane alignment of nanocylinders, leading to

the orthogonal orientation to the LPL direction. When the films prepared on hydrophobic substrates, cylinders exhibited upright orientation for any thickness of the film.

In Chapter 3, the relief structure formation via photo-triggered mass migration was studied using Az-containing diblock copolymer thin films. For this copolymer, no relief structure was formed. In contrast, relief formation was observed in high efficiency in the hybrid films containing 5CB due to the enhancement of the film fluidity.

In Chapter 4, patterning of the cylinder orientation after holographic irradiation was demonstrated. The cylinders were aligned parallel and normal at the trough and crest, respectively, when the film thicknesses at the crests and troughs range above and below the criterion level of 70 nm. By selecting the polarization mode of holographic irradiation, the in-plane control for the laid cylinders at the trough was attained. Thus, the 3D alignment and patterning of nanocylinders in block copolymer films were attained for the first time by the photoprocess.

In Chapter 5, the PS-based diblock copolymer having Az polymer was dealt with. The 3D photoalignment and reorientation of the nanocylinders by the photoprocess were demonstrated in this thin film, resulting in optional rewriting of the alignment. The on-demand 3D photoreorientation of nanocylinders was also demonstrated.

In Chapter 6, lamella-forming diblock copolymer consisting of PS and Az polymer was used. The photoaligned lamellar structures gave rise to strong memory effect in the orientation of the azobenzene mesogenic groups. The strong role of anchoring of Az mesogens at the IMDS surface is suggested.

As described above, the on-demand 3D photoalignment and patterning process of hierarchical structures from molecules to nanostructures was newly developed. This

process is not the simple mixture of bottom-up approach and top-down one, but the fusion of two approaches, in which alignment control of nanostructures can be achieved only by the one-step photoprocess. The achievement obtained in this study should be useful for fabrication of the advanced materials involving high density memory device, nanoporous membrane, nanotemplate and so forth.

Publications

(1) Y. Morikawa, S. Nagano, K. Watanabe, K. Kamata, T. Iyoda and T. Seki ; All Optical Alignment and Patterning of Nanoscale Microdomains in a Block Copolymer Thin Film, *Adv. Mater.*, 18, 883-886 (2006)

(2) Y. Morikawa, S. Nagano, K. Watanabe, K. Kamata, T. Iyoda and T. Seki ; Liquid Crystal- Assisted Photo-triggered Mass Migration in Liquid Crystalline Diblock Copolymer, *Trans. Mater. Res. Soc. Jpn.*, 31, 269-272 (2006)

(3) Y. Morikawa, T. Kondo, S. Nagano and T. Seki ; 3D Photoalignment and Patterning of Microphase Separated Nanostructure in Polystyrene-based Block Copolymer, *Chem. Mater.*, Submitted.

(4) Y. Morikawa, T. Kondo, S. Nagano and T. Seki ; Optical Control of Microphase Separated Nanostructures in Polystyrene-based Liquid Crystalline Diblock Copolymer Thin Film, *Trans. Mater. Res. Soc. Jpn.*, Submitted.

Award

Excellent Presentation Awards for Encouragement, Chemical Society of Japan

Other related publication

Y. Morikawa, K. Arimitsu, T. Gunji, Y. Abe, K. Ichimura ; Characteristics of Silicone Resins as Base Amplifiers and Their Applications to Photopatterning, *J. Photopolym. Sci. Technol.*, 16, 81-82 (2003)

International Conference

(1) Y. Morikawa, S. Nagano, K. Watanabe, T. Iyoda and T. Seki ; Photogenerated Alignment Patterns of Cylindical Nanostructure in Liquid Crystalline Diblock Copolymer Thin Film, The 11th International Cnference of Organized Molecular Film, Sapporo, Japan, June 27 (2005).

(2) Y. Morikawa, S. Nagano, K. Watanabe, T. Iyoda and T. Seki ; Micro-patterning of Nanocylinder Alignment in Liquid Crystalline Diblock Copolymer Film Corrugated via Photoinduced Mass Transfer, The 8th SPSJ International Polymer Conference, Fukuoka, Japan, July 28 (2005).

(3) Y. Morikawa, S. Nagano, K. Watanabe, K. Kamata, T. Iyoda and T. Seki ; Micro-patterning of alignment of microphase separation in liquid crystalline diblock copolymer film corrugated via photoinduced mass transfer, The 14th International Conference on Composites/nano Engineering, Boulder, Colorado, America, July 3 (2006).

Acknowledgement

This investigation has been executed at the Laboratory of Professor Takahiro Seki of Department of Molecular Design and Enginneering, Graduate School of Engineering, Nagoya University, Japan.

I would like to express my sincere gratitude to Professor Takahiro Seki for his helpful discussions, his constant encouragement and continuous guidance throughout the duration of this study.

I would like to thanks Associate Professor Yukikazu Tkeoka of Seki laboratory, Nagoya University for his helpful discussion.

I am very grateful to express sincere thanks Assistant Professor Shusaku Nagano of Seki laboratory, Nagoya University for his helpful discussion and very substantial supporting throughout the duration of this work.

I would like to thank to Professor Tomokazu Iyoda of Tokyo institute of technology for providing me the poly(ethyrene oxide)-*block*-liquid crystalline Az polymer.

I would like to also thank to Mr. Tatsuo Hikage of high intensity X-ray diffraction laboratory, Nagoya University for WAXS measurement.

I wish to thank to Mr. Takeshi Kondo, Mr. Mitsuo Hara and Mr. Toshinobu Ogasawara of Seki laboratory, Nagoya University for supporting my study.

I wish to express my special thank to all members in Seki laboratory, Nagoya University for their general support and excellent dairy life with their.

Finally, I sincerely thanks to my family for supporting my life.